# Ferromagnetic Semiconductor-Metal Transition in Europium Monoxide

Dissertation
zur
Erlangung des Doktorgrades (Dr. rer. nat.)
der
Mathematisch-Naturwissenschaftlichen Fakultät
der
Rheinischen Friedrich-Wilhelms-Universität Bonn

vorgelegt von
Michael Arnold
aus
Saarbrücken

Bonn 2007

Angefertigt mit Genehmigung der Mathematisch-Naturwissenschaftlichen Fakultät der Rheinischen Friedrich-Wilhelms-Universität Bonn

Referent: Prof. Dr. J. Kroha
Korreferent: Prof. Dr. R. Flume
Tag der Promotion: 24.10.2007

Diese Arbeit ist auf dem Hochschulschriftenserver der ULB Bonn
*http* : *//hss.ulb.uni − bonn.de/diss_online* elektronisch publiziert.

# Ferromagnetic Semiconductor-Metal Transition in Europium Monoxide

Michael Arnold

# Contents

# 1 Introduction

The physics of many-particle and in particular solid state systems is full of fascinating phenomena. The scope of the challenges one encounters can thereby range from principle questions of quantum field theory to the very practical development of novel types of storage media. From the theoretical point of view the diversity of macroscopic manifestations of many-particle quantum effects might be the most-intriguing observation. Unfortunately the many-particle character usually leads to significant complications. For instance, the complexity can be either due to many-particle correlations, quantum impurities interacting with the bulk electrons, structural disorder, surface effects or many other origins. Nowadays, especially the coexistence of several complex properties in one material lead to interesting fields of research and application. It is certainly one appealing aspect of solid state physics in general that a possible application of recent research results is sometimes only one step in the future.

In this thesis we will investigate europium monoxide (EuO), as one example of a system with competing interactions. As we will describe in detail in the next chapter the properties of EuO are strongly determined by a magnetic exchange interaction and by the existence of dilute quantum impurities. At room temperature stoichiometric EuO is a paramagnetic semiconductor [1] with a large energy gap of 1.2 eV. Below the critical temperature $T_c = 69K$ it becomes one of the very rare ferromagnetic semiconductors.

Additionally to the stoichiometric case it is in particular interesting to supply excess charge carriers to the system. This is realized either by oxygen vacancies in the Eu-rich compound or for instance by replacing bivalent Eu with trivalent Gd. In both cases the physical properties are qualitatively different in comparison to the pure compound. Namely $EuO_{1-x}$ as well as $Gd_xEu_{1-x}O$ does not only become ferromagnetic below the critical temperature $T_c$. Simultaneously the transport properties change rapidly such that the system is metallic in the low temperature phase [2]-[7]. In fact one can observe a resistivity drop of more than 8 orders of magnitude below $T_c$ for certain samples. Additionally the free charge carriers appear to be nearly 100 per cent spinpolarized in the metallic phase. Furthermore, an applied external magnetic field leads to a considerable shift of the critical temperature and therefore to a colossal magnetoresistance (CMR) effect. Actually the CMR in EuO is one of the strongest effects of that kind ever observed in nature. The strong interplay between magnetism and electronic transport makes electron-doped EuO a natural candidate for many applications

and basic research, for instance in the field of spintronic. All together the striking properties mentioned above make EuO a material which is worth to be studied in detail in order to obtain a principle theoretical understanding of this interesting compound.

In the following we will develop a detailed theory containing the interactions and features, which from our point of view dominate the physical properties of europium monoxide. As usual in modern theoretical condensed matter physics it turns out to be necessary to apply various different approximation schemes to solve such a complex model. Each of them will be explained in the corresponding chapters. Our approach is based on the well known Anderson impurity model [9] in order to account properly for the crucial influence of the dilute quantum impurities in the present case. Already at this point one encounters very basical theoretical problems which are usually referred to as Kondo and Kondo lattice physics. Briefly one can explain the so called Kondo effect to be due to the strong Coulomb repulsion on the impurity site. Thus, the impurity appears to be single occupied and therefore forms a local moment. Resonant scattering off these local moments leads to the so called Kondo resonances in the scattering matrix [11]. From the theoretical perspective this leads to a diverging perturbation expansion and thus to a breakdown of (finite order) perturbation theory. The first attempt to resolve that problems was made by P.W. Anderson [10] and consists of a perturbative renormalization group approach, leading to a diverging (*running*) coupling constant between the local conduction electron spin and the corresponding impurity spin, which are therefore forced to align antiparallel. According to this the ground state of the system could be shown to form a spin singlet. The next important step was due to K.G. Wilson, who developed a numerical renormalization group (NRG, [12]) method to derive the ground state and later also dynamical properties of the Anderson impurity model. Of course there have also been important analytical approaches concerning the (single channel) Kondo model [13, 14]. For details we refer for instance to [15]. Throughout this thesis we concentrate on a diagrammatic method to solve the Anderson impurity part of the model, namely the non crossing approximation (NCA)[16]-[21]. In spite of its shortcomings the NCA turns out to be a convenient method in the present case, particularly because of its diagrammatical and thus at least semi-analytical character. Hence, a fully selfconsistent treatment which is necessary for a model with a higher complexity than the conventional Anderson impurity model can sufficiently be realized. The details of this method and its advantages and disadvantages are presented in Chapter 4 of this thesis. The application to the present model requires a slightly modified NCA which is formulated in Chapter 5.

In addition to the impurity physics in particular the magnetic properties of EuO are known to be essentially determined by the influence of local moments with total spin $S = 7/2$ attached to the $4f^7$ shell of Eu. It is known [22] that

the magnetism of the 4f-moments can be conveniently described according to the Heisenberg exchange model. Additionally, the exchange interaction between the 4f-moments and the conduction band electrons is of crucial importance since it is responsible for the experimentally observed [6] spin dependent splitting of the conduction band. The Heisenberg model of the 4f-moments as well as the spin exchange between the local moments and the conduction band are treated within mean field theory. In spite of this simplification the theory can qualitatively cover the physical properties of the system.

In Chapter 6 we present the corresponding results, restricted to a parameter regime, representing the physical properties of EuO. In contrast to previous studies [35] we solve the complete model selfconsistently. Furthermore, we assume the impurity states to be singly occupied, leading to an equivalence of the Gd-doped and the Eu-rich compound, as specified in Chapter 5. Indeed we find, that the ferromagnetic phase transition in electron-doped EuO is accompanied by a dramatic change of the transport properties, what can essentially be explained by a spin dependent shift of the conduction band under consideration of the overall particle number conservation. Furthermore, we obtain, as a consequence of the selfconsistency, that the strength of the shift as well as the Curie temperature is strongly dependent on the impurity concentration. These properties are in excellent agreement with various recent experimental results [6, 7]. Another possibility to supply charge carriers to the system consists of applying an external bias voltage, shifting the chemical potential in the sample. We show, that in particular the magnetic properties can indeed be switched by such a procedure, which might provide an interesting perspective for future experiments and applications.

The competition between Kondo physics and ferromagnetism is one of the most interesting aspects of the presented model. Although we will demonstrate that in the EuO-regime resonant spin flip processes will be widely suppressed, we will discuss in Chapter 7, how the influence of the Kondo effect might become more important for different realizations of the model, away from the EuO case. In particular, it turns out that a non-magnetic metal to insulator transition can be observed similar to the Mott-Hubbard transition for the Hubbard model.

# 2 Properties of EuO

Since its discovery [1] there have been many experimental and theoretical studies concerning europium monoxide EuO. In this chapter we provide an overview over the physical properties of EuO and its theoretical background. Therefore we summarize the most important experimental results, leading to the current understanding of this compound. Because of the long history of the research in this field we can certainly not mention all the details and thus refer to the corresponding literature whenever it is necessary. As already mentioned before, the physical properties of EuO are remarkable from the theoretical as well as from the experimental point of view. In particular depending on its stoichiometry it can experience tremendous changes in its magnetic and transport properties. Here, we will mainly concentrate on those previous results which are related to the simultaneous para-to-ferromagnetic and semiconductor-metal phase transition observed in Eu-rich $EuO_{1-x}$ or the Gd-doped compound $Gd_xEu_{1-x}O$, respectively. In the following it will be shown that this behavior is accompanied by a change of the electronic band structure, stemming from a complex interplay between the magnetic properties of the different constituents of the system, which we try to identify in order to derive a convenient model description.

## 2.1 Electronic structure

In order to derive a model for EuO we need to know its basic structural properties. EuO has a rocksalt structure with a lattice constant $a = 5.144\mathring{A}$. It is composed of $Eu^{2+}O^{2-}$ and its electronic configuration is $4f^7 5d^0 6s^0$ for $Eu^{2+}$ and $1s^2 2s^2 2p^6$ for $O^{2-}$, respectively. The conduction band is built of the Eu $5d-6s$ orbitals and initially empty. The stoichiometry of EuO is highly influenced by the conditions of the fabrication process, in particular by the temperature at which the crystals are grown (usually ranging from 1000-2000 K, [23]). In the Eu-rich compound it comes to an excess of negative charge carriers which are bound at the oxygen vacancy sites. Hence, the existence of excess Eu provides one possibility of doping the stoichiometric compound. Experimentally one is restricted to 1% doping at maximum in that case. An alternative way of doping the system is given by substituting divalent Eu by trivalent Gd. In particular Gd also obtains a half filled $4f$ shell and thus one expects that it does not change the magnetic properties of the compound. The influence of the impurity concentration on the

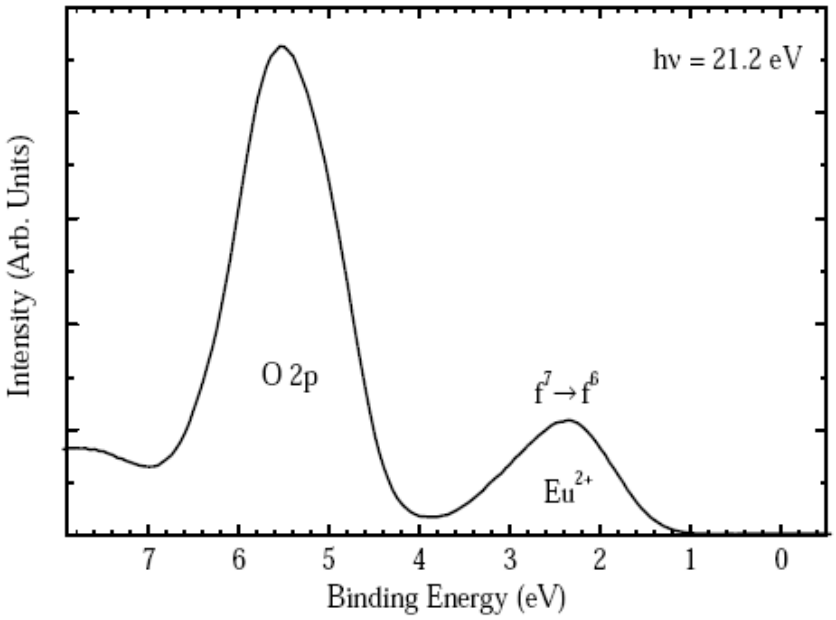


***Figure 2.1:*** Photoemission spectrum (taken from [6]) of EuO demonstrating the occupied O 2p valence band and the Eu 4f states.

magnetic properties, like for instance the Curie temperature, is discussed in the next section. However, as explained later, the model we propose in this thesis does not distinguish between these different types of impurities and therefore can describe the Eu-rich compound as well as the Gd-doped one.

Many properties of EuO can be studied experimentally by investigating the electronic band structure. The O $2p$ and the Eu $4f$ orbital are in general occupied and can be studied using emission spectroscopy. This has been done by Steeneken [6] and Eastman [24] and the results are presented in Fig. 2.1. Due to Hund's rule the 4f moments are in the $S = 7/2$ state and the polarization is about 100% [6], remaining very stable. The Eu 4f-states are strongly localized and hybridize therefore only weakly with other orbitals. As a consequence they do not contribute significantly to the electron transport in the system, which therefore is determined by the $5d - 6s$ conduction band hybridizing with the O $2p$ level. In Chapter 5 this is reflected by the theoretical expression we derived for the conductivity of a model containing localized impurities. Moreover, the exchange integral $\Delta_{4f-5d} \approx 0.3eV$ between the 4f moments and the conduction band is of crucial importance since it it responsible for the shift of the conduction band, as it is shown below.

Since the majority of the conduction band is not occupied one usually has to use absorption spectroscopy methods. In Fig. 2.2 we show results of a recent x-ray

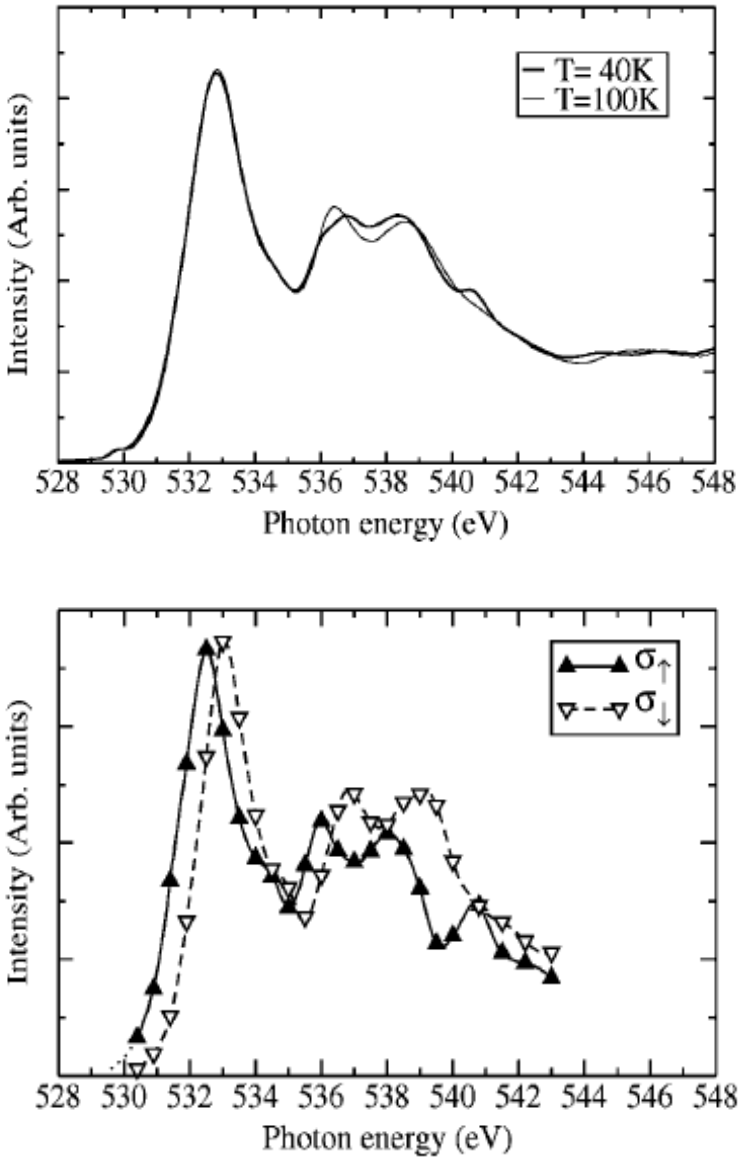


***Figure 2.2:*** Conduction band density of states (DOS) measured with x-ray absorption spectroscopy (taken from [6]). In the upper panel the not spin resolved measurement shows a significant change in the DOS below $T_c$. The spin resolved result in the lower panel proofs this change to be due to a spin dependent shift of the conduction band. The small peak at $529eV$ in the upper panel may be an impurity induced band (see Chapter 5, 6).

absorption spectroscopy (XAS) experiment [6]. These results are very interesting because of several reasons. First, they can clearly show that the conduction band is shifted spin dependently below the critical temperature $T_c \approx 69K$. The observed deformation of the total conduction band (Fig. 2.2, upper panel) is thus only due to the shift of the different spin directions. Hence, the coupling $\Delta_{4f-5d}$ of the conduction band and the local 4f-moment indeed leads to a splitting of the conduction band. Furthermore the conduction electrons appear to be nearly completely spin polarized.

## 2.2 Magnetism

As mentioned before, the magnetism of EuO is mainly determined by the magnetic moments in the half-filled Eu $4f$ shell which align parallel according to Hund's rule. As a consequence even stoichiometric EuO shows ferromagnetic behavior. Because an exchange interaction via free electrons is very unlikely in a semiconductor, the existence of a ferromagnetic semiconductor or insulator has been doubted for a long time. In fact the discovery of $CrBr_3$ [25] and EuO [1] provided the first proof of the existence of such compounds. Furthermore, there exist several other magnetic ordering Eu chalcenogides, namely EuS, EuSe and EuTe, which orders antiferromagnetically. However, today it has been shown by neutron scattering experiments [26] that in particular the spin-wave spectrum of EuO can be described conveniently in terms of the well known Heisenberg exchange model [27]. We will comment on the particular realization of the Heisenberg model in the Eu 4f subsystem of EuO in the next chapter. The magnetic behavior of EuO has been investigated in various theoretical [28]-[31] and experimental [32, 7] studies. In Fig. 2.3 [32] and Fig. 2.4 [7] the measured magnetization for Gd-doped EuO at several doping concentrations $n_I$ is presented. It is particularly remarkable that the magnetization as well as the Curie temperature clearly depends on the impurity or doping concentration in the compound as one can see in Fig. 2.3, lower panel. In recent experiments [33, 34], this behavior could also be observed for Eu-rich EuO without explicit Gd-doping, which is in contradiction to previous theories [35, 36]. Since the Eu 4f moments themselves contain no information about the impurity concentration the $n_I$-dependence of the magnetization and the Curie temperature $T_c$ hints to fact that the magnetization of the local 4f-moments and of the conduction band finally needs to be determined selfconsistently. In our approach this will be realized by a s-f-model type coupling between the conduction electrons and the 4f-states. We will demonstrate that the effective field due to the conduction band magnetization influences the local Eu 4f moments and vice versa. In particular this will explain the existence of the shoulder in the magnetization close to the Curie temperature (cf. Fig. 2.4).

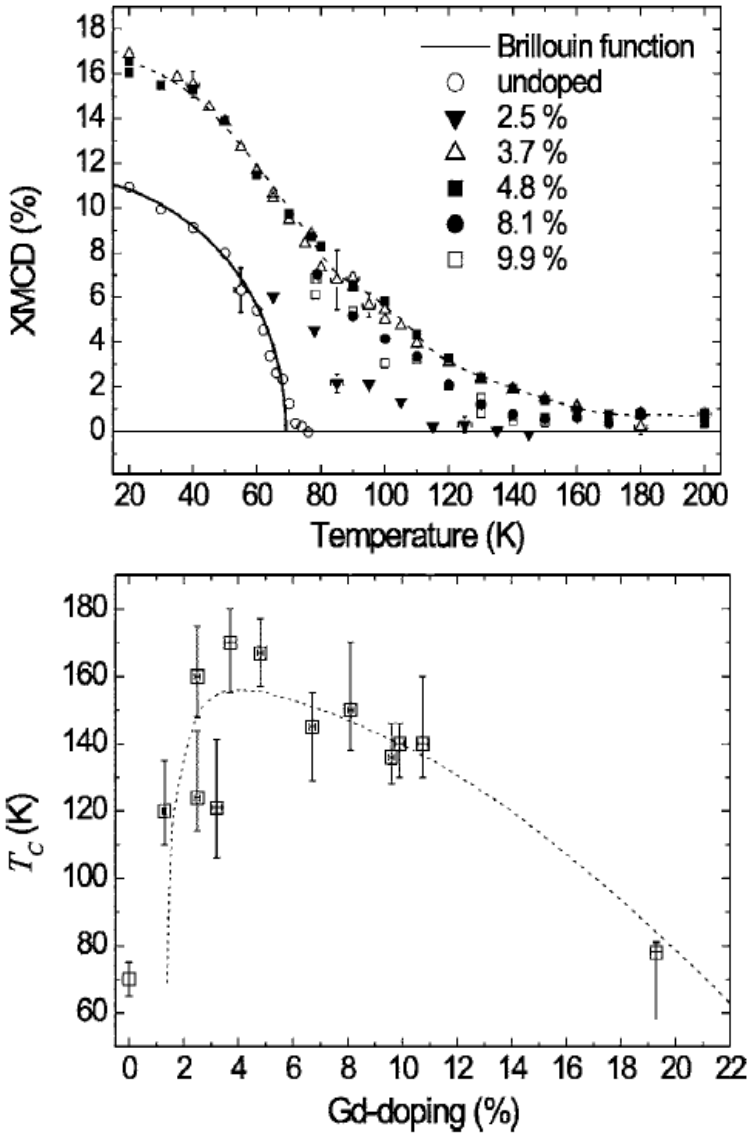


***Figure 2.3:*** Magnetization and Curie temperature $T_C$ measured for Gd-doped EuO. The dependence of $T_C$ on the doping concentration is demonstrated. (taken from [32])

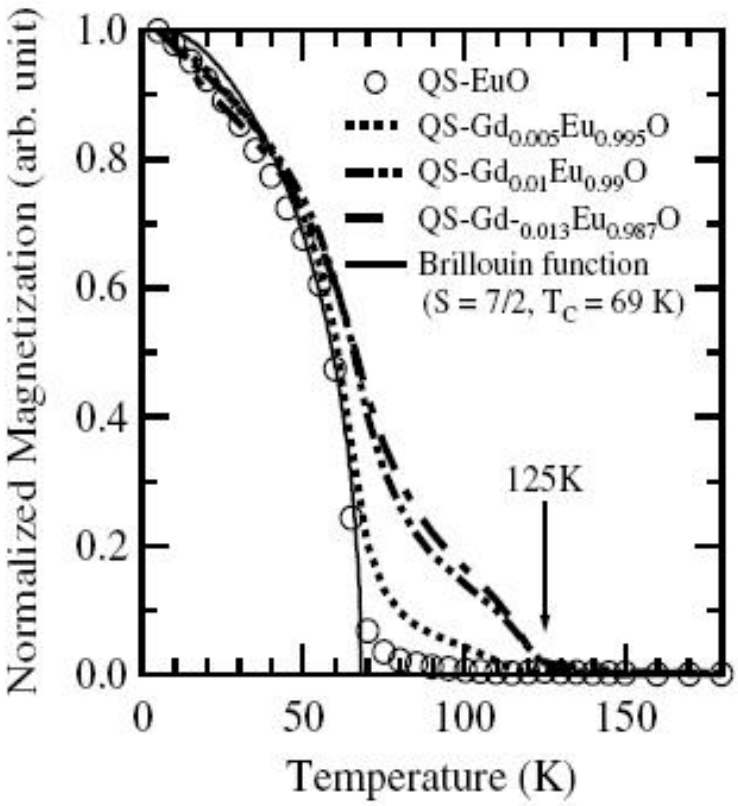


***Figure 2.4:*** Normalized magnetization of Gd-doped compared to quasi-stoichiometric (QS) EuO (taken from [7]). The strong influence of the Gd-concentration on the magnetic properties is remarkable. In particular the Curie temperature can assume values much larger than in the pure compound.

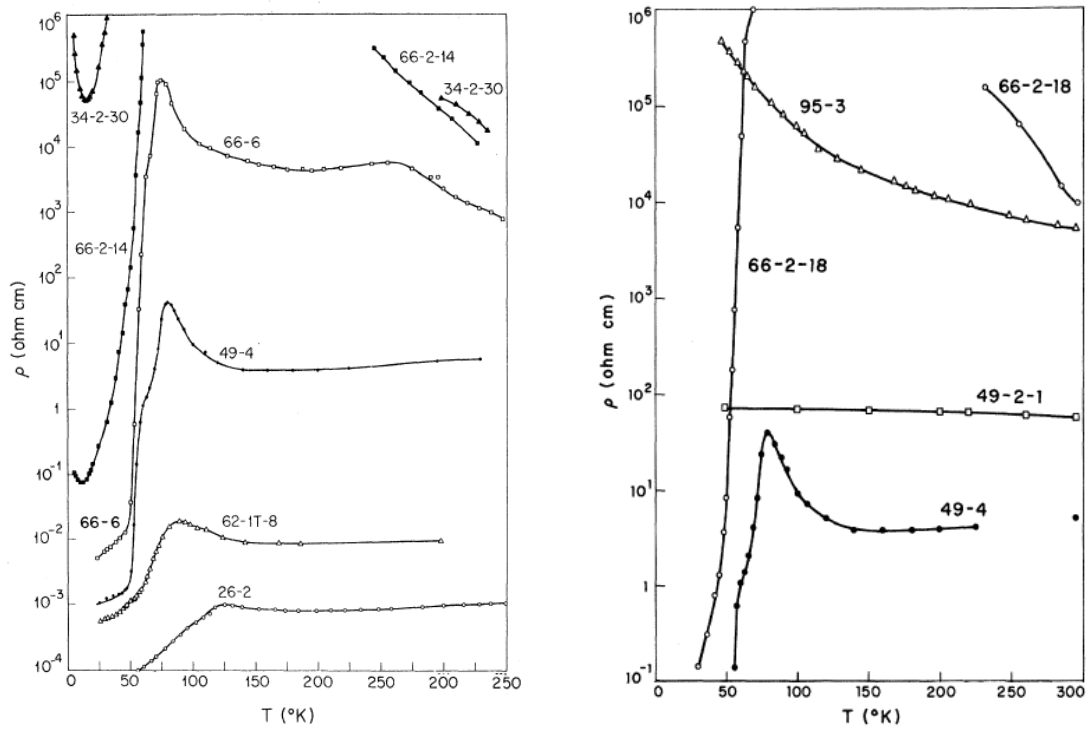


***Figure 2.5:*** Resistivity measurements under various fabrication conditions of the EuO compounds. As mentioned before, in particular the concentration of O-vacancies strongly depends for instance on the temperature under which the crystals are grown. (taken from [2])

## 2.3 Transport properties

Besides the ferromagnetism of the semiconducting stoichiometric EuO the most striking feature is certainly the tremendous change in the conductivity of the electron-doped compound. In Fig. 2.5 we present various resistivity curves [2] measured under different conditions. Thus one can observe semiconductor-like behavior (curve 95-3) for stoichiometric or O-rich EuO. In the Eu-rich case the resistivity above the critical temperature increases by up the 7 orders of magnitude (curve 66-6). We will identify the temperature $T_{max}$ at which the resistivity reaches its maximum with the critical temperature $T_C$. All the samples behaving like the Eu-rich case additionally show a broadened dip on the resistivity edge slightly below the maximum of the resistivity. Later we will explain the dip to be due to the change of the overall conduction electron number. For a long time it has not been clear, whether the spectacular resistivity behavior of Eu-rich EuO is also observed in the Gd-doped compound. Only very recent experiments [7, 33]

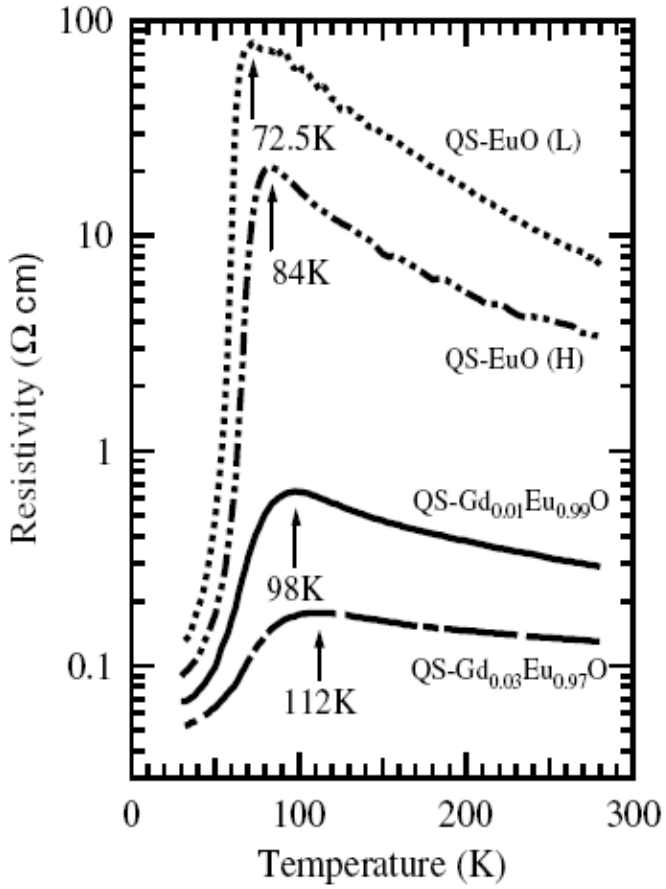


***Figure 2.6:*** Resistivity measurements for very low O-vacancy concentration (QS - quasi-stoichiometric) and with explicit Gd-doping. Both types of electron-doping amounts in a similar effect on the transport properties. (taken from [7])

could clarify, that $Eu_{1-x}$ and $Gd_xEu_{1-x}O$ indeed behave very similar concerning their magnetic as well as their transport properties (cf. Fig. 2.6). In the present work we are exploiting this property by assuming the same model for both types of doping, as demonstrated in Chapter 5.

Besides the strong temperature dependence of the resistivity the application of an external magnetic field leads to another spectacular effect. As one can see in Fig. 2.7 the resistivity of a sample in the vicinity of the critical temperature can be reduced dramatically by applying a magnetic field. In fact, this kind of colossal magnetoresistance effect (CMR) is much larger than for instance in the intensively studied manganates [8].

Up to now the origin of those spectacular transport properties is not finally resolved. However, what all former approaches have in common is the idea that

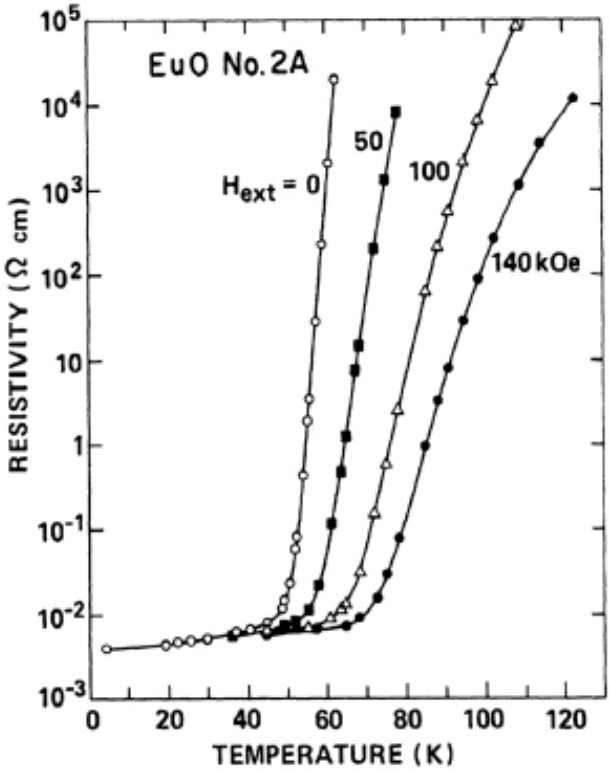


***Figure 2.7:*** Temperature dependent resistivity measurements with various external magnetic fields applied. A colossal magnetoresistance effect can clearly be observed (taken from [4])

below the critical temperature delocalized charge carriers, stemming from the impurity sites are responsible for the transition in the resistivity. This approach is certainly confirmed by the experimental evidence provided in the present chapter. Thus, the importance of impurity physics for a concise theory of doped EuO can hardly be overestimated. We will comment on quantum impurities in general in Chapter 4, while Chapter 5 is dealing with the specific model for EuO with Gd-doping or O-vacancies.

# 3 Stoichiometric EuO - A Heisenberg Ferromagnet

Although magnetism is a phenomenon known for a very long time it is still a vital field in condensed matter physics. The first theoretical attempts to explain the collective magnetism in condensed matter systems considered electrons as interacting spins carrying a magnetic moment. However, the magnitude of the corresponding dipole-dipole interaction is of the order $1K$ and hence far to small to explain typical magnetic transition temperatures. Therefore it was realized very early that the mechanisms giving rise to magnetism are due to fundamental properties of the electrons. In particular the interplay between the Pauli exclusion principle, the Coulomb repulsion between electrons at the same site and their kinetic energy determines the magnetic properties of the system. In the following we try to provide a brief overview over the physical principles of the collective magnetic phenomena due to exchange interactions as they occur in EuO. For a complete overview we refer to the corresponding literature (for instance [41, 42]). Furthermore, we introduce the Heisenberg model [27] describing insulators and semiconductors with magnetic order. In particular stoichiometric EuO is one of the rare ferromagnetic semiconductors and a typical example of a Heisenberg ferromagnet.

## 3.1 Exchange interactions

The interaction between the magnetic moments at sites $\vec{R}_i, \vec{R}_j$ in a many-particle system often can be written as

$$w_{i,j} = -J_{i,j}\vec{S}_i\vec{S}_j \tag{3.1}$$

Here, $J_{i,j}$ is called exchange integral, including the microscopical information about the system. Usually one distinguishes between direct exchange processes between neighboring lattice sites, indirect exchange processes and superexchange processes due to virtual excitations. In the following we will introduce the basic mechanisms and specify the exchange interaction as it appears between the local Eu 4f moments in EuO.

### 3.1.1 Direct exchange

As an example, illustrating the underlying principles of the direct exchange mechanism, we consider two electrons that are localized by an external potential. Furthermore, we assume a repulsive Coulomb interaction $v(x_1, x_2)$ between the two states. The two particle wave function $\Psi(x_1, x_2)$ in this case has to be antisymmetric. If the two spins align parallel the two particles are therefore spatially separated, thus reducing the total Coulomb energy. On the other hand the kinetic energy is increased. In that sense the exchange integral in this situation counts the energy difference due to an exchange of the particles. The competition between Coulomb repulsion and kinetic energy thus determines the sign of the exchange integral $J_{1,2}$ and therefore the magnetic properties of the system. In this simplified fashion for $J_{1,2} > 0$ the ferromagnetic exchange interaction is completely analogous to Hund's rule, claiming that two spins localized in energetically closed orbitals tend to align parallel.

### 3.1.2 Indirect exchange between local moments

In many cases the contribution to the exchange integral $J_{i,j}$ stemming from the direct exchange is negligible because the electrons are strongly localized around the lattice sites $\vec{R}_i, \vec{R}_j$. This is in particular fulfilled in many systems containing local magnetic moments due to not completely filled ($3d, 4d, 4f$ or $5f$) orbitals, like for instance the rare earth compounds. According to Hund's rule the electrons in one orbital align such that their total spin is maximized. Actually, this formation of a local moment can be understood to be a special case of a ferromagnetic exchange interaction between electrons in one shell, as we already noted above. In spite of the local character of the magnetic moments one can often observe a magnetic ordering that can be described in terms of an exchange interaction. Since the direct exchange interaction between neighboring sites can be excluded, the finite exchange integral $J_{i,j}$ must be induced by other constituents of the total system. The most common example for such an interaction is certainly the so called $RKKY$ interaction [37, 38, 39]. Here, an effective oscillating long range interaction between local moments is mediated by conduction band electrons. The coupling of a local moment $\vec{S}_i$ at site $\vec{R}_i$ to the conduction electron spin $\sigma_i$ can be described by an $s-d$ interaction

$$V_i = -J_{sd}\vec{S}_i\vec{\sigma}_i \tag{3.2}$$

Hence, in second order an effective interaction between two local moments $\vec{S}_i, \vec{S}_j$ can be induced. This type of exchange interaction is often responsible for the magnetic order observed in metallic systems.

However, in an insulator or semiconductor like EuO the situation is completely different. Because of the empty conduction band a $RKKY$ interaction between

local moments cannot be induced. In fact there is an analogous exchange interaction (BR) [40] for semiconductors with local moments. In particular for EuO [22] it can be understood the following way. In contrast to the $RKKY$ interaction the BR interaction is due to the direct exchange between the local $4f$ moments polarizing the valence band electrons. Hence, an effective ferromagnetic interaction is induced between the $4f$ moments as a higher order process of the 4f moments valence band interaction.

## 3.2 The Heisenberg model

Independent on the origin of the interaction between two magnetic moments at sites $\vec{R}_i, \vec{R}_j$ one can define a general effective model for such a system. The Hamiltonian of the so called Heisenberg model yields

$$H = -\sum_{i,j} J_{i,j} \vec{S}_i \vec{S}_j \tag{3.3}$$

In fact the Heisenberg model is one of the paradigms in condensed matter and theoretical physics in general. In spite of its simplicity it turns out to describe a rich variety of physical phenomena. In particular the ferromagnetism of many insulating or semiconducting systems is conveniently reflected within Eq. (3.3), provided $J_{i,j} > 0$. Unfortunately, up to now there exists no exact solution for the Heisenberg model in general. Many important aspects of Eq. (3.3) can be understood at least qualitatively in terms of the mean field approximation, which we therefore decide to utilize in the following chapters. In particular in the limit of infinite coordination number the mean field approximation becomes exact [43]. However, for completeness we will mention the shortcomings in lower dimensions (for instance $d = 3$) as well. First, for low temperatures $T \to 0$ collective excitations of the ordered spins $\vec{S}_i$ at site $i$, so called spin waves [44, 41], have to be taken into account. According to this one obtains the Bloch law $M_0 - M(T) \propto T^{3/2}$ describing the magnetization $M(T)$ relative to its value at zero temperature. The other limit in which the mean field approximation fails for dimensions lower than $d = 4$ is approached in the vicinity of the critical temperature $T_C$. At temperatures $T \approx T_C$ the characteristic physical quantities are given in terms of $\tau = (T_C - T)/T_C$. In particular the magnetization within the Heisenberg model yields $M \propto \tau^\beta$, where $\beta$ is a so called critical exponent. Comparing the experimental result $\beta \approx 0.365$ [45] for stoichiometric EuO to the theoretical estimations [43] one can show that the critical behavior of EuO is in excellent agreement with the Heisenberg model. Within mean field theory $\beta$ is given by $\beta = 1/2$, in contradiction to the experiment. As we will show in Chapter 6 this result is reproduced by our calculations. However, we believe that the deviation from the exact critical behavior of the magnetization does not affect the qualitative results too strongly.

# 4 Some Aspects of Quantum Impurities

Over the last 30 years the physics of quantum impurities has become a paradigm in condensed matter theory. Not only, because in a real system the existence of quantum impurities can be an important issue. Furthermore, the problem of correlated electrons on a lattice, which is certainly a central theme of solid state physics turned out to be strongly related. In particular the development of the Dynamical Mean Field Theory (DMFT) in the 90's [46, 47, 48] led to a pursuit for an accurate solution of the so called Anderson impurity model [9]. Within the framework of the DMFT the initial Hubbard model [49], which is a lattice model, as mentioned above, is mapped onto an effective impurity, selfconsistently coupled to a surrounding bath. Thus the kernel of each DMFT calculation consists of an impurity problem that needs to be solved. Unfortunately, until today there exists no perfect solution of the Anderson model as it occurs in complex systems. In the first section we will discuss the model in detail and also address the different approaches developed over the last decades.

Furthermore, we review a selfconsistent diagrammatic method, called non-crossing approximation (NCA) as it is utilized in this thesis. The advantages and shortcomings are summarized with respect to the intended application. Additionally an alternative formulation developed with A.Georges at the Ecole Polytechnique, Palaiseau is presented in the last section of this chapter.

## 4.1 The Anderson impurity model

Quantum impurity models such as the single impurity Anderson model (SIAM) were discussed first in the context of magnetic impurities in metals. In these models a spin degenerate local impurity level hybridizes with the conduction band. Provided that the local level lies sufficiently far below the Fermi energy and the onsite Coulomb repulsion $U$ between two impurity electrons is strong enough, the local level will be singly occupied and a local magnetic moment forms. In general the hybridization between a N-fold degenerate impurity with a M-fold conduction band can be described by the $SU(N) \times SU(M)$ multichannel Anderson model. In the following we well restrict to the single channel (M=1) case.

### 4.1.1 Single channel quantum impurity model

In this section we will formulate the many-particle model corresponding to a local impurity at level $E_d$ relative to the Fermi energy coupling to an arbitrary conduction band. Thus, we will consider the prototype Anderson impurity Hamiltonian

$$H = H_c + H_d + H_{hyb} \tag{4.1}$$

with the conduction electron part

$$H_c = \sum_{k\sigma} \epsilon_k c^\dagger_{k\sigma} c_{k\sigma} \tag{4.2}$$

the local impurity Hamiltonian

$$H_d = E_d \sum_\sigma d^\dagger_\sigma d_\sigma + U \sum_{\sigma<\sigma'} n_{d\sigma} n_{d\sigma'} \tag{4.3}$$

and the hybridization

$$H_{hyb} = V \sum_{k\sigma} \left( c^\dagger_{k\sigma} d_\sigma + h.c. \right) \tag{4.4}$$

Introducing the width of the local d-level $\Gamma = \pi V^2 N(0)$ with the conduction electron density of states at the Fermi energy $N(0)$, one can define the so called Kondo limit by $E_d < 0 < E_d + U$ and $\Gamma/|E_d|, \Gamma/|2E_d + U| \ll 1$. In this limit a local magnetic moment forms on the impurity site and thus the Anderson model can be mapped onto the so called Kondo model [50, 51]. Hence the physics can be described by an antiferromagnetic exchange interaction between the local conduction electron spin and the local d-electron spin mediated via the coupling constant $J = V^2 \left(1/|E_d| + 1/|2E_d + U|\right)$. This exchange interaction is responsible for the Kondo effect as it is known for a long time in metals containing magnetic impurities [52] or as it has quite recently been discovered in quantum dots [53].

The properties of these models have been intensively studied in the past using various different approaches, like the Bethe ansatz (BA) method [13, 14] or the Numerical Renormalization Group (NRG) [12]. In the Kondo limit the system is governed by the low temperature scale given by the Kondo temperature

$$T_K = \sqrt{2\Gamma D}\, e^{-\frac{\pi E_d}{2\Gamma}} \tag{4.5}$$

where $D = 1/N(0)$ is the high energy cutoff of the constant conduction electron density of states. For temperatures $T \gtrsim T_K$ resonant spin flip scattering of conduction electrons off the impurity degenerate level leads to logarithmic corrections to the temperature dependent resistivity $\rho(T)$, such that the perturbation theory breaks down at $T \simeq T_K$. Below the Kondo temperature a many-body spin singlet

state forms in which the local impurity is screened by conduction electron cloud leaving a pure potential scattering center in the limit $T \to 0$. Thus the ground state of the single channel Anderson model can be described within Fermi liquid theory. Despite the great success concerning the principle understanding of the Anderson model alternative approaches instead of the Bethe ansatz or the NRG might be favorable in some cases. In particular, if one is interested in an at least semi-analytical formulation of the problem for an arbitrary conduction electron density of states both approaches are not appropriate anymore. One method to overcome this problems is provided by conserving diagrammatic approximations as we will present later.

However, any diagrammatic approach being due to perturbation theory in $V$ encounters two severe problems in the present case. The first problem consists of the breakdown of finite order perturbation theory in the limit $T \simeq T_K$. This issue is resolved within the non crossing approximation as it is discussed later. Furthermore, the conventional quantum field theoretical methods like Wick's theorem and Feynman diagrams in general do not apply to a strongly correlated impurity system.

### 4.1.2 Pseudo particle representation

The applicability of the standard diagrammatic calculus as it is widely used in condensed matter theory can be recovered by the introduction of a pseudo particle representation of the impurity states [54]-[57]. The dynamics of an electron occupying a local impurity state will be strongly determined by the impurity occupancy, in particular in the strongly correlated limit with a large Coulomb repulsion $U$ on the impurity site. Therefore it is useful to divide the impurity Hilbert space depending on the occupation number. The empty, single occupied and double occupied states are thus created by $|0\rangle = b^\dagger|vac\rangle$, $|\sigma\rangle = f_\sigma^\dagger|vac\rangle$ and $|2\rangle = a^\dagger|vac\rangle$ out of the vacuum $|vac\rangle$. Furthermore an fermionic operator acting on the occupation number states is defined

$$d_\sigma^\dagger = f_\sigma^\dagger b + \eta_\sigma a^\dagger f_{-\sigma} \tag{4.6}$$

such that $|\sigma\rangle = d_\sigma^\dagger|0\rangle$ and $|2\rangle = \eta_\sigma d_\sigma^\dagger|-\sigma\rangle$ with $\eta_\sigma = \pm 1$ for $\sigma = \uparrow, \downarrow$. In comparison to the physical impurity states the Fock space of the pseudo particles is artificially enlarged. Therefore the subspace corresponding to the physical impurity electrons is defined by the requirement that the impurity is in a unique pseudo particle state, as it is expressed via

$$Q = \sum_\sigma f_\sigma^\dagger f_\sigma + b^\dagger b + a^\dagger a = 1 \tag{4.7}$$

The operator definition Eq. (4.6) together with the constraint Eq. (4.7) can be used to transform the Hamiltonian Eqs. (4.1-4.4).

The Anderson impurity model in terms of the pseudo particle operators can finally be rewritten

$$H = H_c + E_d \sum_\sigma f_\sigma^\dagger f_\sigma + (2E_d + U) a^\dagger a + V \sum_{k\sigma} \left[ c_{k\sigma}^\dagger \left( b^\dagger f_\sigma + \eta_\sigma f_{-\sigma}^\dagger a \right) + h.c. \right] \quad (4.8)$$

It is remarkable that the constraint Eq. (4.7) as well as the Hamiltonian Eq. (4.8) is diagonal in each pseudo particle operator besides of the hybridization part. Therefore standard perturbation theory in $V$ becomes applicable in the pseudo particle space. As another consequence Eq. (4.7) can be regarded as a statement of charge conservation. Similar to other quantum field theories this is related to a local $U(1)$ gauge symmetry of the field operators. According to this Eq. (4.8) remains invariant under simultaneous transformations $f_\sigma \to e^{i\Phi(\tau)} f_\sigma$, $b \to e^{i\Phi(\tau)} b$ and $a \to e^{i\Phi(\tau)} a$ of the pseudo particle operators. In this thesis we will restrict ourselves to the case of infinite Coulomb repulsion $U$ and thus the terms containing $a$-operators can be neglected in the Hamiltonian

$$H = H_c + E_d \sum_\sigma f_\sigma^\dagger f_\sigma + V \sum_{k\sigma} \left[ c_{k\sigma}^\dagger b^\dagger f_\sigma + h.c. \right] \quad (4.9)$$

with the modified constraint

$$Q = \sum_\sigma f_\sigma^\dagger f_\sigma + b^\dagger b = 1 \quad (4.10)$$

reflecting the fact that for $U \to \infty$ the impurity cannot be doubly occupied.

### 4.1.3 Exact projection onto the physical Fock space

The U(1) gauge symmetry of the Hamiltonian Eq. (4.8) or Eq. (4.9) guarantees the conservation of the total particle number Q. However, the physical Fock space is defined by $Q = 1$ and thus a appropriate projection procedure needs to be found. Following the method proposed in [54] we consider the grand canonical density operator:

$$\rho_G = \frac{1}{Z_G} e^{-\beta(H + \lambda Q)} \quad (4.11)$$

with the grand canonical partition function $Z_G = \mathrm{tr}\left[\exp(-\beta(H + \lambda Q))\right]$ and a chemical potential $\lambda$. The trace is taken over the complete Fock space, including a summation over Q. Hence the expectation value of an operator $\hat{A}$ is defined by

$$\langle \hat{A} \rangle_G = \mathrm{tr}\left[ \rho_G \hat{A} \right] \quad (4.12)$$

in the grand canonical ensemble. The physical expectation value of $\hat{A}$ is calculated in the canonical ensemble with $Q = 1$ and is related to the expectation value in

the grand canonical ensemble by

$$\langle \hat{A} \rangle_C = \lim_{\lambda \to \infty} \frac{\langle Q\hat{A} \rangle_G}{\langle Q \rangle_G} =^{(*)} \lim_{\lambda \to \infty} \frac{\langle \hat{A} \rangle_G}{\langle Q \rangle_G} \tag{4.13}$$

while the equality $(*)$ only holds for an operator $\hat{A}$ with $\hat{A}|Q = 0\rangle = 0$. This is valid for any physically observable operator acting on the impurity. One example is given by the physical electron operators $d_\sigma, d_\sigma^\dagger$. In particular the physical d-electron Green's function is given by

$$G_d(\omega) = \lim_{\lambda \to \infty} \frac{G_d(\omega, \lambda)}{\langle Q \rangle_\lambda} \tag{4.14}$$

where $G_d(\omega, \lambda)$ is the Green's function in the grand canonical ensemble. All the upcoming derivations can be performed in the grand canonical (enlarged) Hilbert space and thus the grand canonical Green's function $G_d(\omega, \lambda)$ can be expressed in terms of the pseudo particle Green's functions

$$\mathcal{G}_{f,b} = \left( \left[ \mathcal{G}^0_{f,b}(i\omega_n) \right]^{-1} - \Sigma_{f,b}(i\omega_n) \right)^{-1} \tag{4.15}$$

with the bare Green's functions

$$\mathcal{G}^0_f(i\omega_n) = (i\omega_n - E_d - \lambda)^{-1} \tag{4.16}$$

$$\mathcal{G}^0_b(i\omega_n) = (i\omega_n - \lambda)^{-1} \tag{4.17}$$

Since, in the limit $\lambda \to \infty$ the energy scale of the so defined pseudo particles scales to infinity it is useful to gauge the auxiliary particle spectrum relative to the chemical potential $\lambda$. Thus the projected Green's functions are given after analytical continuation by

$$G_{f,b}(\omega) = \lim_{\lambda \to \infty} \mathcal{G}^0_{f,b}(\omega + \lambda) \tag{4.18}$$

The energy scale of physical quantities, defined by the difference of the pseudo-fermion and the slave-boson energy is not affected by this procedure. This will be extensively exploited in the subsequent sections.

### 4.1.4 Disorder and dilute impurities

Up to now we were only dealing with one single Anderson impurity hybridizing with an electron conduction band. However, in real system and in particular in the model we are dealing with in this thesis, a dilute concentration of impurities is randomly distributed over the solid. Thus in general it becomes necessary to average over the impurity distribution. In this section we derive the resulting expression for the electron selfenergy. It follows immediately from the Hamiltonian

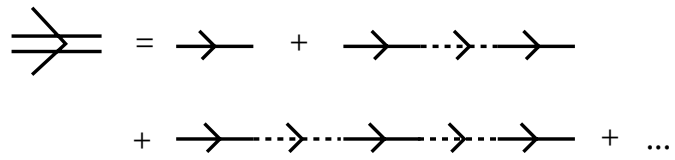

***Figure 4.1:*** Diagram of the local conduction electron Green's function (double solid line). Solid lines represent the local, bare conduction electron propagator, while dashed lines are d-electron Green's functions.

Eqs. (4.1)-(4.4), that the canonical local conduction electron t-matrix $t_\sigma(i\omega_n)$ defined by the local conduction electron Green's function $G_{loc} = G^0_{loc}\,(1 + tG^0_{loc})$ (cf. Fig. 4.1) yields

$$t_\sigma(i\omega_n) = |V|^2 G_{d\sigma}(i\omega_n) \tag{4.19}$$

Knowing the local t-matrix Eq. (4.19) the conduction electron selfenergy $\Sigma_{k\sigma}(i\omega_n)$ for a dilute impurity concentration $n_{imp}$ is given by

$$\Sigma_{k\sigma}(i\omega_n) = n_{imp} \cdot t_\sigma(i\omega_n) = n_{imp} \cdot |V|^2 G_{d\sigma}(i\omega_n) \tag{4.20}$$

This relation holds under the assumption of independent impurities, which is fulfilled for low impurity concentrations. The derivation of Eq. (4.20) is presented in Appendix A.

## 4.2 The Non Crossing Approximation

At the heart of each impurity problem is the calculation of the impurity Green's function as it is defined in Eq. (4.14). In particular in Eq. (4.20) in the case of a dilute impurity concentration $G_d$ is even influencing the full conduction electron Green's function. In this section we present the so called non crossing approximation (NCA) as one efficient method to derive $G_d$ for the single impurity Anderson model in the limit of infinite local Coulomb repulsion on the impurity states. The NCA has been pioneered by Keiter and Kimball [16] and later by Kuramoto [18, 19, 20, 21], who was the first to recognize its conserving character. We will not follow the historical way, but instead we directly introduce the NCA as a conserving approximation derived from its generating functional.

### 4.2.1 Conserving approximations and the generating functional

Before demonstrating the non crossing approximation as one efficient method to solve the Anderson impurity model some general aspects on conserving ap-

proximations (where the NCA is one example for) will be discussed. Conserving approximations are based on selfconsistent approximations to the one-particle Green's function. It turns out that the intrinsic conservation laws at each vertex in a diagrammatic expansion is a necessary but not sufficient condition for the over-all conservation of particle number, momentum and energy. Therefore a specific approximation needs to fulfill further conditions to obey the conservation laws. It has been shown by L. Kadanoff and G. Baym [58, 59] that any conserving approximation can be formulated in terms of a generating functional $\Phi$ such that the one-particle selfenergy yields

$$\Sigma(1,1') = \delta\Phi/\delta G(1,1') \tag{4.21}$$

where $1, 1'$ are the space-time coordinates of the Green's function G and $\delta$ denotes the functional derivative. As an example for the conserving character of such an approximation we proof the over-all particle number conservation due to a selfenergy defined in that way (we follow directly [58, 59]). Under variation of $G$ the generating functional transforms by

$$\delta\Phi = \int d1d1' \frac{\delta\Phi}{\delta G(1,1')} \delta G(1',1) \tag{4.22}$$

The first order change of $\Phi$ due to the gauge transformation

$$G(1,1') \to e^{i\lambda(1)} G(1,1') e^{-i\lambda(1')} \tag{4.23}$$

yields

$$\begin{aligned} \delta\Phi &= \int d1d1' \Sigma(1,1') i \left[\lambda(1') - \lambda(1)\right] G(1',1) \\ &= -i \int d1d1' \left[\Sigma(1,1')G(1',1) - G(1,1')\Sigma(1',1)\right] \lambda(1) \end{aligned} \tag{4.24}$$

Since the generating functional $\Phi$ is a functional of $G$ and the number of incoming and outgoing lines at each vertex are equal, the variation $\delta\Phi$ under a gauge transformation Eq. (4.23) must vanish. Therefore it follows

$$\int d1' \left[\Sigma(1,1')G(1',1) - G(1,1')\Sigma(1',1)\right] = 0 \tag{4.25}$$

Finally, the equations of motion of the Green's function are subtracted

$$\int d\bar{1} \left[G_0^{-1}(1,\bar{1}) - \Sigma(1,\bar{1})\right] G(\bar{1},1') = \delta(1-1') \tag{4.26}$$

$$\int d\bar{1} G(1,\bar{1}) \left[G_0^{-1}(\bar{1},1') - \Sigma(\bar{1},1')\right] = \delta(1-1') \tag{4.27}$$

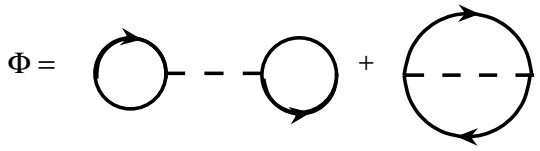


***Figure 4.2:*** Generating functional Φ of the Hartree Fock approximation. The selfenergy is obtained by cutting one Green's function, represented by a full line. The dashed line stands for the interaction.

with $G_0^{-1}(1,1') = (i\partial/\partial t_1 + \nabla_1^2/2m)\delta(1-1') = (-i\partial/\partial t_{1'} + \nabla_{1'}^2/2m)\delta(1-1')$. Substituting $1' = 1^+$ one therefore obtains the continuity equation for the particle number $n(1)$ and the particle current $\vec{j}(1)$

$$\partial\langle n(1)\rangle/\partial t_1 + \nabla_1\langle\vec{j}(1)\rangle = 0 \tag{4.28}$$

Similar relations can be derived for the other conserved quantities under the condition that the selfenergy is defined via a generating functional Φ, being a functional of the fully renormalized Green's functions. An example for such a conserving approximation is given by the Hartree Fock approximation (Fig. 4.2) or the non crossing approximation (Fig. 4.3) discussed in the next section.

### 4.2.2 The non crossing approximation (NCA)

Following the general discussion of the previous section we will now give an example of a conserving approximation particularly applied to the single impurity Anderson model Eq. (4.9) in the limit of infinite local Coulomb repulsion and in terms of the pseudo particle operators. Hence, the generating functional Φ in this case would consist of all vacuum skeleton diagrams built of fully renormalized Green's functions $G_{f,b,c}$. This leads to a set of equations representing the selfenergy of each particle species

$$\Sigma_{b,f,c} = \delta\Phi/\delta G_{f,b,c} \tag{4.29}$$

As before, the choice of a generating functional determines the corresponding approximation. First, the existence of a small parameter (in the present case $V/D$, where $D$ is the conduction electron band width) implies a renormalized low order perturbation theory approach. However, one still has to account for the leading physical processes. In the present case the generating functional Fig. 4.3 is chosen in lowest order, renormalized perturbation theory in $V/D$. The physical interpretation of this approximation can be discussed regarding the conduction electron - pseudo fermion c-f vertex function. In terms of the generating functional

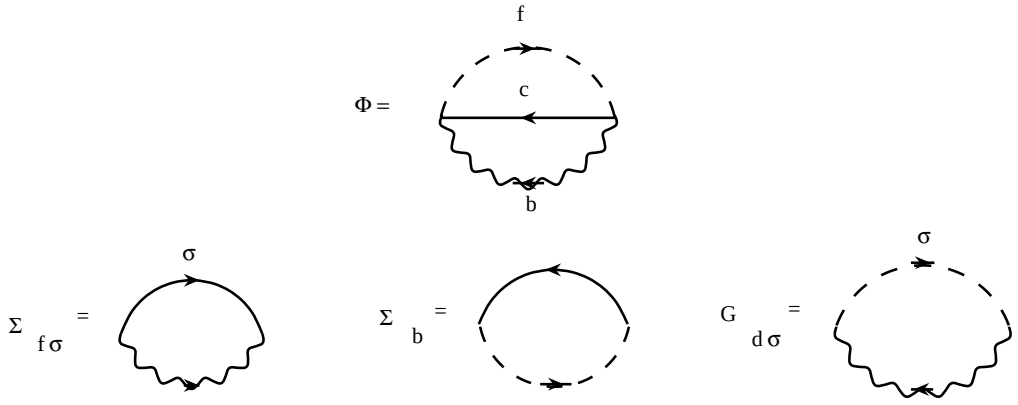


***Figure 4.3:*** Generating functional $\Phi$ of the non crossing approximation for the pseudo particle representation of the Anderson impurity model Eq. (4.9). Full lines represent conduction electron, dashes lines pseudo fermion $f$ and wavy lines slave boson $b$ propagators.

the irreducible c-f vertex function can be derived taking the second functional derivative of $\Phi$ with respect to the Green's functions $G_f$ and $G_c$. Hence, for the NCA the irreducible c-f vertex function is given by $V^2 G_b$. Thus, the advantage of the NCA basically consists of its relative simplicity compared to other techniques. Evaluating the selfenergy equations, defined by Eq. (4.29) and diagrammatically illustrated in Fig. 4.3, the selfconsistent NCA equations for the pseudo particle selfenergies $\Sigma_{f,b}$ and the impurity Green's function $G_d$ read

$$\Sigma_{f\sigma}(\omega) = \Gamma \int \frac{d\epsilon}{\pi} \left[1 - f(\epsilon)\right] A^0_{c\sigma}(\epsilon) G_b(\omega - \epsilon) \tag{4.30}$$

$$\Sigma_b(\omega) = \Gamma \sum_\sigma \int \frac{d\epsilon}{\pi} f(\epsilon) A^0_{c\sigma}(\epsilon) G_{f\sigma}(\omega + \epsilon) \tag{4.31}$$

$$G_{d\sigma}(\omega) = \int d\epsilon \; e^{-\beta\epsilon} \left[G_{f\sigma}(\omega + \epsilon) A_b(\epsilon) - A_{f\sigma}(\epsilon) G_b(\epsilon - \omega)\right] \tag{4.32}$$

where $\omega$ is regarded as $\omega \pm i0$ for the retarded/advanced functions, $\Gamma = \pi V^2$, $A^0_{c\sigma} = \pm(1/\pi)\mathrm{Im}G^0_{c\sigma}$ is the bare conduction electron density of states per spin and $f(\epsilon) = 1/(\exp(\beta\epsilon) + 1)$ is the Fermi distribution function. The set of equations can be evaluated numerically [19, 60] and analytically in the limit of low energies at $T = 0$ [61]. In the upcoming section we will present an efficient way to treat the Eqs. (4.30)-(4.32) and to compute the impurity Green's function.

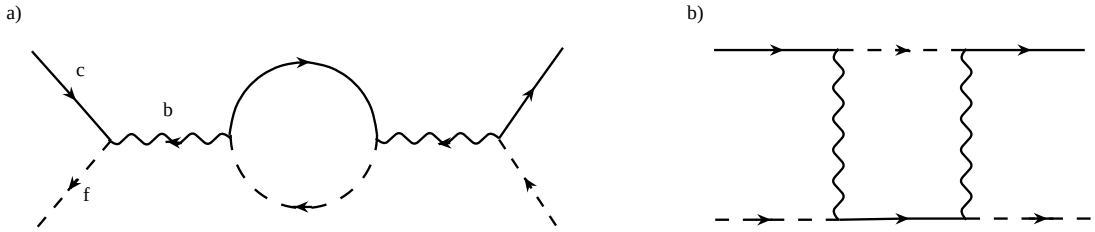


***Figure 4.4:*** a) Constituent of the Bethe-Salpeter equation for the c-f vertex function as it appears in the NCA. The full c-f vertex with NCA is given by $V^2 G_b$, where $G_b$ is the full slave boson propagator b) Spin flip scattering contribution to the c-f vertex neglected within NCA

For $U \to \infty$ the NCA reproduces correctly the Kondo energy scale. Additionally the formation of the Kondo resonance for $T > T_K$ is qualitatively well described. Therefore the NCA provides a convenient tool to evaluate the Anderson impurity model, in particular above the Kondo temperature. However, in the low energy regime $T \ll T_K$ the NCA fails [62], leading to spurious infrared singularities in physical quantities in contradiction to the expected Fermi liquid behavior. Furthermore, the NCA fails in the presence of an external magnetic field, producing a spurious resonance in the impurity Green's function $G_d$ at $\omega = 0$ even in the temperature regime $T > T_K$ above the Kondo temperature. The influence of these failures of the NCA on the subject of this thesis is discussed in the corresponding chapter.

To understand the origin of the NCA shortcomings one needs to regard the c-f vertex function as defined above. In Fig. 4.4 a) one constituent of the Bethe-Salpeter equation for the c-f vertex function in terms of the NCA is presented. Since the slave boson propagator $G_b$ cannot carry any spin the NCA obviously does not account for coherent spin flip scattering processes. Similar considerations for the c-b vertex show, that also charge transfer processes are neglected within the NCA. However, these two processes are known to be responsible for the coherent collective behavior below the Kondo temperature. It could be shown by means of perturbative renormalization group [63] that indeed the missing terms Fig. 4.4 b) are responsible for the spurious singularities mentioned above. For completeness it should be mentioned that the shortcomings of the NCA can be cured by including the vertex contributions like they are given in Fig. 4.4 b). Thus a new generating functional can be derived, taking into account in particular the coherent spin flip scattering processes. However, the resulting conserving T-matrix approximation (CTMA,[64, 65]) gives an essentially correct description of the Anderson impurity model over the whole temperature range, but is numerically very demanding.

### 4.2.3 Evaluation of the NCA equations

Here, we present an efficient way to evaluate the NCA Eqs. (4.30)-(4.32) even in the low temperature regime $T \ll T_K$. It can be shown [66] that all quantities involving pseudo particle operators at $T = 0$ vanish for energies $\omega < 0$. In particular the $f, b$ spectral function behaves like

$$A_{f,b}(\omega) \sim |\omega - E_0|^{-\alpha_{f,b}} \theta(\omega - E_0) \tag{4.33}$$

at a threshold $E_0$ and with the critical exponents $\alpha_f, \alpha_b$, which can be derived for instance within the Numerical Renormalization Group (NRG) approach [12]. In order to solve the NCA equations numerically by iteration, the threshold behavior needs to be sufficiently resolved. We therefore apply a method proposed in [66]. The numerical evaluation of physical expectation values like the impurity Green's function $G_{d\sigma}(\omega, \lambda \to \infty)$ Eq. (4.32) is non-trivial, because of two reasons. First, at $T = 0$ the auxiliary functions $A_{f,b}(\omega)$ according to Eq. (4.33) diverge at a threshold $E_0$ which is initially not known. Furthermore, the Boltzmann factor $e^{-\beta\epsilon}$ as it appears in Eq. (4.32) diverges exponentially for $\omega < 0$. The first step to overcome the threshold problem consists of exploiting the gauge freedom of the pseudo particle Green's functions. The pseudo particle operators are gauged time dependently according to $f_\sigma \to e^{i\lambda_0 t} f_\sigma$, $b \to e^{i\lambda_0 t} b$. As mentioned before this gauge freedom is an intrinsic property of the Anderson impurity model. For the auxiliary particle spectral functions this procedure amounts in a shift of the energy spectrum $\omega \to \omega + \lambda_0$, such that the physical spectral functions are defined as

$$A_{f,b}(\omega) = \lim_{\lambda \to \infty} \mathcal{A}_{f,b}(\omega + \lambda_0 + \lambda) \tag{4.34}$$

where $\mathcal{A}_{f,b}(\nu) = \pm(1/\pi) \cdot \mathrm{Im}\mathcal{G}(\nu)$ for the retarded/advanced function according to the definition Eq. (4.18) of the auxiliary particle Green's function. Consequently, the chemical potential $\lambda_0$ is determined within each iteration such that the following relation holds:

$$\int d\omega e^{-\beta\omega} \left[ \sum_\sigma A_{f\sigma}(\omega) + A_b(\omega) \right] = 1 \tag{4.35}$$

Note, that this procedure must not be mixed up with the exact projection procedure due to the limit $\lambda \to \infty$. The introduction of $\lambda_0$ is for purely numerical reasons. For $T = 0$ the Boltzmann factor $e^{-\beta\omega}$ in Eq. (4.35) can only be compensated if $\lambda_0$ is determined such that the threshold of the spectral functions is at a fixed energy $\omega \approx 0$. Thus, the threshold $E_0$ mentioned above is resolved with each iteration. Numerically, this procedures amounts in the possibility of choosing a fixed energy mesh with a accumulation of grid points around $\omega = 0$ for the integration of the NCA equations. This is increasing as well the speed as the accuracy of the computation. Furthermore, the divergence of the Boltzmann

factor implies that the solution for the pseudo particle spectral functions at a finite temperature vanishes exponentially $A_{f,b}(\omega) \sim e^{\beta\omega}$ for negative frequencies, confirming the threshold behavior. According to this it is convenient to formulate the NCA equations (4.30)-(4.32) in terms of new defined functions $\tilde{A}_{f,b}(\omega)$ and $\mathrm{Im}\tilde{\Sigma}_{f,b}(\omega)$, such that

$$A_{f,b}(\omega) = f(-\omega)\, \tilde{A}_{f,b}(\omega) \tag{4.36}$$
$$\mathrm{Im}\Sigma_{f,b}(\omega) = f(-\omega)\, \mathrm{Im}\tilde{\Sigma}_{f,b}(\omega) \tag{4.37}$$

where the threshold behavior is completely absorbed in the prefactor $f(-\omega)$. In terms of the so defined functions the NCA equations can be formulated for the advanced functions ($\omega \leftrightarrow \omega - i0^+$)

$$\mathrm{Im}\tilde{\Sigma}_{f\sigma}(\omega) = \Gamma \int d\epsilon \frac{f(-\epsilon)(1-f(\omega-\epsilon))}{f(-\omega)} A^0_{c\sigma}(\epsilon)\tilde{A}_b(\omega-\epsilon) \tag{4.38}$$
$$\mathrm{Im}\tilde{\Sigma}_{b}(\omega) = \Gamma \int \sum_\sigma d\epsilon \frac{f(\epsilon)(1-f(\omega+\epsilon))}{f(-\omega)} A^0_{c\sigma}(\epsilon)\tilde{A}_{f\sigma}(\omega+\epsilon) \tag{4.39}$$
$$\mathrm{Im}G_{d\sigma}(\omega) = \int d\epsilon \left[f(\epsilon+\omega)f(-\epsilon) + f(-\epsilon-\omega)f(\epsilon)\right] \tilde{A}_{f\sigma}(\omega+\epsilon)\tilde{A}_b(\epsilon) \tag{4.40}$$

with Eq. (4.35) determining the $\lambda_0$ being transformed to

$$\int d\omega f(\omega) \left[\sum_\sigma \tilde{A}_{f\sigma}(\omega) + \tilde{A}_b(\omega)\right] = 1 \tag{4.41}$$

This set of equations is solved iteratively using the explicit form of the auxiliary functions, including the chemical potential $\lambda_0$

$$\tilde{A}_{f\sigma}(\omega) = \frac{1}{\pi} \frac{\mathrm{Im}\tilde{\Sigma}_{f\sigma}(\omega)}{(\omega+\lambda_0-i0-E_d-\mathrm{Re}\Sigma_{f\sigma}(\omega))^2 + \mathrm{Im}\Sigma_{f\sigma}(\omega)^2} \tag{4.42}$$
$$\tilde{A}_{b}(\omega) = \frac{1}{\pi} \frac{\mathrm{Im}\tilde{\Sigma}_{b}(\omega)}{(\omega+\lambda_0-i0-\mathrm{Re}\Sigma_{b}(\omega))^2 + \mathrm{Im}\Sigma_{b}(\omega)^2} \tag{4.43}$$

The method described in this section is capable to solve the NCA Eqs. (4.38)-(4.40) down to temperatures of $T \simeq 10^{-4} T_K$. In Fig. 4.5 we present the results for the impurity Green's function $G_{d\sigma}$ at various temperatures. One can clearly see how the Kondo resonance in the imaginary part of the impurity Green's function $A_{d\sigma}$ is evolving as the temperature approaches the Kondo temperature. The Anderson impurity problem treated in this thesis is slightly modified compared to the model presented in this section. However, the technique applied here can easily be modified and will be presented in the next chapter.

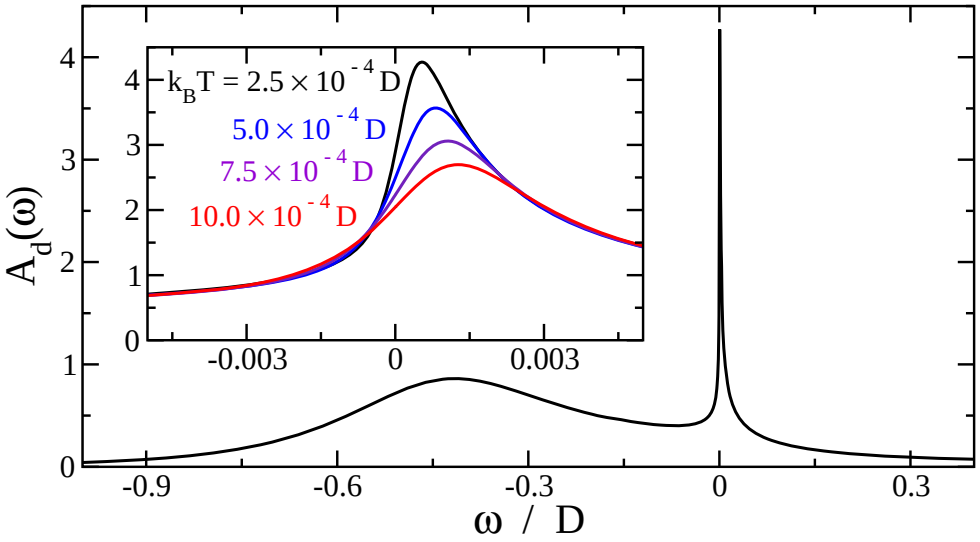


***Figure 4.5:*** Imaginary part $A_{d\sigma}(\omega) = (1/\pi)G_{d\sigma}(\omega)$ of the impurity Green's function, plotted for $k_BT = \{2.5, 5.0, 7.5, 10.0\} \cdot 10^{-4}D$. The parameters are chosen such that the Kondo temperature is given by $T_K \approx 7 \cdot 10^{-4}D$ in units of the half conduction band width.

## 4.3 A new slave boson formulation of the NCA

Auxiliary particle methods provide a powerful tool in condensed matter theory. As we demonstrated in the previous sections they could be used to simplify the Anderson impurity model significantly in order to make it capable for standard diagrammatic perturbation theory. Of course, the choice of a set of auxiliary particles to formulate the present Hamiltonian is not unique. In this section we present an alternative formulation of the NCA applied to the single impurity Anderson model. Here, the problem will be transformed utilizing Kotliar-Ruckenstein slave bosons [67] which were initially applied to the Hubbard model. This formulation has been suggested by Prof. A. Georges and the work has been done in his group at the Ecole Polytechnique/Palaiseau.

### 4.3.1 The Anderson model in terms of Kotliar-Ruckenstein slave bosons

Motivated by earlier works concerning a pseudo particle representation for the Hubbard model [67] we formulate the single impurity Anderson model Eqs. (4.1)-(4.4) in terms of so called Kotliar-Ruckenstein slave bosons.Therefore we assume four auxiliary boson fields to define the impurity states $e \leftrightarrow |0\rangle, p_\sigma \leftrightarrow |\sigma\rangle, a \leftrightarrow |2\rangle$ together with two pseudo fermion operator $f_\sigma$.The physical impurity operator $d_\sigma$

is then defined as

$$d_\sigma = (e^\dagger p_\sigma + p_{-\sigma}^\dagger a) f_\sigma \tag{4.44}$$

Similar to the method of the previous sections the Hilbert space is again vastly enlarged due to the introduction of the pseudo particles. To perform the projection onto the physical subspace the following two constraints have to be fulfilled:

$$e^\dagger e + a^\dagger a + \sum_\sigma p_\sigma^\dagger p_\sigma = 1 \tag{4.45}$$

$$f_\sigma^\dagger f_\sigma = p_\sigma^\dagger p_\sigma + a^\dagger a \tag{4.46}$$

Physically these conditions can be understood to guarantee the impurity to be in a unique bosonic state Eq.(4.45). Simultaneously the overall fermion number can assume all possible values, while it is strictly correlated to the corresponding bosonic occupation number Eq.(4.46). In that sense the $f$-operators in this approach must be understood as total pseudo fermion operators on the impurity site and not only counting the single occupied states. Utilizing these constraints the Anderson impurity Hamiltonian can be transformed the following way:

$$\begin{aligned} H &= \sum_{k\sigma} \epsilon_{k\sigma} c_{k\sigma}^\dagger c_{k\sigma} + E_d \sum_\sigma f_\sigma^\dagger f_\sigma + U a^\dagger a + V \sum_{k\sigma} c_{k\sigma}^\dagger f_\sigma \left( e^\dagger p_\sigma + p_{-\sigma}^\dagger a \right) + h.c. \\ &+ \lambda_0 \left[ \sum_\sigma p_\sigma^\dagger p_\sigma + e^\dagger e + a^\dagger a - 1 \right] \\ &+ \sum_\sigma \lambda_1^\sigma \left[ (f_\sigma^\dagger f_\sigma - p_\sigma^\dagger p_\sigma) - a^\dagger a \right] \end{aligned} \tag{4.47}$$

where the constraints are implemented via three Lagrange multipliers $\lambda_0, \lambda_1^\sigma$, acting similar to an additional chemical potential for the corresponding fields. Thus the form of the full auxiliary spectral functions yields

$$A_{f\sigma}(\omega) = -\frac{1}{\pi} \frac{\mathrm{Im}\Sigma_{\mathrm{f}\sigma}(\omega)}{(\omega - \lambda_1^\sigma - E_d - \mathrm{Re}\Sigma_{\mathrm{f}\sigma}(\omega))^2 + \mathrm{Im}^2\Sigma_{\mathrm{f}\sigma}(\omega)} \tag{4.48}$$

$$A_{p\sigma}(\omega) = -\frac{1}{\pi} \frac{\mathrm{Im}\Sigma_{\mathrm{p}\sigma}(\omega)}{(\omega - \lambda_0 + \lambda_1^\sigma - \mathrm{Re}\Sigma_{\mathrm{p}\sigma}(\omega))^2 + \mathrm{Im}^2\Sigma_{\mathrm{p}\sigma}(\omega)} \tag{4.49}$$

$$A_e(\omega) = -\frac{1}{\pi} \frac{\mathrm{Im}\Sigma_{\mathrm{e}}(\omega)}{(\omega - \lambda_0 - \mathrm{Re}\Sigma_{\mathrm{e}}(\omega))^2 + \mathrm{Im}^2\Sigma_{\mathrm{e}}(\omega)} \tag{4.50}$$

$$A_a(\omega) = -\frac{1}{\pi} \frac{\mathrm{Im}\Sigma_{\mathrm{a}}(\omega)}{(\omega - \lambda_0 + \lambda_1^\uparrow + \lambda_1^\downarrow - U - \mathrm{Re}\Sigma_{\mathrm{a}}(\omega))^2 + \mathrm{Im}^2\Sigma_{\mathrm{a}}(\omega)} \tag{4.51}$$

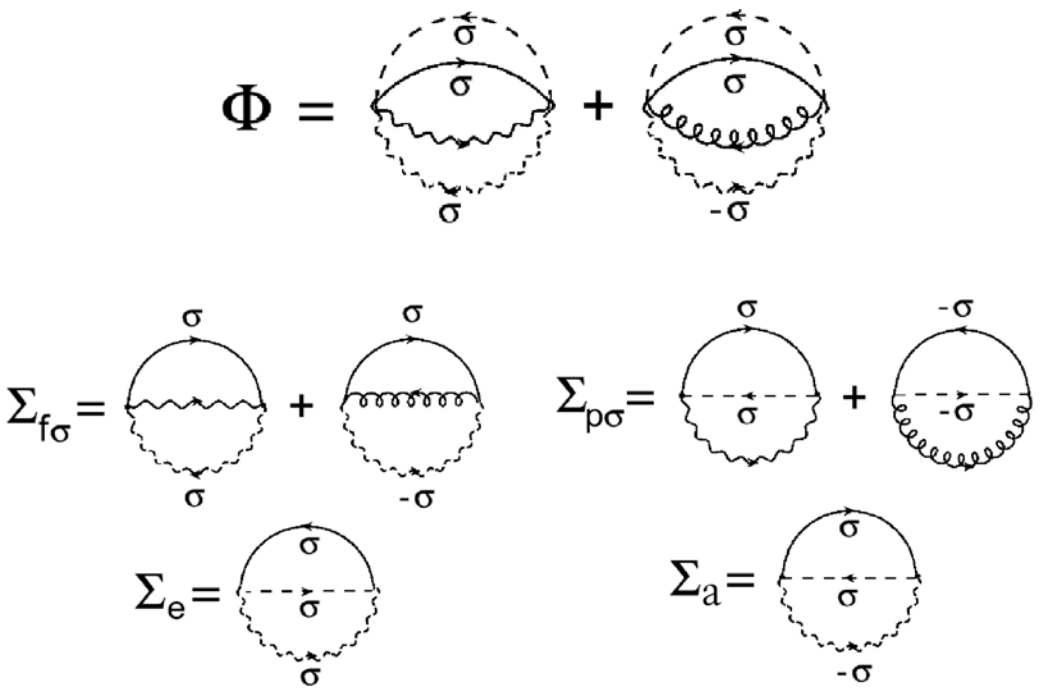


***Figure 4.6:*** The generating Luttinger-Ward functional. Solid lines represent conduction electrons $c$, dashed lines pseudo fermions $f$, wavy dashed lines single occupation bosons $p$, wavy solid lines empty impurity bosons $e$, curly lines double occupation bosons $a$. The lower diagrams show the auxiliary particle selfenergies.

### 4.3.2 Formulation of the NCA equations

Analogous the the former auxiliary particle formulation we develop the NCA in terms of a generating functional $\Phi$ for the Kotliar-Ruckenstein fields, such that the selfenergies are derived according to

$$\Sigma_{f,p,e,a} = \delta\Phi/\delta G_{f,p,e,a} \tag{4.52}$$

Hence, a non crossing approximation for the Hamiltonian Eq. (4.47) leads to the generating functional and selfenergies, which are presented in Fig. 4.6. The most striking feature of the NCA diagrams in terms of Kotliar-Ruckenstein slave particles is due to the fact that each hybridization term in the Hamiltonian Eq. (4.47) consists of four different operators. As a consequence the lowest ($2^{nd}$) order diagram of $\Phi$ consists of four pseudo particle propagators. Therefore the pseudo particle selfenergies contain three propagators in each diagram, which is in particular inconvenient since it results in a two dimensional integration for the selfenergies. As in the previous section we derive the imaginary part of the

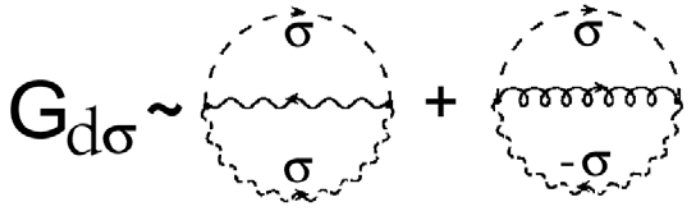


***Figure 4.7:*** The physical impurity Green's function is derived via cutting the (bare) conduction electron line in the Luttinger-Ward functional Fig.4.6. The proportionality factor is discussed below.

advanced selfenergies Eqs. (4.53)-(4.56), while the corresponding real part can be obtained by a Kramers-Kronig relation. Finally we therefore obtain

$$\begin{aligned}
\mathrm{Im}\Sigma_{\mathrm{f}\sigma}(\omega) &= \Gamma \int d\epsilon d\epsilon' A_{c\sigma}(\epsilon) A_e(\epsilon') A_{p\sigma}(\epsilon + \epsilon' - \omega) \\
&\quad \cdot [(f(\epsilon) + b(\epsilon + \epsilon' - \omega)) \cdot (b(\epsilon') + f(\epsilon' - \omega))] \\
&- \Gamma \int d\epsilon d\epsilon' A_{c\sigma}(\epsilon) A_a(\epsilon') A_{p-\sigma}(\epsilon' - \epsilon + \omega) \\
&\cdot \quad [(f(\epsilon) + b(\epsilon - \epsilon' - \omega)) \cdot (b(\epsilon') + f(\epsilon' + \omega))] \qquad (4.53) \\
\mathrm{Im}\Sigma_{\mathrm{p}\sigma}(\omega) &= \Gamma \int d\epsilon d\epsilon' A_{c\sigma}(\epsilon) A_{f\sigma}(\epsilon') A_e(\omega + \epsilon' - \epsilon) \\
&\cdot \quad [(f(\epsilon) + b(\epsilon - \epsilon' - \omega)) \cdot (f(\epsilon' + \omega) - f(\epsilon'))] \\
&+ \Gamma \int d\epsilon d\epsilon' A_{c-\sigma}(\epsilon) A_{f-\sigma}(\epsilon') A_a(\omega - \epsilon' + \epsilon) \\
&\cdot \quad [(f(\epsilon) + b(\epsilon - \epsilon' + \omega)) \cdot (f(\epsilon' - \omega) - f(\epsilon'))] \qquad (4.54) \\
\mathrm{Im}\Sigma_{\mathrm{a}}(\omega) &= \Gamma \sum_\sigma \int d\epsilon d\epsilon' A_{c\sigma}(\epsilon) A_{f\sigma}(\epsilon') A_{p-\sigma}(\omega + \epsilon' - \epsilon) \\
&\cdot \quad [(f(\epsilon) + b(\epsilon - \epsilon' - \omega)) \cdot (f(\epsilon' + \omega) - f(\epsilon'))] \qquad (4.55) \\
\mathrm{Im}\Sigma_{\mathrm{e}}(\omega) &= \Gamma \sum_\sigma \int d\epsilon d\epsilon' A_{c\sigma}(\epsilon) A_{f\sigma}(\epsilon') A_{p\sigma}(\omega - \epsilon' + \epsilon) \\
&\cdot \quad [(f(\epsilon) + b(\epsilon - \epsilon' + \omega)) \cdot (f(\epsilon' - \omega) - f(\epsilon'))] \qquad (4.56)
\end{aligned}$$

where as usual $f(\epsilon)$ denotes the Fermi distribution function and $b(\epsilon) = 1/(e^{\beta\epsilon} - 1)$ is the Bose distribution function.

From the auxiliary particle spectral functions one can finally derive the physical impurity Green's function. Diagrammatically the result is obtained by cutting

the (bare) conduction electron in the Luttinger-Ward functional Fig.4.6, leading to the diagram in Fig.4.7.

$$\begin{aligned} A_{d\sigma}(\omega) &= \frac{\alpha_N}{V^2}\int d\epsilon d\epsilon' A_{f\sigma}(\epsilon)A_a(\epsilon')A_{p-\sigma}(\epsilon+\epsilon'-\omega) \\ &\quad \cdot[(f(\epsilon)+b(\epsilon+\epsilon'-\omega))\cdot(b(\epsilon')+f(\epsilon'-\omega))] \\ &- \int d\epsilon d\epsilon' A_{f\sigma}(\epsilon)A_e(\epsilon')A_{p\sigma}(\epsilon'-\epsilon+\omega) \\ &\quad \cdot[(f(\epsilon)+b(\epsilon-\epsilon'-\omega))\cdot(b(\epsilon')+f(\epsilon'+\omega))] \end{aligned} \tag{4.57}$$

The set of Eqs. (4.53)-(4.56) can be solved iteratively. Within each iteration the Lagrange multipliers $\lambda_0, \lambda_1^\sigma$ are determined such that the particle number constraints Eqs. (4.45),(4.46) are obeyed on average. In Fig. 4.8 the results for the pseudo particle spectral functions are presented for a particular set of parameters. The change of sign at $\omega = 0$ is a characteristic feature of the bosonic spectral functions in order to provide a positive particle number. It has been argued previously [68], that spurious Bose condensation is inhibited by the negative bosonic spectral weight for $\omega < 0$. In the symmetric case where $|2E_d| = U$ the double occupancy spectral function $A_a$ and the empty impurity function $A_e$ are supposed to be equal, as it is confirmed in Fig. 4.8 b). According to Eq. (4.57) the physical impurity spectral function is given by a convolution of the pseudo particle spectral functions. In contrast to the previous auxiliary particle approaches in the present case it is necessary to normalize the impurity spectral function $A_{d\sigma}$ via a normalization factor. This can be understood the following way. Transforming the impurity occupation number yields: $d_\sigma^\dagger d_\sigma = f_\sigma^\dagger f_\sigma \cdot \left(p_\sigma^\dagger p_\sigma + a^\dagger a + p_\sigma^\dagger p_\sigma e^\dagger e + p_{-\sigma}^\dagger p_{-\sigma} a^\dagger a\right)$. The exact implementation of the constraints Eqs.(4.45),(4.46) reproduces the expected result $d_\sigma^\dagger d_\sigma = f_\sigma^\dagger f_\sigma$. In the present case the result differs in general from that due to the averaged realization of the constraints. Therefore a normalization factor $\alpha_N$ needs to be introduced in front of the conventual impurity diagram such that $\int d\omega A_{d\sigma} = 1$ holds. It turns out that the normalization factor indeed yields $\alpha_N \approx \langle p_\sigma^\dagger p_\sigma + a^\dagger a + p_\sigma^\dagger p_\sigma e^\dagger e + p_{-\sigma}^\dagger p_{-\sigma} d^\dagger d\rangle$, hence lifting the deviation of the physical electron occupation number due to the averaged projection procedure. In Fig. 4.9 we present an example of the physical impurity spectral function in comparison to the corresponding function obtained utilizing the pseudo particle representation introduced in the previous sections. Concerning the Kondo resonance the agreement of both method turns out to be reasonably good, while the one particle peaks at $\omega \approx \pm 0.4D$ differ significantly due to the different projection methods. The technical applicability of the NCA formulation developed in this section is certainly hindered by the high computational effort that is needed to evaluate the NCA Eqs. (4.53)-(4.56). However, it might be useful to investigate the principle properties of the Kotliar-Ruckenstein representation and compare the results to the existing mean field approximation.

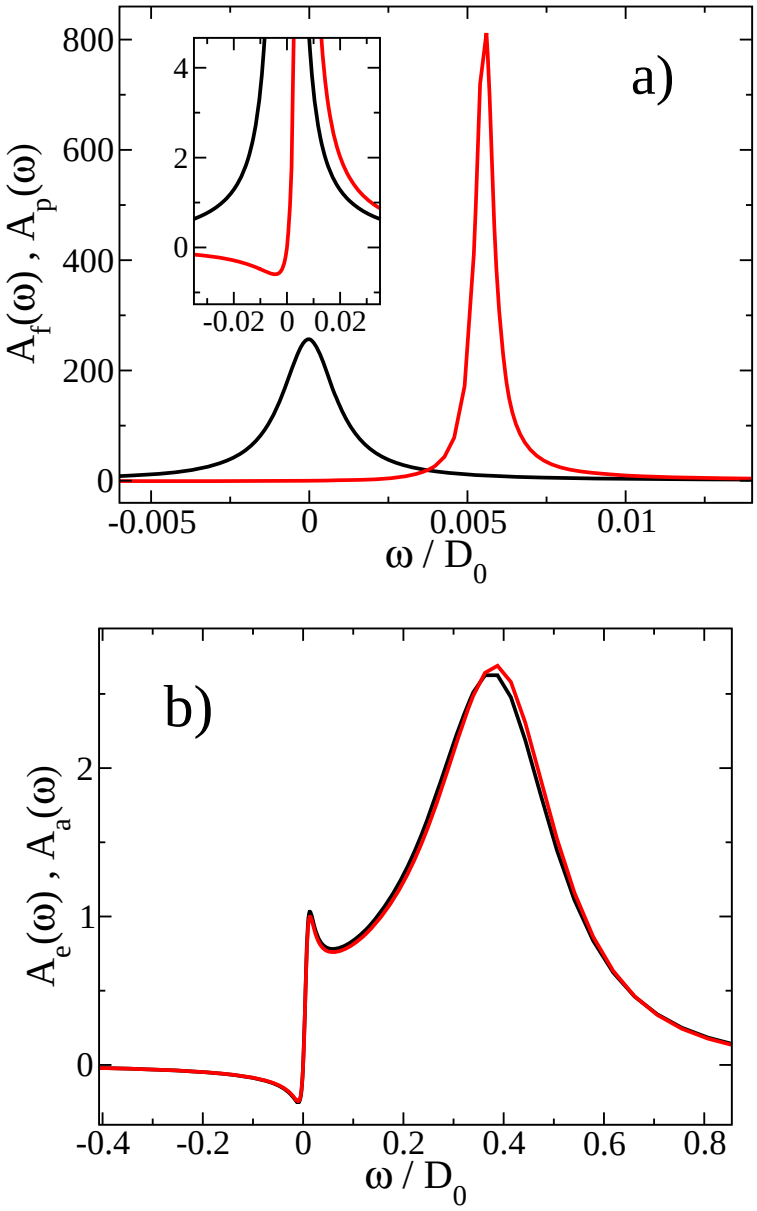


***Figure 4.8:*** The auxiliary particles spectral functions. a) black line: f-fermion, red line: p-boson. b) black line: e-boson, red line: d-boson. The e- and d-boson are equal when $|2E_d| = U$. The system parameters are: $E_d = -0.35D_0$, $U = 0.7D_0$, $\Gamma = 0.1D_0$, temperature $T = 0.005D_0$

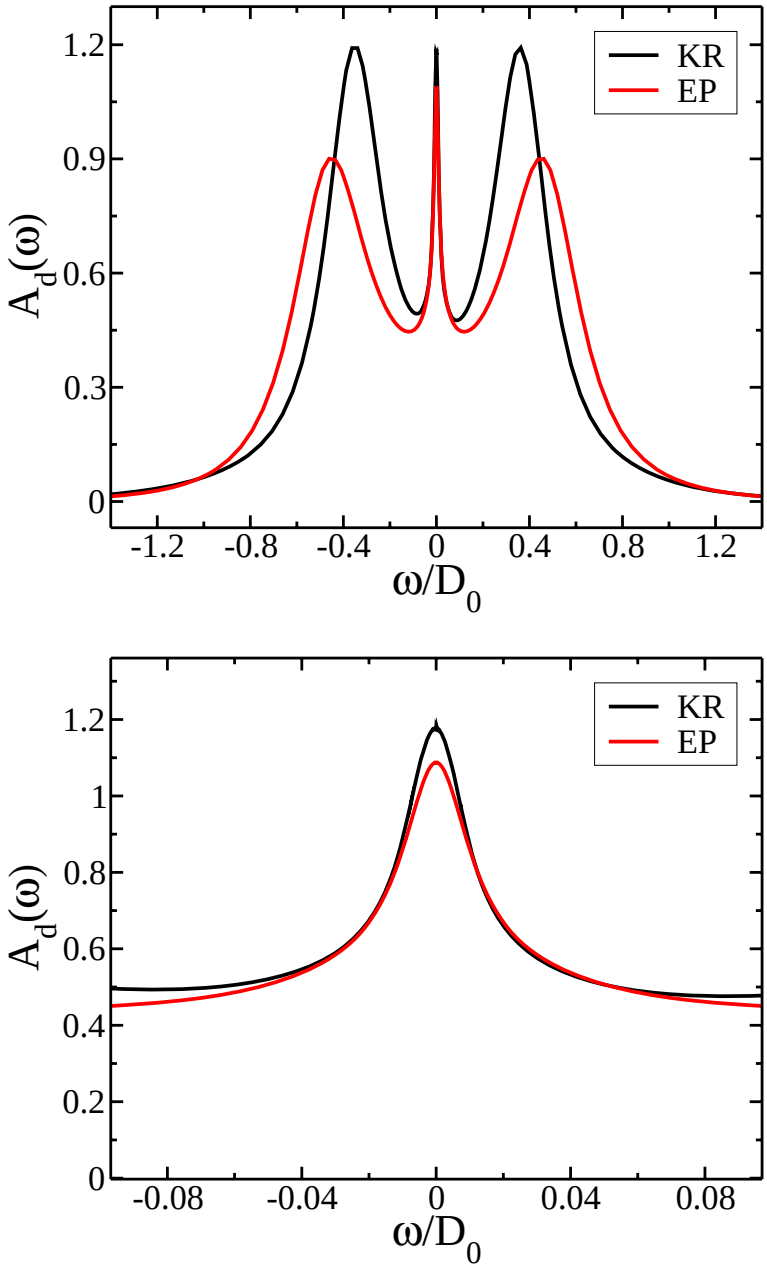


***Figure 4.9:*** The physical impurity spectral function, obtained by the Kotliar-Ruckenstein NCA-method (KR), and the auxiliary particle NCA with exact projection (EP), described in the previous sections. The system parameters are: $E_d = -0.35D_0$, $U = 0.7D_0$, $\Gamma = 0.1D_0$ at a temperature $T = 0.005D_0$

# 5 An Impurity Model for EuO

After the general remarks on quantum impurity models in the previous chapter, now we will come back to the real physical system provided by oxygen-depleted europium monoxide $EuO_{1-x}$ or the Gd-doped compound $Gd_xEu_{1-x}O$ respectively. As we stated in the introduction in particular the transport properties are tremendously influenced by the existence of impurities, embedded in the off-stoichiometric compound. In the following we define the circumstances under which a model consisting of dilute Anderson impurities coupled to an electron conduction band can exhibit the experimentally observed behavior. Furthermore, the magnetic properties coinciding with those features have to be taken into account. Additionally we want to investigate the principle theoretical properties of the model. Especially the interplay between coherent spin flip scattering processes, leading to the well known Kondo effect and the magnetic phase transition, being of crucial importance for EuO, is of great theoretical interest.

Due to the complexity of the model it becomes necessary to utilize various approximations. We will comment on the technical details of the calculation as well as on the validity and the limits of the chosen approximations. Therefore we refer to the methods described in the previous chapters and demonstrate how they need to be modified in the present case. Our main remark will be on magnetic as well as on the transport properties. Thus we will derive the necessary expression for the resistivity and the conductance of the electronic system.

## 5.1 A Hamiltonian representing EuO

As mentioned before, we first want to refer strongly to the specific system EuO, before we come to the general properties of the presented model. Therefore it is useful to summarize the main ingredients which are experimentally known to determine the properties of this compound and to include them systematically in the theoretical approach. The main experimental observations about EuO are:

a) Stoichiometric EuO is a ferromagnetic semiconductor with a Curie temperature of $T_C \approx 69K$

b) Inserting impurities into the system leads to a simultaneous semiconductor-metal transition for $T < T_C$

The first feature a) is basically reflected by two properties. First, the electron conduction band of EuO, consisting of the Eu $5d-6p$ orbitals is initially empty. The free electron Hamiltonian is given by

$$H_c = \sum_{k\sigma} (\epsilon_k - \mu) c^\dagger_{k\sigma} c_{k\sigma} \tag{5.1}$$

with a chemical potential $\mu$. The initially empty conduction band is represented by a semi-elliptical band with half width $D_0$

$$N^0(\epsilon) = \frac{2}{\pi} \sqrt{1 - \left( \frac{\epsilon - \Delta_0}{D_0} \right)^2} \tag{5.2}$$

where $\Delta_0 \geq D_0 + \mu$ guarantees that the lower band edge is above the chemical potential. Later, the electron conduction band will be further modified due to the selfenergy in the interacting system, in particular in the off-stoichiometric or Gd-doped regime. As mentioned in the introduction the ferromagnetism of stoichiometric EuO can reasonably be described in terms of a Heisenberg model representing the exchange interaction between the local Eu $4f$ moments arranged on a lattice

$$H_{4f} = -\sum_{i,j} J_{i,j} \vec{S}_i \vec{S}_j \tag{5.3}$$

where $\vec{S}_i$ represents a 4f-spin at site $i$ and $J_{i,j}$ is the exchange integral between two spins at sites $i, j$. Furthermore, we add an exchange interaction with the strength $J_{cf}$ between the local conduction electron spin $\vec{\sigma}_i = (1/2) \sum_{\sigma\sigma'} c^\dagger_{i\sigma} \vec{\tau}_{\sigma\sigma'} c_{i\sigma'}$, with $c_{i\sigma} = \sum_{\mathbf{k}} \exp(i\mathbf{k}\mathbf{x_i})\, c_{\mathbf{k}\sigma}$ and $\vec{\tau}_{\sigma\sigma'}$ the vector of Pauli matrices, at site $i$ and the corresponding Eu $4f$ moment. Thus, one obtains

$$H_{st} = \sum_{k\sigma} (\epsilon_k - \mu) c^\dagger_{k\sigma} c_{k\sigma} - \sum_{i,j} J_{i,j} \vec{S}_i \vec{S}_j - J_{cf} \sum_i \vec{\sigma}_i \vec{S}_i \tag{5.4}$$

It has been shown [28] that this Hamiltonian together with ab initio band structure calculations, taking into account the full electronic band can successfully describe the magnetic phase transition in stoichiometric EuO, leading to a good agreement with the experiment. However, the so defined system is known to remain in the semiconducting phase for all temperatures. This is due to the fact that there are no free charge carriers at zero temperature, even in the interacting system. Let $A^{st}_{c\sigma}(\epsilon, \mu)$ be the interacting conduction electron density of states according to the Hamiltonian given in Eq. (5.4). In the stoichiometric case the chemical potential $\mu$ is determined such that the total number of free electrons in the low temperature limit yields

$$\sum_\sigma \int d\epsilon f(\epsilon) A^{st}_{c\sigma}(\epsilon, \mu) = 0 \tag{5.5}$$

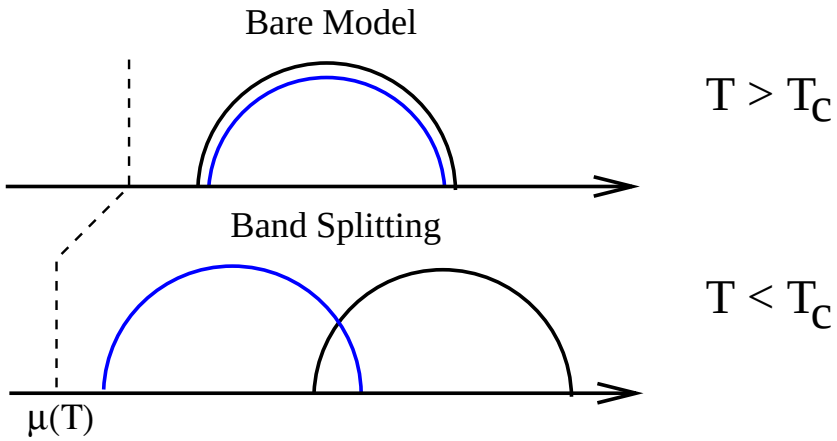


***Figure 5.1:*** Sketch of the band structure shifted spin dependently due the the coupling between the conduction band and the Eu $4f$ moments. The chemical potential $\mu(T)$ is determined for each temperature $T$ such that the total particle number is conserved.

Although the conduction band certainly splits, according to Fig. 5.1, spin dependently below the Curie temperature $T_c$, no overlap with the chemical potential could be generated without violating particle number conservation.Therefore the whole magnetization must be carried by valence band electrons, which are not contributing to the transport in the system.

The situation changes completely when impurities are incorporated into the system. According to b) in that case EuO turns into a metal below the critical temperature $T_c$. In the model, proposed in the following this fact is reflected by two features. First, dilute Anderson impurities ($d_{i\sigma}$) at site $i$ hybridizing with the corresponding conduction electron states are added to the stoichiometric model Eq. (5.4). Hence, we obtain the full Hamiltonian of $Eu0_{1-x}$ or $Gd_xEu_{1-x}0$ with an impurity concentration $n_I = x$ and the hybridization matrix element $V$

$$H = \sum_{k\sigma}(\epsilon_k - \mu)c^\dagger_{k\sigma}c_{k\sigma} + H_{cd} + H_{cf} \tag{5.6}$$

$$H_{cd} = E_d \sum_{i\sigma} d^\dagger_{i\sigma}d_{i\sigma} + V\sum_{i\sigma}(c^\dagger_{i\sigma}d_{i\sigma} + h.c.) + U\sum_i d^\dagger_{i\uparrow}d_{i\uparrow}d^\dagger_{i\downarrow}d_{i\downarrow} \tag{5.7}$$

$$H_{cf} = -\sum_{i,j} J_{i,j}\vec{S}_i\vec{S}_j - J_{cf}\sum_i \vec{\sigma}_i\vec{S}_i \tag{5.8}$$

In Eq. 5.7 we assume an infinite onsite Coulomb repulsion $U$ on the impurity site. Hence, the impurity finally appears to be singly occupied even for $EuO_{1-x}$ where each O-vacancy provides two excess electrons (compared to only one when replacing bivalent Eu by trivalent Gd). Therefore we claim that the particle

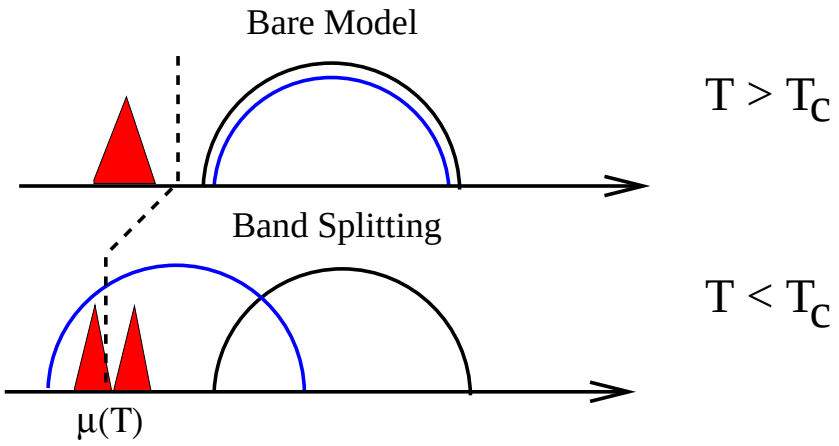


***Figure 5.2:*** Sketch of the spin dependent band structure due the the coupling between the conduction band and the Eu $4f$ moments in the presence of a finite impurity density of states (red). Again, the chemical potential $\mu(T)$ is determined for each temperature $T$ such that the total particle number is conserved. But here, spin split impurity states may be transferred into free charge carriers.

number constraint for $EuO_{1-x}$ as well as for $Gd_xEu_{1-x}O$ transforms into

$$\sum_{\sigma} \int d\epsilon f(\epsilon) \left[ A_{c\sigma}(\epsilon, \mu) + n_I A_{d\sigma}(\epsilon, \mu) \right] = n_I \tag{5.9}$$

where $A_{c\sigma}(\epsilon, \mu)$ is the full conduction electron and $A_{d\sigma}(\epsilon, \mu)$ the full impurity density of states. The meaning of this condition is illustrated in Fig. 5.2, where we sketch the possible exchange process of spectral weight between the impurity states and the electron conduction band. In that sense the low temperature phase of the system can become metallic. At least the limit $n_I \to 0$ is clearly determined by Eq. (5.9), leading analytically to the corresponding expression Eq. (5.5) of the stoichiometric case and hence to the semiconducting compound. Of course, the dynamics of the impurity states at finite impurity concentrations leads to a complicated selforganized interaction between impurity states and conduction band electrons, including the whole variety of possible physical processes.

## 5.2 Approximations and physical interpretation

The model Hamiltonian, as given in Eqs. (5.6)-(5.8) provides many different complications. In particular the electron conduction band is coupled to dilute Anderson impurities, represented by Eq. (5.7). As stated in Chapter 4, a Hamiltonian like this usually leads directly to strongly correlated electron physics. Thus, one

can expect the system to be widely dominated by the occurrence of collective behavior leading for instance to a Kondo resonance in the impurity Green's function. Additionally, the conduction band is coupled to the local Eu $4f$ moment system. Strictly, the Hamiltonian $H_{cf}$ amounts in a Kondo lattice problem. Thus it is in fact very similar to the problem defined by $H_{cd}$, including the possibility of resonant spin flip scattering processes. In the present approach we decided to treat the Kondo lattice problem $H_{cf}$ only in terms of a mean field theory. Within this approximation the local Eu $4f$ moment should only provide the effective magnetic field, shifting the spin states of the conduction band. We hope that this approximation describes the ferromagnetic phase transition at least qualitatively correct.

According to feature b) given in the previous section we treat the influence of the doping impurities more concisely. Since the existence of these impurities strongly affects the transport properties, in particular the impurity density of states at the Fermi energy can be of crucial importance, including eventually occurring Kondo resonances. Therefore we will treat the $H_{cd}$ part of the Hamiltonian Eqs. (5.6)-(5.8) within the non-crossing approximation.

Since we want to derive the electronic conductance and the magnetization of the conduction band, we need to derive the full interacting conduction band density of state $A_{c\sigma}(\omega) = (1/\pi)\mathrm{Im}G_{c\sigma}(\omega)$ for each spin direction. Therefore we first have to obtain the interacting conduction band Green's function

$$G_{c\sigma}(k,\omega) = [\omega + \mu - \epsilon_k - \Sigma_{c\sigma}(\omega)]^{-1} \tag{5.10}$$

The electronic selfenergy $\Sigma_{c\sigma}(\omega)$ consists of two parts. First, there is a contribution from the dilute impurities, as described in Chapter 4, stemming from the local conduction electron t-matrix. This part is proportional to the impurity concentration $n_I$ and hence responsible for the formation of an impurity side band as sketched in Fig. 5.2. The second part consists of the coupling to the effective field $\langle S\rangle$ built of the local $4f$ moments. Finally one therefore obtains

$$\Sigma_{c\sigma}(\omega) = n_I|V|^2 G_{d\sigma}(\omega) - J_{cf}\langle S\rangle\sigma \tag{5.11}$$

We will see below that this relation implies a fully selfconsistent problem, since in the present case $G_{d\sigma}$ as well as $\langle S\rangle$ depends on the electron Green's functions $G_{c\sigma}$ and hence on the selfenergy Eq. (5.11) itself. In that sense Eq. (5.11) is very similar to the well known DMFT equation [46] for the local conduction electron selfenergy. Additionally, the local Eu $4f$ moment $\langle S\rangle$ appears to be responsible for the lifting of the spin degeneracy in Eq. (5.11) and hence for the magnetization of the conduction band. It is one of the most interesting questions of the present model, whether the phase transition is dominated by strongly correlated physics due to the hybridization of the conduction band and the local impurity states, or by the band shift induced by the $4f$ moments. In particular the decoupled system

with $J_{cf} = 0$ might show as well a metal-insulator transition (MIT), driven by the Kondo resonance of the impurity spectral function $G_{d\sigma}$. Thus, the present model Eqs. (5.6)-(5.8) implies two completely different types of MIT. The energy scale of the magnetic phase transition is given by the Curie temperature $T_C$ which will in general be much larger than the Kondo temperature $T_K$ determining the other type of MIT. Furthermore these two types are obviously competing, since the occurrence of a Kondo resonance is due to resonant spin flip scattering of conduction band states off the impurity. Hence, these processes are suppressed by a conduction band polarization of nearly 100 per cent as it is experimentally known for EuO.

### 5.2.1 Magnetization and mean field approximations

In mean field approximation the expectation value $\langle S \rangle$ of the local $4f$ moment (which is independent on the lattice site $i$ in the isotropic case) yields

$$\langle S \rangle = \frac{\sum_S S e^{-\beta(2J_{4f}\langle S\rangle + J_{cf}m)S}}{\sum_S e^{-\beta(2J_{4f}\langle S\rangle + J_{cf}m)S}} \tag{5.12}$$

$$m = \frac{1}{2}\int d\omega f(\omega)\left[A_{c\uparrow}(\omega) - A_{c\downarrow}(\omega)\right] \tag{5.13}$$

Hence, the conduction electron magnetization $m$ influences the local $4f$ moment similar to an external magnetic field and vice versa. The effective exchange couplings $J_{4f} = \sum_i J_{i,j} = \sum_j J_{i,j}$ and $J_{cf}$ determine the magnetization of the $4f$ system and the splitting of the conduction band respectively. In the case of stoichiometric EuO the magnetization $m$ of the (empty) conduction band vanishes. Thus Eq. (5.12) is decoupled from the conduction band and can be solved separately. In Fig. 5.3 we present the result for $\langle S \rangle$ and various different exchange couplings $J_{4f}$.To obtain a Curie temperature of $T_c \approx 69K$ corresponding to stoichiometric EuO we have chosen $J_{4f} = 7 \cdot 10^{-5} D_0 \approx 6.5 k_B K$, where $D_0 = 8eV$ is approximately the half bandwidth of EuO and $k_B$ is the Boltzmann factor. Experimentally the exchange integrals are given by $J_1/k_B = 0.606K$ for the nearest neighbor and $J_2/k_B = 0.119K$ for the next nearest neighbor exchange. For a fcc lattice this yields $J_{4f}^{exp}/k_B \approx 7.75K$ for the mean field exchange integral. Since we are not specifically interested in a quantitative correct description of the magnetic phase transition the agreement with the experimental result is sufficient.

As soon as impurities are incorporated in the system Eq. (5.12) and Eq. (5.13) are non-trivially coupled. However, already at this point one can estimate the influence of the conduction band on the local $4f$ moments. Actually, the term $J_{cf}m$ appearing in Eq. (5.12) acts similar to an external magnetic field. In Fig. 5.4 we investigate $\langle S \rangle$ assuming constant contributions $B_0 = J_{cf}m$. As expected, the additional term increases the Curie temperature significantly even for low values of the field $B_0$. For the selfconsistent solution one might further

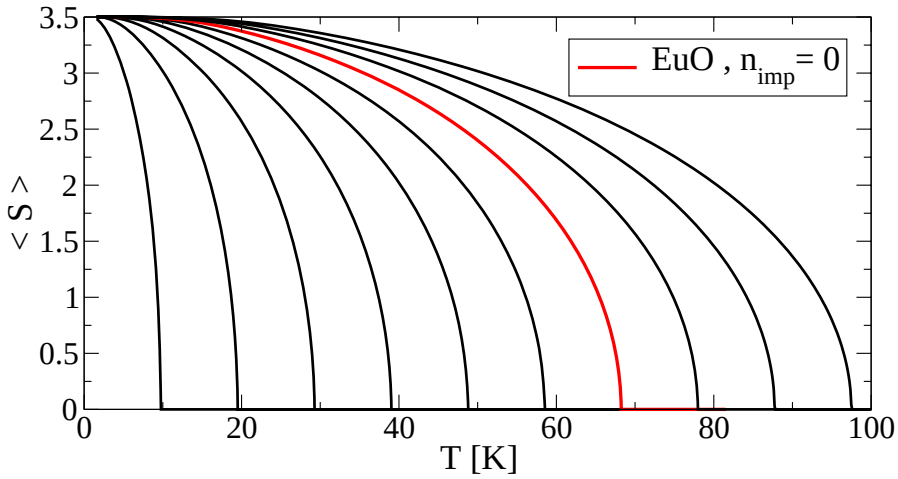


***Figure 5.3:*** Local Eu $4f$ moment for stoichiometric EuO at various different exchange couplings $J_{4f} = \{8, 16, 24, ..., 72, 80\}10^{-5}eV$. The red line corresponds to $J_{4f} = 5.6 \cdot 10^{-4}eV$ and a Curie temperature $T_c \approx 69K$ according to EuO. Experimentally one obtains $J_{4f} \approx 6.6 \cdot 10^{-4}eV$, which is in sufficient agreement for our purpose.

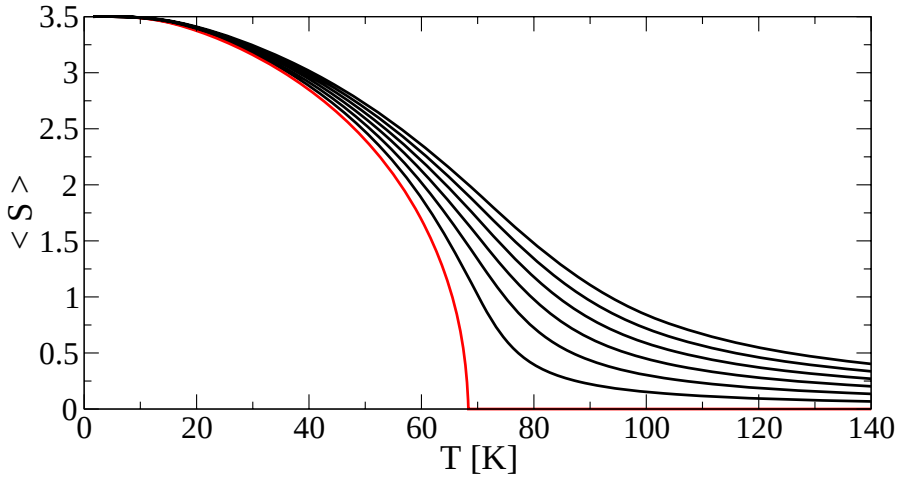


***Figure 5.4:*** Local Eu $4f$ moment for stoichiometric EuO at $J_{4f} = 5.6 \cdot 10^{-4}eV$ and a Curie temperature $T_c \approx 69K$ according to EuO. We applied a constant magnetic field $B_0 = J_{cf}m = \{8, 16, 24, 32, 40, 48\}10^{-5}eV$ in Eq. (5.12) to estimate the influence of the conduction band magnetization $m$ on the $4f$ moment formation. Therefore we expect an increasing Curie temperature due the existence of excess free charge carriers in the doped compound.

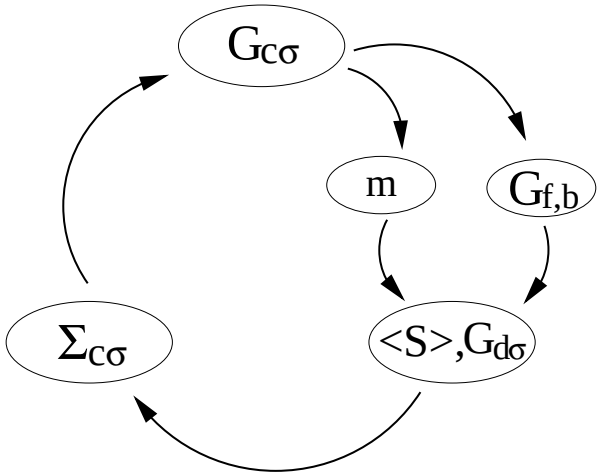


***Figure 5.5:*** Selfconsistence loop, representing the coupled Eqs. (5.10)-(5.16). Additionally the particle number constraint Eq. (5.9) has to be obeyed.

expect that $\langle S \rangle$ will not vanish as an asymptotic tail. Instead, the non-magnetic limit $m = 0$, $\langle S \rangle = 0$, which is always a solution of Eqs. (5.12), (5.13) should be approached selfconsistently below a certain value of the two magnetizations. This is in contrast to the application of a constant external field.

### 5.2.2 Modified non-crossing approximation

After deriving the mean field equations for the magnetization Eq. (5.12), (5.13) we still need to solve the impurity part of Eq. (5.11). Therefore we have to evaluate the quantum impurity problem. Here, we use the NCA as impurity solver according to the description in Chapter 4. As before, we choose a pseudo particle representation of the system and we regard the limit $U \to \infty$ of infinite local Coulomb repulsion. Hence, one obtains the following set of equations

$$\Sigma_{f\sigma}(\omega) = \Gamma \int \frac{d\epsilon}{\pi} \left[1 - f(\epsilon)\right] A_{c\sigma}(\epsilon) G_b(\omega - \epsilon) \tag{5.14}$$

$$\Sigma_b(\omega) = \Gamma \sum_\sigma \int \frac{d\epsilon}{\pi} f(\epsilon) A_{c\sigma}(\epsilon) G_{f\sigma}(\omega + \epsilon) \tag{5.15}$$

$$G_{d\sigma}(\omega) = \int d\epsilon \; e^{-\beta\epsilon} \left[G_{f\sigma}(\omega + \epsilon) A_b(\epsilon) - A_{f\sigma}(\epsilon) G_b^*(\epsilon - \omega)\right] \tag{5.16}$$

There is one remarkable difference compared to the conventional NCA equations, given in Eqs. (4.30)-(4.32). In contrast to the single impurity case, where the full conduction electron propagator reduces to the bare one, in the present case the Eqs. (5.15)-(5.15) contain the full interacting $A_{c\sigma}(\omega) = (1/\pi)\mathrm{Im}G_{c\sigma}(\omega)$. This

is due to the finite impurity concentration entering via impurity averaging into the conduction band selfenergy. All together the Eqs. (5.10)-(5.16) form a fully selfconsistent set of equations, yielding the conduction electron density of states. We present a sketch of these equations in Fig. 5.5 to emphasize the selfconsistence. At this point we want to stress again the importance of the particle number constraint Eq. (5.9), which has to be obeyed within the selfconsistent set of equations.

### 5.2.3 Numerical remarks

We want to comment briefly on the technical aspects concerning the numerical solution of the system of equations Eqs. (5.10)-(5.16) including the particle number constraint Eq. (5.9). The kernel of the selfconsistence loop Fig. 5.5 consist of an impurity problem, which we solve, following the procedure presented in the previous chapter. In particular we stick to the $\lambda_0$ gauge transformation in order to fix the auxiliary spectral functions at $\omega \approx 0$. Therefore we start the selfconsistence loop, assuming a magnetization $m$ and the pseudo particle selfenergies $\Sigma_{f,b}$ and determining the corresponding spectral functions

$$A_{f\sigma}(\omega) = \frac{1}{\pi} \frac{\mathrm{Im}\Sigma_{f\sigma}(\omega)}{(\omega + \mu + \lambda_0 - i0 - E_d - \mathrm{Re}\Sigma_{f\sigma}(\omega))^2 + \mathrm{Im}\Sigma_{f\sigma}(\omega)^2} \quad (5.17)$$

$$A_b(\omega) = \frac{1}{\pi} \frac{\mathrm{Im}\Sigma_b(\omega)}{(\omega + \lambda_0 - i0 - \mathrm{Re}\Sigma_b(\omega))^2 + \mathrm{Im}\Sigma_b(\omega)^2} \quad (5.18)$$

where the chemical potential $\mu$ and the gauge potential $\lambda_0$ are determined via a bisection method, obeying the condition Eq. (4.41) and the particle number constraint Eq. (5.9), respectively. Here, it must be emphasized that the application of the bisection method is possible for two reasons. First, we utilize the exact relation

$$\sum_\sigma \int d\omega f(\omega) A_{f\sigma}(\omega) = \sum_\sigma \int d\omega f(\omega) A_{d\sigma}(\omega) \quad (5.19)$$

in order to replace the $A_{d\sigma}$ in Eq. (5.9) by the pseudo fermion function $A_{f\sigma}$. At least for the converged solution this must be valid. Furthermore, $A_{d\sigma}$ is independent on $\lambda_0$, as we have shown in Chapter 4. Hence, $\mu$ does not depend on $\lambda_0$ and a coupled bisection for both variables can be applied. In particular for those parameters representing the paramagnetic phase of EuO it turned out to be necessary to add a small constant contribution to the imaginary part of the pseudo particle selfenergies. This is due to the gap, appearing in the conduction band density of states. As a consequence a slight deviation ($n_I \to 0.998 n_I$) from the particle number constraint Eq. (5.9) is enforced, in order to keep the chemical potential lying in center of the gap in the paramagnetic phase. Having determined $\mu$ and $\lambda_0$ we can finally derive the impurity Green's function $G_d$.

## 5.3 Transport properties and resistivity of impurity models

Besides the semiconductor-metal transition indicated by the temperature dependent conduction band density of states, we also want to derive the transport properties of our model. In particular we are interested in the conductivity and the resistivity, respectively. For convenience we evaluate the conductivity within linear response theory. Hence we apply the Kubo formula [69], where the conductivity tensor $\sigma^{\alpha\beta}$ is given by an integral over the current-current correlation function

$$\sigma^{\alpha\beta}(\omega) = \int_0^\beta d\lambda \int_0^\infty dt \langle j^\beta(0) j^\alpha(t + i\lambda)\rangle e^{i(\omega+i0^+)t} \tag{5.20}$$

In a cubic system $\sigma^{\alpha\beta}(\omega) = \delta_{\alpha\beta} \cdot \sigma(\omega)$ the diagonal components are equal, while the off-diagonal components vanish. To derive an expression for the current $j$ appearing in Eq. (5.20) we start with the continuity equation for the particle current $\mathcal{J}$ and the particle density $\rho$

$$\frac{\partial \rho}{\partial t}(\vec{r}, t) + \nabla_r \mathcal{J}(\vec{r}, t) = 0 \tag{5.21}$$

In the Heisenberg picture one therefore obtains after Fourier transforming to momentum space the following equation for the electrical current $j = -e\mathcal{J}$, with the elementary charge $e$

$$\vec{q}^H \cdot j^H(\vec{q}, t) = -\frac{e}{\hbar}\left[\rho^H(\vec{q}, t), H\right] \tag{5.22}$$

Transforming into the conventional Schrödinger picture and assuming without loss of generality $\vec{q}$ and $\vec{j}$ to point into $x$-direction, one obtains for the integrated total current

$$j_x = -\lim_{\vec{q}\to 0} \frac{e}{\hbar|\vec{q}|}\left[\rho(\vec{q}), H\right] \tag{5.23}$$

Because of the cubic symmetry of EuO, we can assume an isotropic current. Hence the current into each spatial direction is derived from the commutator of the total charge operator $\rho(\vec{q})$ of the system with the full Hamiltonian Eqs. (5.6)-(5.8). Performing these calculations, which are presented in Appendix B, leads to the remarkably simple result (compare [70, 71])

$$j_x = \frac{e}{\hbar} \sum_{k\sigma} \frac{\partial \epsilon_k}{\partial k_x} c^\dagger_{k\sigma} c_{k\sigma} \tag{5.24}$$

In particular, the total current is obviously provided only by conduction electron states, and not by impurity electrons. This is not surprising, since all electrons

besides the ones in the conduction band are local states. If there would be a hopping between different $d$-electron states included in the Hamiltonian, the impurities would contribute to the total current. In the present case the situation is the same as for the Hubbard model within DMFT where the conduction electron selfenergy is momentum independent as well. Hence, we can use the expression for the conductance derived in [72, 73]. Additionally we averaged over the spatial directions, such that $\sigma = (\sigma_{xx} + \sigma_{yy} + \sigma_{zz})/3$

$$\sigma = \frac{\pi e^2}{3\hbar V} \sum_{k\sigma} \int d\omega \left( -\frac{\partial f}{\partial \omega} \right) A^2_{c\sigma}(k,\omega) \left( \frac{\partial \epsilon_k}{\partial k} \right)^2 \tag{5.25}$$

where $f(\omega)$ is the Fermi distribution function. The conduction electron spectral function $A_{c\sigma}(k,\omega)$ is proportional to the imaginary part of Eq. (5.10), and is therefore obtained within our calculations. The dispersion relation $\partial\epsilon_k/\partial k$ is taken with respect to the absolute value of the momentum $k = (k_x + k_y + k_z)^{1/2}$. Assuming $\epsilon_k$ to depend only on the absolute value $k$ one can obtain $\partial\epsilon_k/\partial k$ according to the bare conduction electron density of states Eq. (5.2) $N(\epsilon) = N^0(\epsilon) = \frac{2}{\pi}\left(1 - (\epsilon - \Delta_0)^2\right)^{1/2}$ with the energy $\epsilon$ in units of the half bandwidth $D_0$. In this case one can replace any $\vec{k}$ summation by an integral like

$$\sum_{\vec{k}} = \frac{V}{(2\pi)^3} \int d^3k = \frac{a^3}{2\pi^2} \int dk k^2 = \frac{a^3}{6\pi^2} k^3 = \int_{\Delta_0 - 1}^{\epsilon} d\epsilon' N(\epsilon') = g(\epsilon) \tag{5.26}$$

where $V = a^3$ is the volume corresponding to one lattice site and $a$ is the lattice constant. Hence one can derive the dispersion relation as

$$\frac{\partial \epsilon}{\partial k}(\epsilon) = \frac{3a}{(6\pi^2)^{1/3}} \frac{g^{2/3}(\epsilon)}{N(\epsilon)} \tag{5.27}$$

Finally, the conductivity yields

$$\sigma = \left( \frac{3}{4\pi} \right)^{1/3} \frac{e^2}{\hbar a} \sum_{\sigma} \int d\omega d\epsilon \left( -\frac{\partial f}{\partial \omega} \right) A^2_{c\sigma}(\epsilon,\omega) \frac{g^{4/3}(\epsilon)}{N(\epsilon)} \tag{5.28}$$

As one can see, the conductivity $\sigma$ at low temperatures is essentially determined by the spectral function $A_{c\sigma}(k, \omega = \mu)$ in the vicinity of the chemical potential. In that sense it can be compared to the Drude conductivity which is basically given by the density of states at the Fermi energy. In the next chapter we use Eq. (5.28) to derive the resistivity $\rho = 1/\sigma$ within the present model.

# 6 Analysis of the EuO Model

In the following we discuss the solution of the EuO model introduced in the previous chapter. As mentioned before the theoretical phase space of the present model is very large, leading to many different physical manifestations. In this chapter we restrict ourselves to one set of model parameters, which is typical for stoichiometric EuO. Furthermore we vary the temperature $T$ systematically and add different impurity or doping concentrations $n_I$ to the model. Hence, we regard the EuO phase transition as being driven by either the temperature or the impurity concentration. Finally, we compare the most important quantities namely the conduction band magnetization $m(T)$, the 4f-moment $\langle S \rangle$, and the resistivity $\rho(T)$ to the experimental results.

## 6.1 Band structure and particle numbers

From various experiments [6] it is known that a spin dependent band splitting is of crucial importance for the phase transitions in EuO. Additionally we already sketched in the previous chapter that the particle number conservation between impurity and conduction electrons is the precondition for the physical model and can even explain the stoichiometric limit exactly. Therefore we will first present the results for these to properties.

### 6.1.1 Conduction band density of states

As mentioned before we assumed a semi-elliptical bare density of states (Eq. (5.2)). According to the conduction electron selfenergy $\Sigma_c(\omega)$ Eq. (5.11) one can conclude that the semi-elliptical shape is conserved for energies where the imaginary part of the impurity density of states $G_d(\omega)$ becomes small. This turns out to be the case for $\omega \gg \mu$. In this energy regime $\Sigma_c(\omega)$ becomes basically real leading to a shift of the conduction electron spectrum. At those energies where $\mathrm{Im}G_d(\omega)$ is finite we expect an additional structure to be induced to the conduction band. In Fig. 6.1 we present the results for the conduction band density of states at various impurity concentrations. In the upper panel the system is in the paramagnetic phase $T \gtrsim T_C$. Hence, both spin directions are degenerate, lying onto each other. Furthermore, additionally to the upper semi-elliptical conduction band at $\omega - \mu > 0$ one can clearly observe an impurity

induced side band at $\omega - \mu \approx -0.017 D_0$. The width of the side band is determined by the hybridization $\Gamma = \pi V^2$, the impurity concentration $n_I$ and the difference $\Delta_0 - E_d$ between the bare conduction band and the impurity level $E_d$. If $\Delta_0 - E_d$ is sufficiently large a gap between the to components of the conduction band opens like in Fig. 6.1. The width of the gap $\Delta_G \approx 0.02 D_0$ in the present case is of the order of the critical temperature $k_B T_C \approx 0.01 D_0$. Hence, one can assume the system to be in an insulating state, as it will be quantified later. At this point, we want to emphasize that in Fig. 6.1 the band difference $\Delta_0 - E_d = D_0$ is chosen in such a way that it cannot be the only reason for the existence of a gap, assuming a finite width of the impurity Green's function $G_d(\omega)$. Hence the formation of the gap is supported by the real part of the conduction band selfenergy due to the hybridization between the conduction electrons with the impurity states.

Below the critical temperature the spin degeneracy of the conduction band is broken. Depending on the strength of the coupling $J_{cf}$ between the conduction band and the Eu 4f moments the band structure of the two spin directions splits into two components. We demonstrate in Fig. 6.1 that due to a finite overlap of one conduction band component with the chemical potential at $\omega - \mu = 0$ the system obviously becomes (half-)metallic. The precondition for the appearance of a finite density of states at $\omega = \mu$ can be formulated in terms of the effective gap $\Delta_g$ in the paramagnetic phase, which has to be significantly lower than the maximum splitting of the conduction band. In mean field approximation this splitting is proportional to the average 4f magnetic moment $\langle S_{4f} \rangle$. Hence one obtains approximately the criterion

$$k_B T_C < \Delta_g < 7/2 \cdot J_{cf} \tag{6.1}$$

for the appearance of a sufficient metal to insulator transition. Although $T_C$ as well as $\Delta_g$ are determined selfconsistently they can be adjusted by modifying the exchange coupling $J_{4f}$ and the bare interval $\Delta_0 - E_d$, respectively. In particular the upper limit should actually be $\Delta_g \ll 7/2 \cdot J_{cf}$, because for a very small but finite overlap between the impurity and the conduction band states, the density of states at $\omega = \mu$ is very low due to a Fano resonance of the conduction band with the impurity states. This can be seen in Fig. 6.2 where we present the evolution of the conduction band at a given impurity concentration when the temperature is approaching its critical value. The spin splitting is lifted as $T \to T_C$ accompanied by a lowered density of states $N(\mu)$ at the chemical potential. If $N(\mu)$ remains small even for low temperature $T \ll T_C$ we expect the conductance to be very low as well. Additionally, this usually leads to significant numerical problems. In the present case we have chosen the exchange coupling $J_{4f} = 7 \cdot 10^{-5} D_0$ according to the Curie temperature $T_C = 69K$ of stoichiometric EuO and $J_{cf} = 0.05 D_0$ , with $D_0 = 8eV$ such that $7/2 \cdot J_{cf} \approx 1eV$ according to the experiment. With these parameters and $\Delta_0 - E_d = D_0$ the constraint Eq. (6.1) is sufficiently fulfilled.

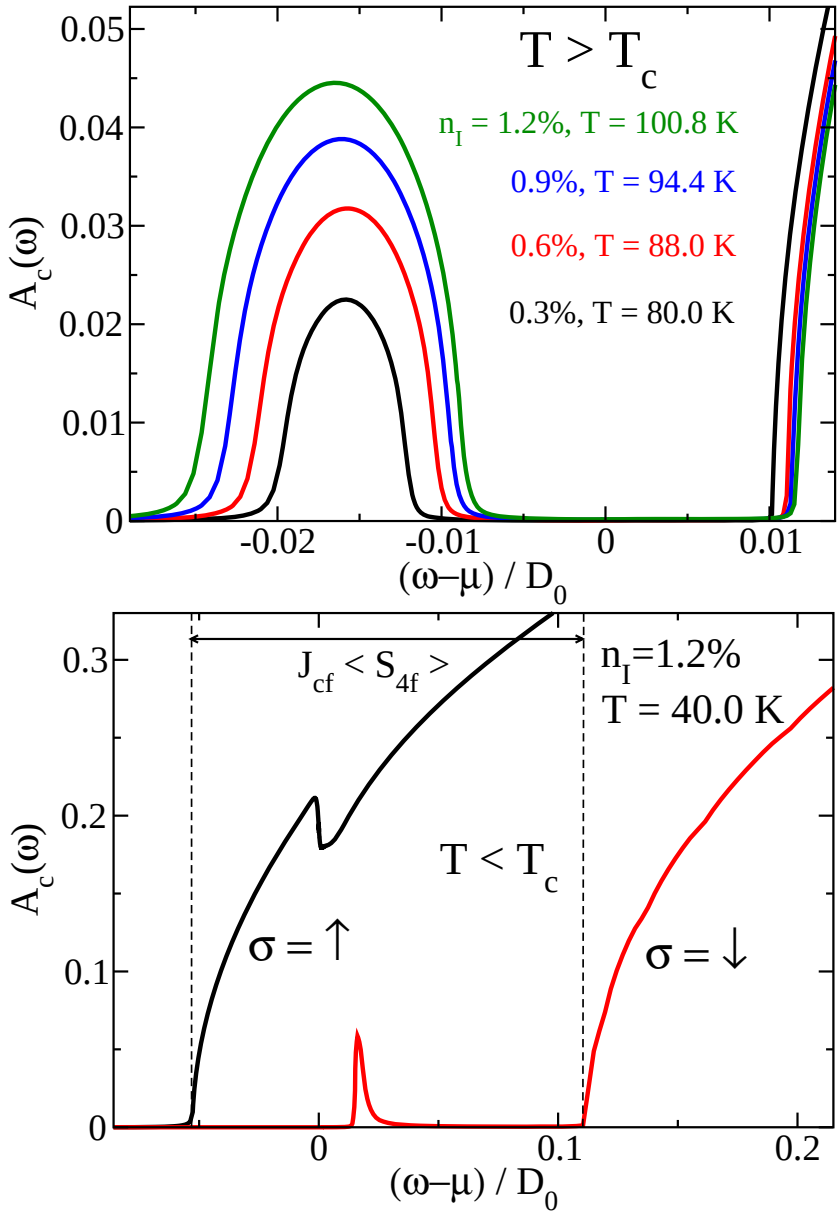


***Figure 6.1:*** Conduction electron density of states relative to the chemical potential $\mu$ for temperatures $T > T_C$ (upper panel) and $T < T_C$ (lower panel). The system parameters are $E_d = -0.4D_0$, $\Gamma = \pi V^2 = 0.05D_0^2$, $J_{4f} = 7 \cdot 10^{-5} D_0$, $J_{cf} = 0.05D_0$, $\Delta_0 = 0.6D_0$, $D_0 = 8eV$ at an impurity concentration $n_I$. In the paramagnetic phase above $T_C$ an $n_I$ dependent gap opens between the impurity induced side band and the bare conduction band ($\omega > 0$). Below $T_C$ the spin degeneracy is lifted and a band splitting of the order $J_{cf}\langle S_{4f}\rangle$ can be observed.

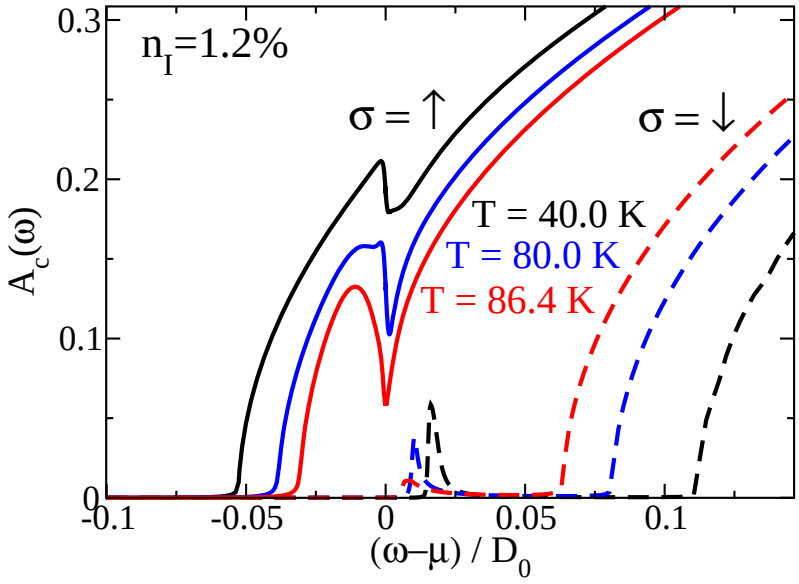


***Figure 6.2:*** Evolution of the conduction electron density of states relative to the chemical potential $\mu$ for various temperatures $T \to T_C$ approaching the critical temperature $T_C \approx 99.4K$. (Parameters like in Fig. 6.1)

### 6.1.2 Impurity density of states

The origin of the side band induced to the electron conduction band is provided by the hybridization with the impurity states. The impurity density of states $A_d(\omega)$ is presented in Fig. 6.3. Above the critical temperature $A_d(\omega)$ is forming a spin degenerate band below the chemical potential. The width of the impurity band is thereby selfconsistently determined from the pseudo particle Green's functions and the conduction band density of states $A_{c\sigma}(\omega)$. One can estimate the width of the impurity induced conduction side band to be of the order $n_I \Gamma A_d^{max}$ where $A_d^{max}$ is the maximum of $A_d(\omega)$. Hence, the conduction side band as well as the impurity band becomes more narrow for vanishing $n_I$. Due to the infinite local Coulomb repulsion the impurity states obtain a local moment. For $T < T_C$ the spin degeneracy is therefore lifted. Hence, the minority component $A_{d\downarrow}(\omega)$ forms a peak above the chemical potential which also induces a peak to the conduction band at the same position. The majority component $A_{d\uparrow}(\omega)$ is centered around $\mu$, leading to a Fano dip in the conduction band. Consequently a relatively large amount of impurity spectral weight is transferred into the conduction band in the ferromagnetic phase, what will be responsible for the increased Curie temperature in the electron-doped compound. In particular close to $T_C$ the spin splitting is small, enforcing a finite density of state at the Fermi energy. Hence, the rising magnetization is expected to be accompanied by an increasing conductivity.

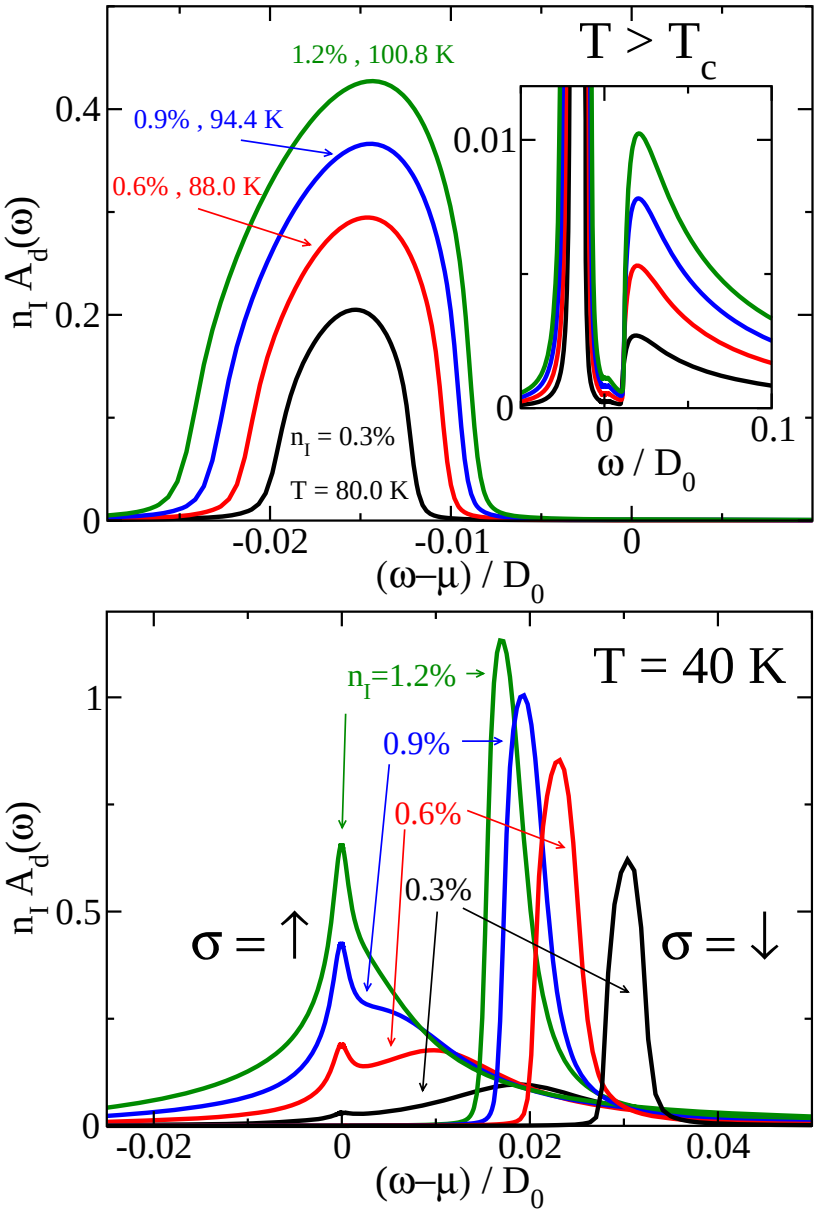


***Figure 6.3:*** Impurity density of states relative to the chemical potential $\mu$ for temperatures $T > T_C$ (upper panel) and $T < T_C$ (lower panel). In the paramagnetic case the impurity density of states is getting more narrow for vanishing impurity concentration. Below the critical temperature the majority spin component is centered around the chemical potential, while the minority band is shifted above $\mu$. (All parameters and temperatures are equal to Fig. 6.1)

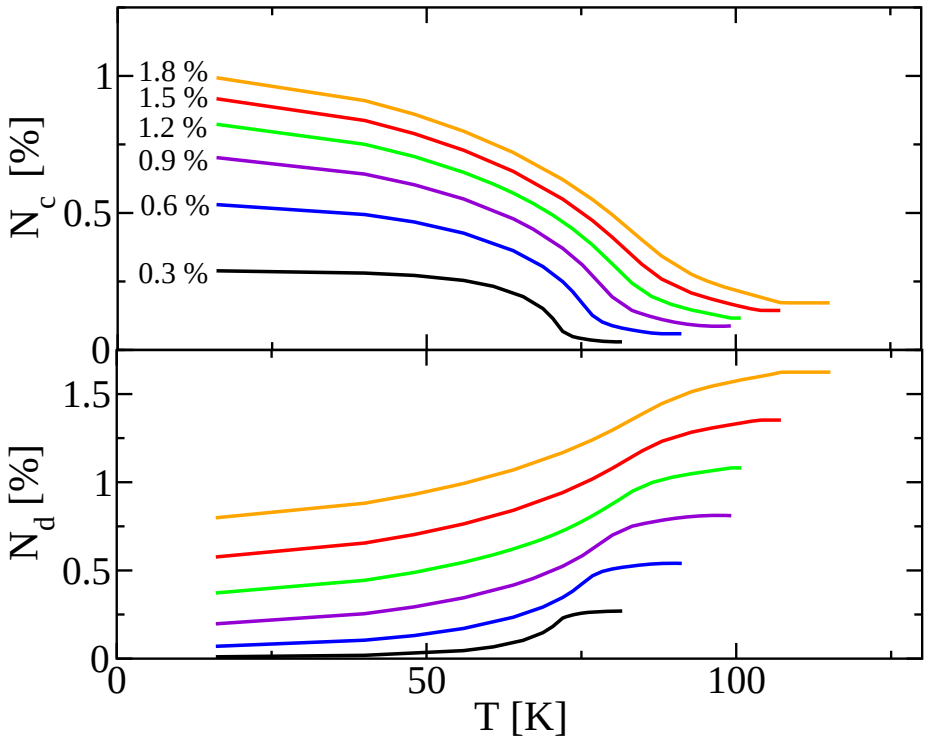


***Figure 6.4:*** Temperature dependent conduction electron $N_c$ and impurity $N_d$ particle numbers for different impurity concentrations. The impurity states are discharged into the conduction band with lowering temperature.(Parameters like in Fig. 6.1)

### 6.1.3 Particle number conservation

We already emphasized the importance of the particle number constraint Eq. (5.9) for the present system. We determine the chemical potential such that the total electron number $N_d + N_c = n_I$ equals the impurity concentration. The question remains how the particle density $n_I$ is distributed over the impurity and the conduction electrons, respectively. In Fig. 6.4 we show the temperature dependent particle numbers at different impurity concentrations for the same set of parameters as in Fig. 6.1. Besides the obviously fulfilled particle number constraint, it is remarkable that the exchange of particle density between the two species of electrons already reflects the metal to insulator transition. As the temperature is lowered the impurity states are discharged into conduction electron states. Actually this is no proof for the metallic state of the system at low temperatures, but together with the information of the previous sections about the interacting conduction band, it hints to a metallic low temperature phase and to an insulating state above the critical temperature.

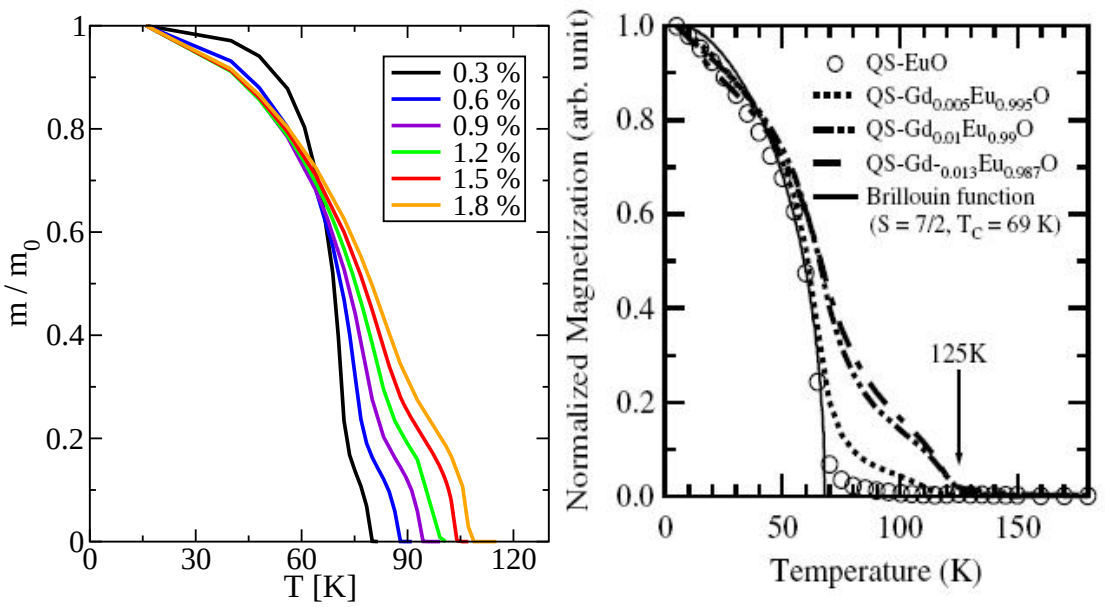


***Figure 6.5:*** Left: Temperature dependent relative magnetization of the conduction band. The system parameters are $E_d = -0.4D_0$, $\Gamma = \pi V^2 = 0.05D_0^2$, $J_{4f} = 7 \cdot 10^{-5} D_0$, $J_{cf} = 0.05D_0$, $\Delta_0 = 0.6D_0$, $D_0 = 8eV$ at various impurity concentrations $n_I$. Right: Experimental relative magnetization at various Gd-doping concentrations [7]

## 6.2 Magnetization

As mentioned before, stoichiometric EuO can be regarded as an archetype for a Heisenberg ferromagnet. Although the presence of O-vacancies or doped Gd impurities does not influence the magnetic as strongly as the transport properties, we still expect a remarkable effect, particularly on the critical temperature. Nowadays, this is confirmed in various experiments [6, 7], which determined the Curie temperature to be increasing with higher impurity concentrations (at least for low $n_I$). In contrast to previous theories [35], a fully selfconsistent study like in the present work should be able to reproduce these results. In Fig. 6.5 we compare the relative conduction band magnetization $m(T)/m(0)$ at various impurity concentrations obtained by our calculations to recent experimental results for the total magnetization of Gd-doped EuO [7]. Furthermore, the Eu 4f moment and the absolute conduction band magnetization is presented in Fig. 6.6. We obtain a qualitatively good agreement between the theory and the experiment. In particular the principle dependence of the magnetic phase transition on $n_I$ turns out to be consistent.

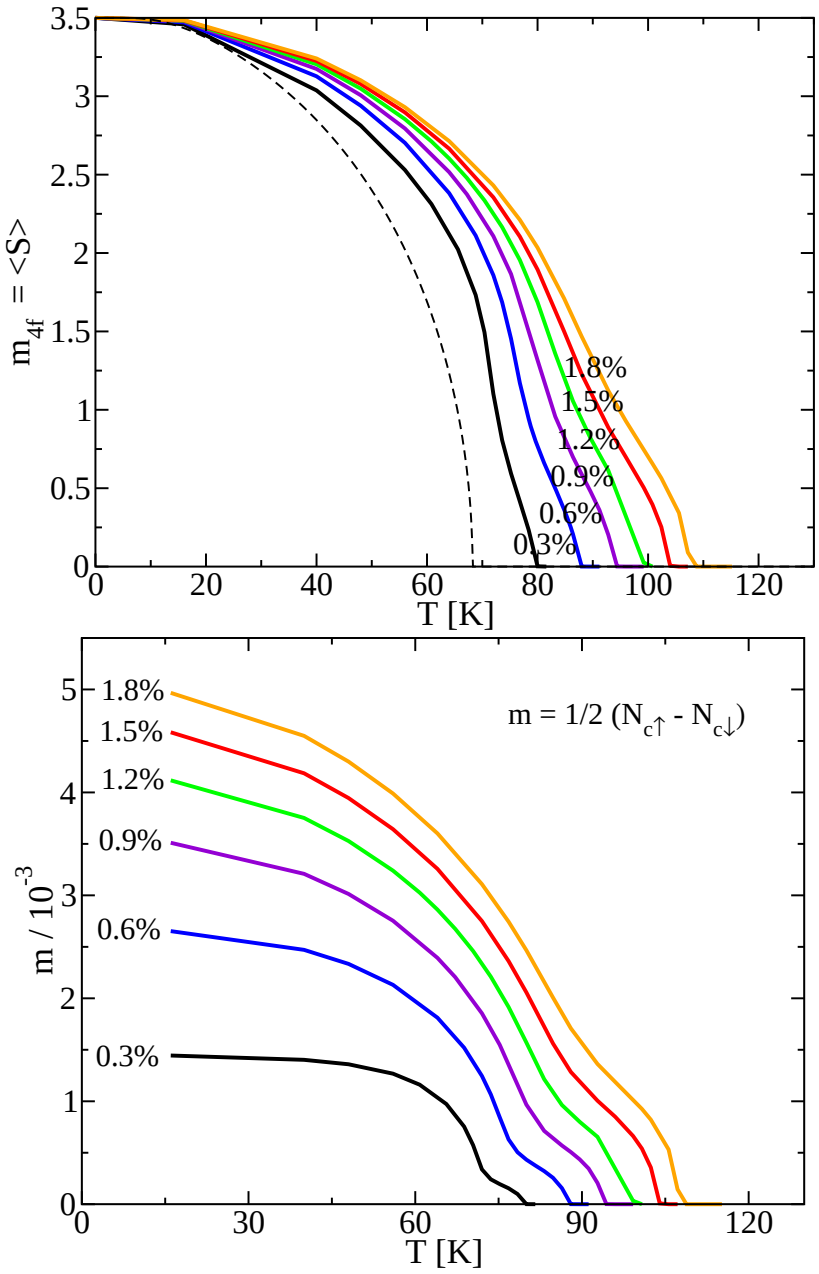


***Figure 6.6:*** Temperature dependent magnetization of the Eu 4f moments (upper panel) and the conduction band (lower panel) at various impurity concentrations (Parameters like in Fig. 6.5)

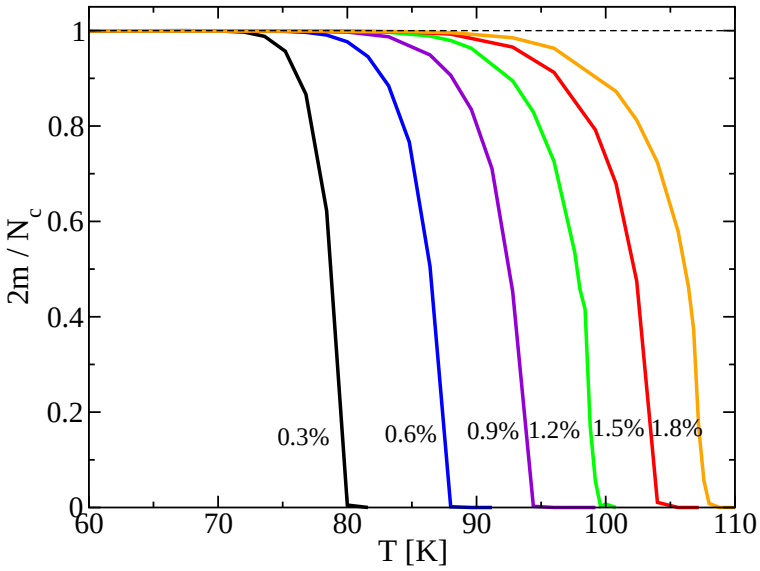


***Figure 6.7:*** Temperature dependent polarization of the conduction band corresponding to the magnetization in Fig. 6.6. The high degree of the polarization up to temperatures $T \lesssim T_C$ is a remarkable property of EuO.(Parameters like in Fig. 6.5)

As predicted in the previous section, the interaction with the magnetic moments of the conduction band deforms the magnetization of the Eu 4f moments in the vicinity of the Curie temperature and vice versa. This behavior is indeed very similar to the magnetization of the Heisenberg model in a constant magnetic field. But in the present case the mean field provided by the conduction band electrons and the local moments is generated selfconsistently. Hence it is not clear at this point if the unique origin of the deformation in the magnetizations close to $T_C$ is mainly due to the 4f moments or the conduction band.

In Fig. 6.7 we present the temperature dependent polarization $m(T)/N_c(T)$ of EuO within our model. In recent experiments [6] it could be shown that EuO is very highly (nearly 100 per cent) polarized in the metallic phase. The high degree of the polarization is one of the most interesting properties of EuO in particular in the context of a possible spintronic application. The experimental behavior is confirmed within our calculations, as one can clearly see in Fig. 6.7. Furthermore the existence of the shoulder in the conduction band and the Eu 4f moment magnetization is not reproduced in the polarization and can hence be shown to be due to the conduction band occupation number $N_c(T)$. The total magnetization can therefore be understood as a superposition of a mean field Heisenberg model for the Eu 4f moment and the condction band with a temperature dependent occupation number, enlarging the Curie temperature depending on $n_I$.

## 6.3 Transport properties

The most striking property of EuO is the strong colossal magneto resistance effect observed for the Eu-rich compound. We already demonstrated that the conduction band Fig. 6.1 and its temperature dependent occupation number Fig. 6.4 hints to a metal to insulator transition in our model. We also claimed that the system parameters are to be chosen such that the condition Eq. 6.1 is fulfilled if one wants to observe a convenient change in the conductance with varying temperature. In particular the difference between the bare conduction band and the impurity level $\Delta_0 - E_d$ is thereby to be adjusted such that a sufficiently large gap can occur in the high temperature phase. As in the previous sections we have chosen the system parameters to be $E_d = -0.4D_0$, $\Gamma = \pi V^2 = 0.05D_0^2$, $J_{4f} = 7 \cdot 10^{-5} D_0$, $J_{cf} = 0.05D_0$, $\Delta_0 = 0.6D_0$, $D_0 = 8eV$ according to the experimental values. We investigate the resistivity in comparison to the experiment as a function of temperature and of the impurity concentration. Thereby we will show that there exist two characteristic types of metal to insulator transitions in the present model, driven by either the temperature $T$ or the impurity concentration $n_I$. In the next chapter we will show that there might even be a third type of metal to insulator transition contained in the present model without magnetic 4f moments.

### 6.3.1 Temperature dependence of the resistivity

At first, we want to discuss the temperature dependence of the resistivity at different impurity concentrations $n_I$. We calculate the resistivity as the inverse $\rho(T) = 1/\sigma(T)$ of the conductivity $\sigma(T)$ derived by Eq. 5.28. The corresponding results are demonstrated in Fig. 6.8 in comparison to the experiment [6]. Indeed, for properly chosen parameters we can observe a very large jump in the resistivity of up to seven orders of magnitude when the temperature $T$ is crossing its critical value. Comparing the strength of the resistivity change to the corresponding quantity in the experimental curves 66-6 in Fig. 2.5 and Fig. 6.8 b) we find a sufficient agreement. Also the principle shape of the resistivity curves is qualitatively reproduced. In particular we can also observe the change of the curvature on the rising edge of the resistivity. This behavior is also seen in Fig. 2.5 but not in Fig. 6.8 b), which may be due to an insufficient experimental resolution on the edge. We can identify this feature with the breakdown of polarization. Its appearance namely coincides with the temperature region where the induced impurity band of the minority spin conduction band in Fig. 6.2 is heading towards the chemical potential. Hence, the resistivity in this region is slightly lowered, leading to a change of its curvature on the narrow resistivity edge. Furthermore, we regard the strength of the observed resistivity jump in dependence on the impurity concentration. The lower $n_I$ becomes the stronger gets the change in $\rho(T)$

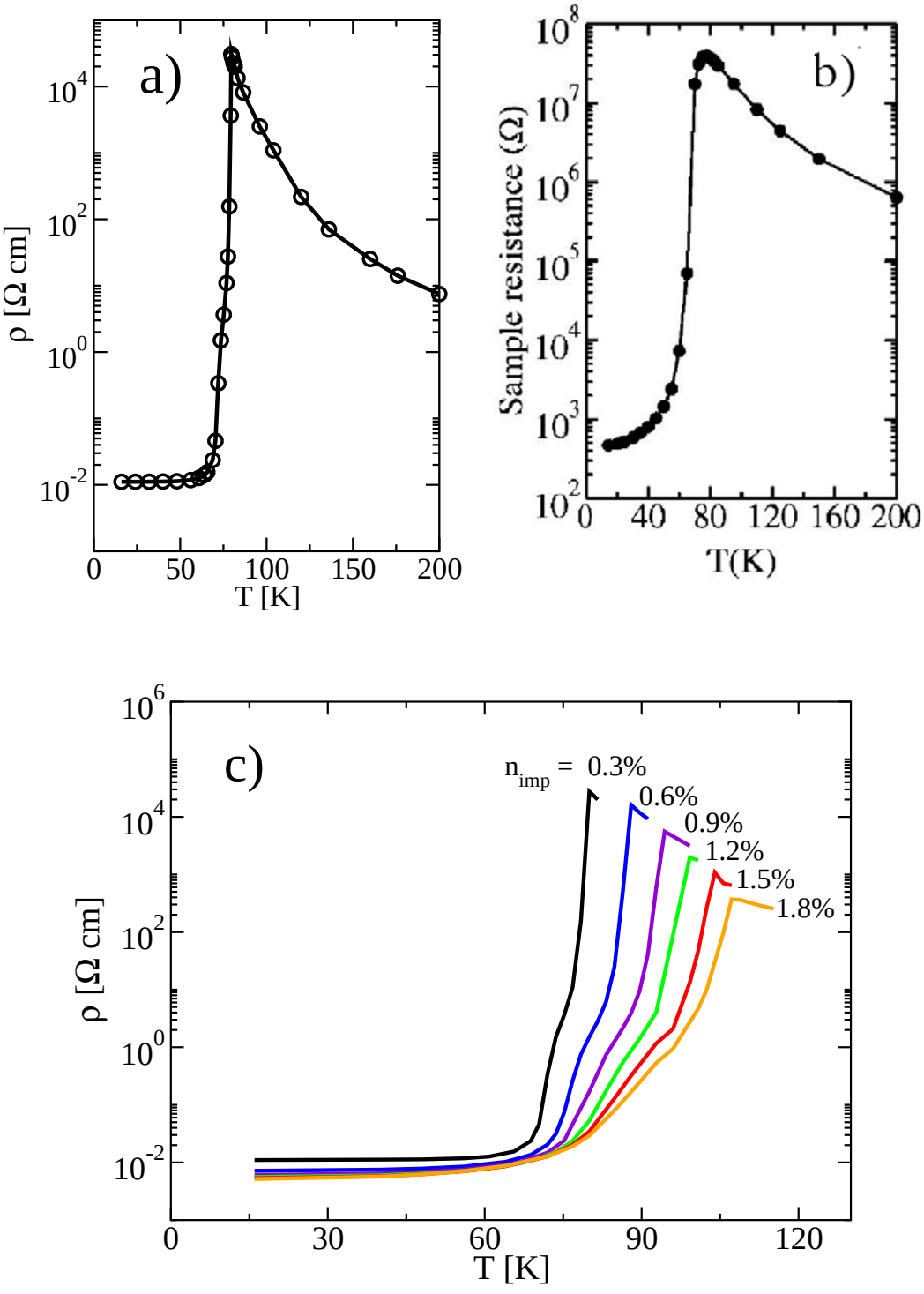


***Figure 6.8:*** Temperature dependent resistivity. a) Theory with the parameters: $E_d = -0.4D_0$, $\Gamma = \pi V^2 = 0.05D_0^2$, $J_{4f} = 7 \cdot 10^{-5} D_0$, $J_{cf} = 0.05D_0$, $\Delta_0 = 0.6D_0$, $D_0 = 8eV$ and $n_I = 0.3\%$ b) experiment [6] and c) theory for various impurity concentrations

at the critical temperature. Although the resistivity at $T \to 0K$ gets lower as well with increasing $n_I$ (which we well discuss in the subsequent section) the decreasing width of the gap in the paramagnetic phase (cf. Fig. 6.1) is the dominant contribution. In fact the height of the resistivity step has experimentally often been used as a measure of the impurity concentration. All together we can show that the relevant experimental features of the temperature dependent resistivity are reproduced within our model for a realistic set of system parameters.

### 6.3.2 Impurity concentration dependence of the conductivity - a quantum critical phase transition

The low temperature behavior of the resistivity in Fig. 6.8 raises the question after the dependence of the conductivity $\sigma_T(n_I)$ on the impurity concentration. In particular far below the critical temperature $\sigma_T(n_I)$ is only weakly temperature dependent while its value is mainly determined by the impurity concentration $n_I$. Furthermore, due to the particle number constraint Eq. (5.9) the limit

$$\lim_{n_I \to 0} \sigma_T(n_I) = 0 \tag{6.2}$$

can analytically be predicted. In fact, this limit even leads to a really vanishing conductivity, while the conductivity for finite impurity concentrations might become very small but finite, due to a finite semiconducting gap in the high temperature phase. In Fig. 6.9 we present the conductivity $\sigma_T(n_I)$ at various temperatures $T$ as a function of $n_I$. For numerical reasons we can solve the system only for impurity concentrations down to $n_I \approx 0.1\%$ and for temperatures $T \approx 0.0001 D_0$. Therefore, we added the data point $\sigma_T(0) = 0$ by hand, according to the analytical limit Eq. (6.2). Furthermore we will show that the temperature dependence of the conductivity for low impurity concentrations saturates quite early. At a temperatures $T = 72K$ and $T = 80K$ above the critical temperature $T_C^0 = 69K$ of stoichiometric EuO ($n_I$=0) the system can be above the Curie temperature for finite impurity concentrations. Hence the vanishing conductivity corresponds the the paramagnetic semiconducting phase characterized by a gap in the conduction band density of states. The impurity concentration $n_I^c$ at which the conductivity is about to vanish is thereby determined by the $n_I$-dependent critical temperature $T_C(n_I)$. The corresponding condition yields $T_C(n_I^c) = 72K$ and $T_C(n_I^c) = 80K$, respectively.

For temperatures $T \ll T_C^0$ the situation is completely different. As one can see in Fig. 6.9 in this regime the conductivity remains finite even at very low impurity concentrations. Furthermore, for low values of $n_I$ the conductivity basically depends on $n_I$ and will vanish in the limit $n_I \to 0$. Hence, we predict a quantum critical (at temperature $T = 0$) phase transition at a critical impurity concentration $n_I = 0$ within our model. Note, that at temperature $T = 0$ the

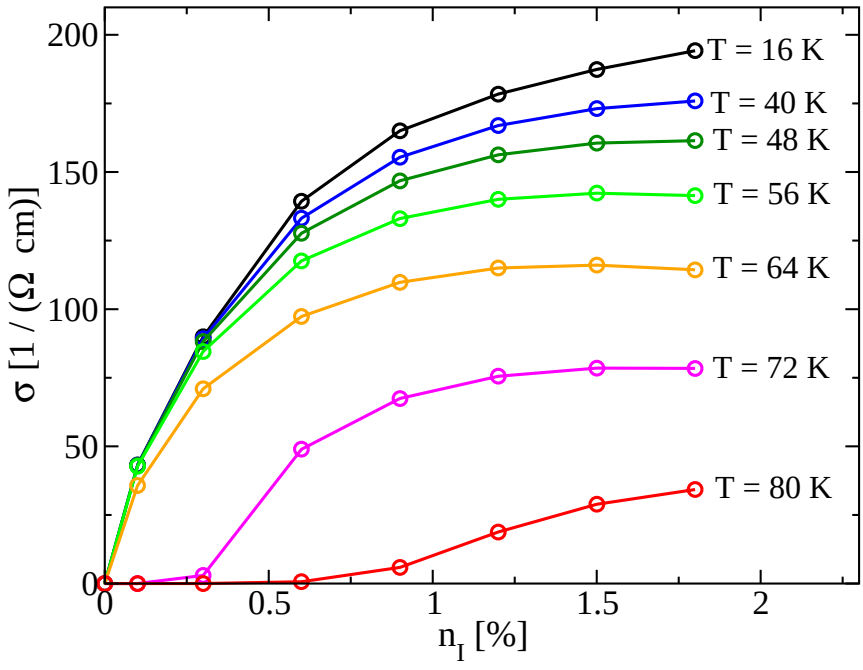


***Figure 6.9:*** Impurity concentration dependence of the conductivity $\sigma_T(n_I)$ at various temperatures $T$. The data points $\sigma_T(0) = 0$ are added according to the analytical limit Eq. (6.2). For temperature sufficiently below the critical temperature $T_C^0 = 69K$ of stoichiometric EuO and for low impurity concentrations $\sigma_T(n_I)$ mainly depends on $n_I$.

present model is always in the ferromagnetic phase. Therefore, in contrast to the temperature dependent the $n_I$-dependent quantum critical conductivity phase transition obviously does not coincide with a change of the magnetic properties.

Actually one should strongly distinguish the two different phase transitions since the corresponding microscopical mechanisms are completely different. First, there is a transition leading to a gapped high temperature phase with a finite number of conduction band electrons. In the other case the system is always ferromagnetic, while the free charge carriers are gradually removed. Of course, the second type is experimentally more difficult to investigate, since it is complicated to adjust the impurity concentration of the sample. Unfortunately, to our knowledge there are no systematical studies, investigating the impurity concentration dependence of the physical properties of EuO for a sufficiently large number of different impurity concentrations, such that we could compare the results to Fig. 6.9. However, the few experiments [32, 7] concerning this issue are in qualitative agreement with our findings.

## 6.4 Simultaneity and Critical Temperature

Up to now, we have not yet discussed the simultaneity of the magnetic phase transition and the dramatic change of the transport properties as a function of temperature. In particular we need to have a closer look at the specific character of the magnetic phase transition at the Curie temperature $T_{Curie}$ and the transition in the resistivity $\rho(T)$. First, we recognize that it is not obvious how one can define a critical temperature characterizing the conductivity transition. The resistivity $\rho(T)$ in Fig. 6.8 contains a well resolved maximum at a temperature $T_{\rho_{max}}$. In table 6.1 and Fig. 6.10 we compare $T_{\rho_{max}}$ to the magnetic Curie temperature $T_{Curie}$. It turns out that both temperatures coincide with a sufficient accuracy as long as the impurity concentration $n_I$ is finite. This result corresponds to the observation that the gap in the conduction band density of states obtains its maximum width as soon as the magnetization has completely vanished. Hence we define a critical temperature $T_C$ as

$$T_C = T_{Curie} = T_{\rho_{max}} \tag{6.3}$$

In that sense one can regard the two phase transition to be simultaneous in agreement with the experimental results. At vanishing impurity concentration $n_I = 0$

| $n_I$ | 0.0 | 0.3 | 0.6 | 0.9 | 1.2 | 1.5 | 1.8 |
|---|---|---|---|---|---|---|---|
| $T_{Curie}[K]$ | 69 | 79.8 | 87.8 | 94.4 | 99.4 | 103.6 | 107.8 |
| $T_{\rho_{max}}[K]$ | - | 79.6 | 88.0 | 94.2 | 99.2 | 104.0 | 107.6 |

***Table 6.1:*** Critical temperatures at various impurity concentrations. We compare the magnetic Curie temperature $T_{Curie}$ of the Eu 4f system to the temperature $T_{\rho_{max}}$ at which the resistivity reaches its maximum. This definition fails at vanishing impurity concentrations $n_I = 0$. The numerical error is $\Delta T = \pm 0.4K$.

the conductivity is zero at low temperatures. Hence the resistivity maximum can not anymore serve as a sufficient definition of the critical temperature. As mentioned before, one therefore has to distinguish between the quantum critical phase transition as $n_I \to 0$ and the temperature dependence of the conductivity. In contrast to the magnetization, the temperature dependent conductivity cannot serve as the order parameter of a phase transition, because it remains finite at all temperatures and can only become zero for vanishing impurity concentration.Strictly, one should therefore understand the temperature dependent evolution of the present system as a magnetic phase transition accompanied by a strong change of the electrical transport properties, instead of the interpretation as two simultaneous phase transitions.

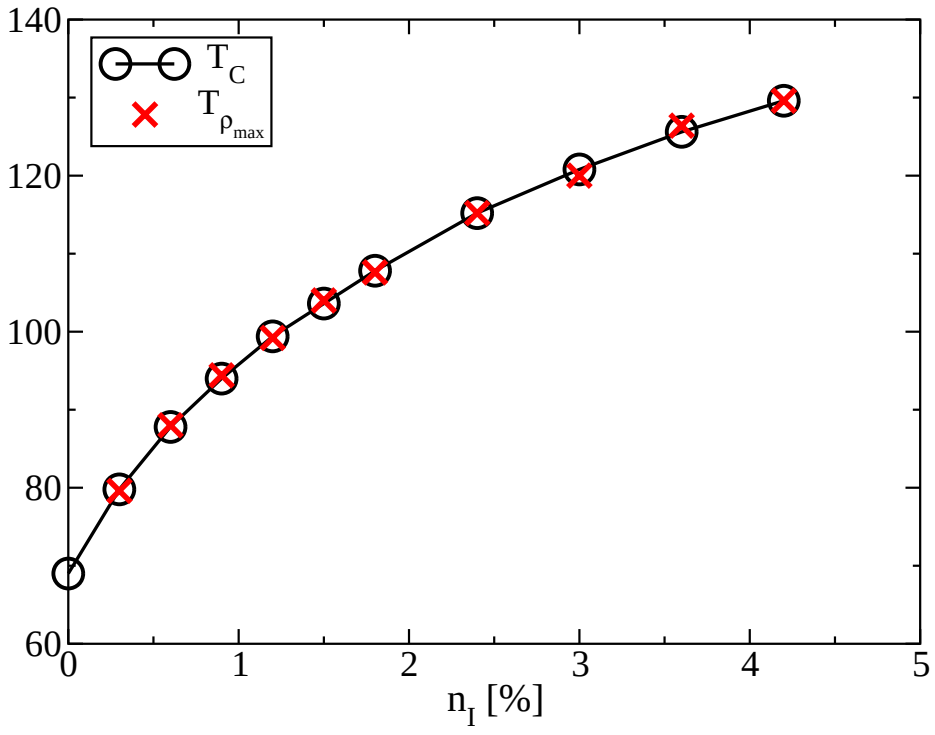


***Figure 6.10:*** Curie temperature $T_C$ as a function of the impurity concentration $n_I$ compared to the temperature $T_{\rho_{max}}$ at which the resistivity reaches its maximum value. The simultaneity of the magnetic and the conductivity transition is confirmed. At least for impurity concentrations $n_I \leq 4\%$ the results are in good agreement with the experiment [32]. In contrast to previous studies [36] we reproduce the $n_I$-dependent of the Curie temperature.

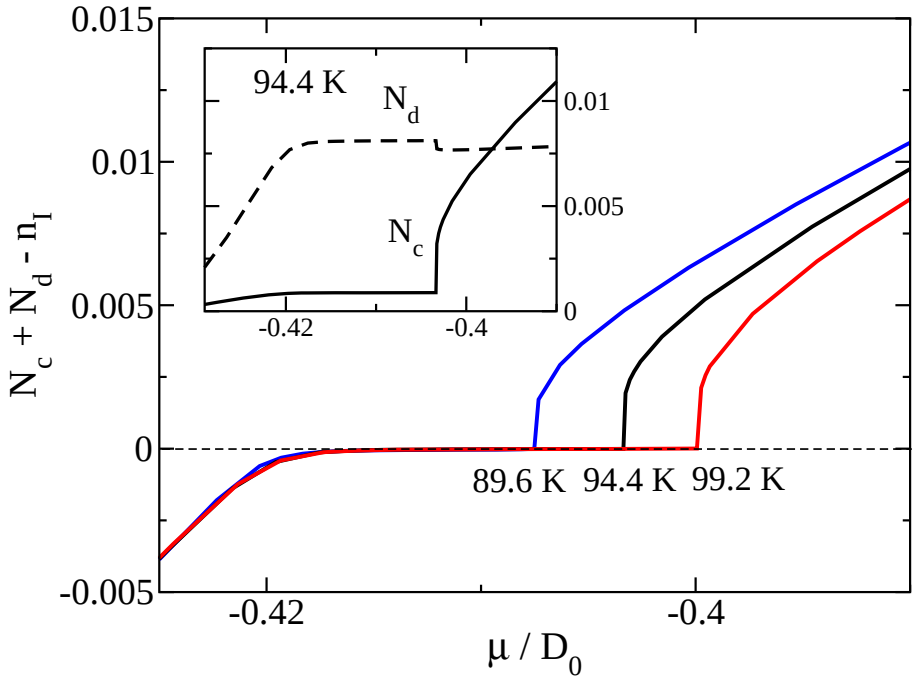


***Figure 6.11:*** Total Fermion number $N_c + N_d - n_I$ as a function of the chemical potential $\mu$ . Above a certain $\mu$ the overall fermion number increases due to bare conduction band states which become occupied in this regime (see inset). For lower $\mu$ the impurity states are shifted gradually above the chemical potential. The system parameters are: $E_d = -0.4D_0$, $\Gamma = \pi V^2 = 0.05D_0^2$, $J_{4f} = 7 \cdot 10^{-5} D_0$, $J_{cf} = 0.05D_0$, $\Delta_0 = 0.6D_0$, $D_0 = 8eV$ , $n_I = 0.9\%$ leading to $T_C \approx 94.4K$.

## 6.5 Controlling the physical properties

In the previous sections we derived the principle behavior of our model in particular as a function of temperature and impurity concentration. We have demonstrated the essentially good agreement with the experimentally observed properties of EuO. Thereby the modification of the impurity concentration is experimentally difficult to achieve since it depends basically on the fabrication process of the compound. In particular for eventual applications it is desirable to have a possibility to adjust the physical properties that can more easily be handled. The canonical approach therefore consists in applying a bias voltage perpendicular to the transport direction of the compound. Thus, the chemical potential $\mu$ in the sample can be adjusted. Concerning our model this amounts in a deviation from the particle number constraint Eq. (5.9). It can certainly be expected that the magnetic and transport properties strongly depend on the overall fermion number.

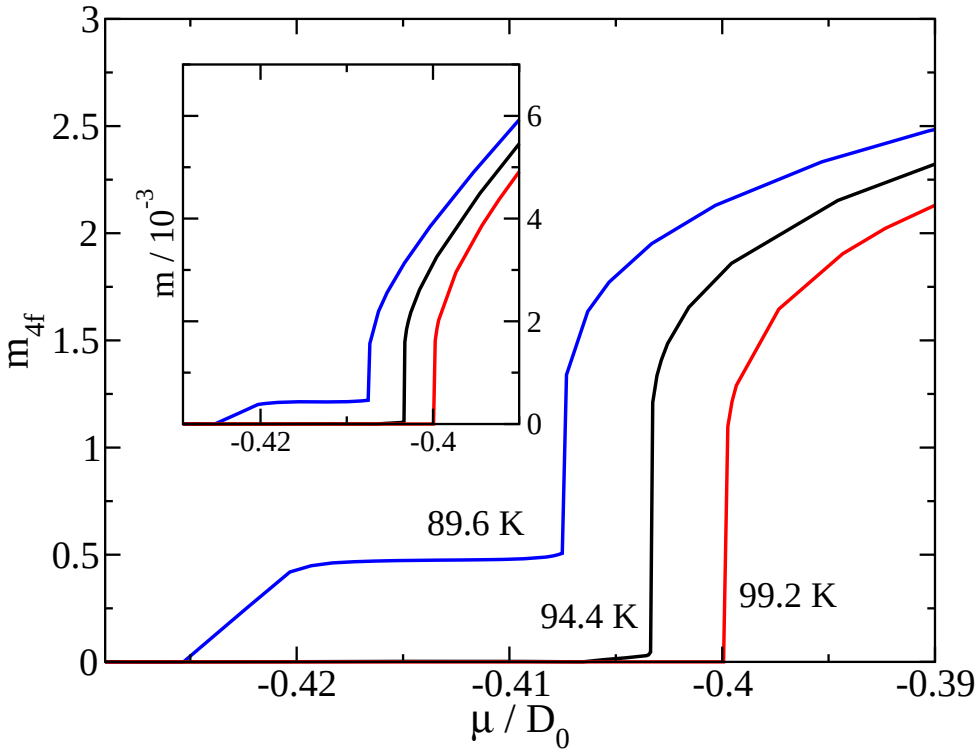


***Figure 6.12:*** Magnetization of the Eu 4f moments and the conduction band (inset) for the parameters as in Fig. 6.11. As expected the increasing conduction electron number can increase the critical temperature such that the magnetization at a given temperature is enhanced.

We investigated the particle number, the magnetization and conductivity as a function of the chemical potential at the temperatures $T = T_C, T = T_C \pm 0.05 T_C$. In Fig. 6.11 we present the total fermion number $N_c + N_d - n_I$ as a function of $\mu$ at an impurity concentration $n_I = 0.9\%$. In this case the critical temperature is $T_C = 94.4K$ (assuming a conduction band width of $D_0 = 8eV$). One can clearly observe a plateau around the chemical potential $\mu_0 \approx -0.41 D_0$ for each investigated temperature. For $\mu \ll \mu_0$ the total fermion number decreases because the impurity states are shifted above the chemical potential. On the other hand if $\mu \gg \mu_0$ the upper conduction band overlaps with $\mu$ leading to an enhanced conduction electron number. This behavior is confirmed in the inset of Fig. 6.11 for $T = T_C$, where the specific occupation number $N_{c,d}$ are presented. From the previous results we know that the critical temperature increases with the total fermion number. Although the origin of the increasing particle number is different in this section we expect the same behavior again. Hence the magnetization at a given temperature should essentially follow Fig. 6.11. We present the calculated

Eu 4f moment magnetization $m_{4f}$ and the conduction band magnetization $m$ (inset) in Fig. 6.12 for the same parameters as in Fig. 6.11. Indeed we obtain a strong $\mu$ dependence of the magnetic properties. For temperatures $T < T_C$ one can thus turnoff the sample magnetization, while for $T > T_C$ the sample becomes ferromagnetic above a certain chemical potential.

Previously we already clarified that the most remarkable feature of EuO consists in the interplay of magnetic and transport properties. Hence, we expect the $\mu$ dependence of the magnetization to be accompanied a drastic change in the conductivity. The result is presented in Fig. 6.13. First, one can see, that the

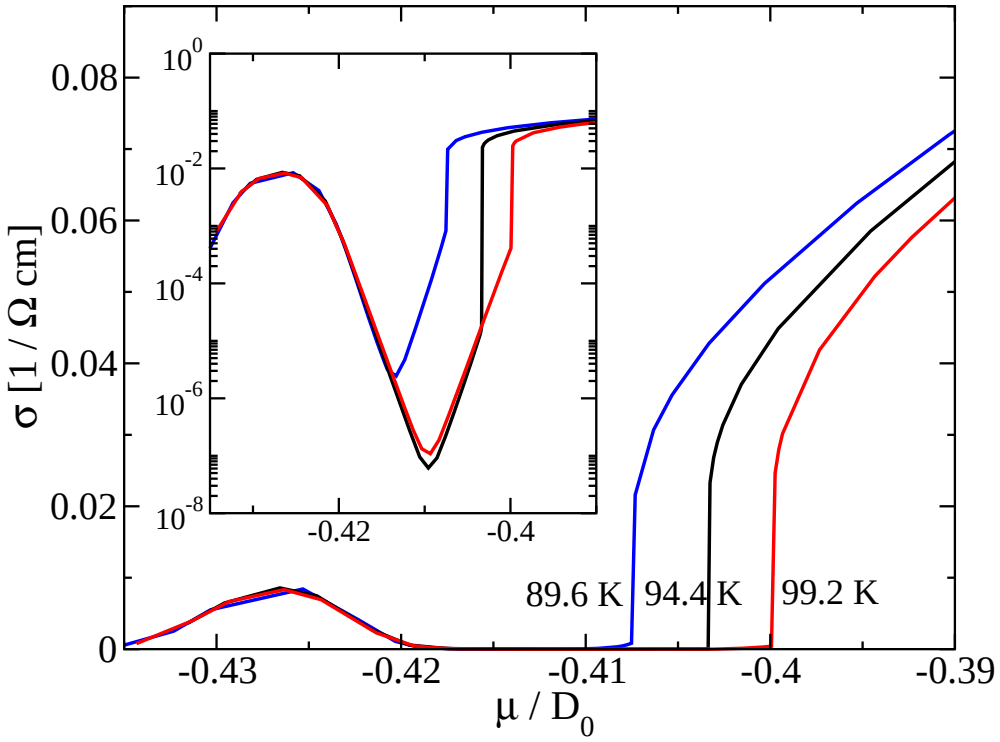


***Figure 6.13:*** Conductivity of the model (parameters like in Fig. 6.11). The $\mu$ dependence of the magnetization is accompanied by a very strong change of the conductivity $\sigma_T(\mu)$ at a given temperature. The conductivity as a function of the chemical potential basically corresponds to the conduction band summed over both spin directions. The inset shows the conductivity on a logarithmic scale. In the gap $\sigma_T(\mu)$ depends exponentially on $\mu$.

conductivity $\sigma_T(\mu)$ as a function of the chemical potential basically corresponds to the conduction band summed over both spin directions. Thus, at the critical temperature $T = T_C$ we observe a gap in the conductivity $\sigma_T(\mu)$ as well. Moreover, in the logarithmic plot (inset of Fig. 6.13) it turns out that the conductivity in the gap depends exponentially on $\mu$, as expected for a semiconductor. At a

certain $\mu_C > \mu_0$ there seems to be a jump in $\sigma_T(\mu)$ which coincides with the onset of the magnetization in Fig. 6.12. We interpret this behavior to be due to the infinite slope at the band edges of the bare conduction band, increasing the conductivity rapidly as soon as the chemical potential is shifted into the band. According to this the $\mu$ dependent as well as the temperature $T$ dependent phase transition would be of $2^{nd}$ order type. Regarding the technical aspect it is remarkable that it is possible to drive such a strong simultaneous phase transition by changing the chemical potential, which can be done in a controlled manner. This may be an interesting perspective for future experiments. The crucial question concerning an eventual application is, if the Curie temperature can be further increased in the voltage-controlled case.

We want to close our investigation of the EuO model with these remarks. As mentioned at the very beginning we strongly focused on the experimentally known properties of EuO and thus we restricted ourselves to the corresponding parameters. In the next chapter we will investigate another possible realization of the general model, which will in particular be paramagnetic at all temperatures.

# 7 A Paramagnetic Model

In any physical model that, as defined in Eqs. (5.6) - (5.8) contains quantum impurities with strong onsite Coulomb repulsion, a serious influence of local moment physics can be expected. In the standard Anderson model this is expressed particularly by the appearance of a Kondo resonance in the impurity density of states at temperatures below the Kondo temperature $T_K$. The physical origin can thereby be traced back to resonant spin flip scattering processes between local conduction band and impurity spin states. We already argued that in the parameter regime reflecting the physical properties of EuO, which is highly spin polarized, we do not expect strong signatures of Kondo behavior.

In the case of a lower conduction band splitting the situation might be completely different. In particular in the limit $J_{cf} \to 0$ where the Eu 4f moments and the conduction band electrons are completely decoupled, the spin degeneracy is recovered . Hence, the resulting Hamiltonian reads

$$H = \sum_{k\sigma} \epsilon_k c^\dagger_{k\sigma} c_{k\sigma} + E_d \sum_{i\sigma} d^\dagger_{i\sigma} d_{i\sigma} + V \sum_{i\sigma} (c^\dagger_{i\sigma} d_{i\sigma} + h.c.) + U \sum_i d^\dagger_{i\uparrow} d_{i\uparrow} d^\dagger_{i\downarrow} d_{i\downarrow} \quad (7.1)$$

As in the previous chapter, we regard the limit $U \to \infty$, leading to a single occupied impurity and the total particle number is conserved according to Eq. (5.9). As in the EuO case we want to emphasize the importance of this condition for the physical properties of the model. In particular in the limit $n_I \to 0$ the system is a perfect insulator at temperature $T = 0K$. The conduction band selfenergy for $J_{cf} = 0$

$$\Sigma_{c\sigma}(\omega) = n_I |V|^2 G_{d\sigma}(\omega) \quad (7.2)$$

is thereby identical to the corresponding quantity Eq. (5.11) in the EuO model with a vanishing 4f moment $\langle S \rangle$. Hence, the high temperature phase of the non-magnetic model Eq. (7.1) should be equivalent to the paramagnetic phase of the corresponding EuO model, provided that all parameters instead of $J_{cf}$ are the same. As before one might therefore choose the center $\Delta_0$ of the bare conduction band and the impurity level $E_d$ such that a gap in the high temperature phase can be observed. However, the low temperature phase will obviously not be ferromagnetic anymore. So far one would therefore assume the conductivity of the system to behave completely like in a semiconductor. In the following we will show that according to our model this will not be the case. At least for a proper choice of the system parameters one can observe a strong metal to insulator transition even in the non-magnetic model.

## 7.1 Density of states

We start our investigation with the conduction band and the impurity density of states, respectively. Since, in the present case the two spin directions are degenerate we restrict ourselves to the investigation of only one spin direction. The system parameters in this section are $E_d = -0.4D_0$, $\Gamma = \pi V^2 = 0.05D_0^2$, $n_I = 5.0\%$ with a varying $\Delta_0 = 0.573..0.576D_0$, adjusting the overlap of the impurity induced side band and the bare conduction band. Hence, compared to the EuO model we have chosen a larger impurity concentration and a lower $\Delta_0$. Thus we expect the gap in the high temperature phase to be smaller than before. In fact it turns out that for those parameters we obtain a small but finite conduction band density of states $A_{c\sigma}(\omega = \mu) = N_0$ at the chemical potential in the high temperature regime. For numerical reasons we need to choose the parameters such that a finite $N_0$ is provided at low temperatures, since the non crossing approximation leads to singularities in the pseudo particle Green's functions as soon as $N_0$ vanishes. We find, that this breakdown of the NCA equations in the low temperature regime coincides with the occurrence of a gap at high temperatures. Hence, we are forced to choose a sufficiently small $\Delta_0$. In the following we try to approach the upper numerically possible limit of $\Delta_0$ in order to observe an eventual metal to insulator transition as a function of temperature.

First, we regard the temperature dependence of the conduction band density of states $A_{c\sigma}(\omega)$ at the maximum of the numerically possible $\Delta_0$. The result is presented in Fig. 7.1. As predicted the high temperature phase exhibits a deep dip around the chemical potential, already indicating a low conductivity. The difference $\Delta_0 - E_d$ is thereby obviously not large enough to give rise to a real gap. With decreasing temperature we observe a very strong peak emerging around the chemical potential which could not be found in the polarized EuO case. To explain the origin of the peak in $A_{c\sigma}(\omega)$ we compare it to the impurity density of states $A_{d\sigma}(\omega)$, which is presented in Fig. 7.2. One can clearly see a Kondo resonance emerging in $A_{d\sigma}(\omega)$ simultaneously with the conduction band peak at the chemical potential. Regarding the conduction band selfenergy Eq. (7.2) we conclude that the Kondo resonance in $A_{d\sigma}(\omega)$ is induced to the conduction band in the same way like the already discussed side band structure. Thus, one can proof the finite low temperature conduction band density of state $A_{c\sigma}(\omega = \mu) = N_0$ at the chemical potential to be due to a resonant spin flip interaction between the conduction band and the impurity states. On the other hand one knows that the Kondo temperature $T_K$ which provides the dominant energy scale for those processes is exponentially suppressed with vanishing $N_0$. Therefore one could not observe a Kondo peak in the impurity density of states without the peak in $A_{c\sigma}(\omega)$ and vice versa. In that sense on can understand the Kondo resonance in the present case to be *self-organized* or at least *self-amplified*, meaning that it creates its own density of states at the Fermi energy.

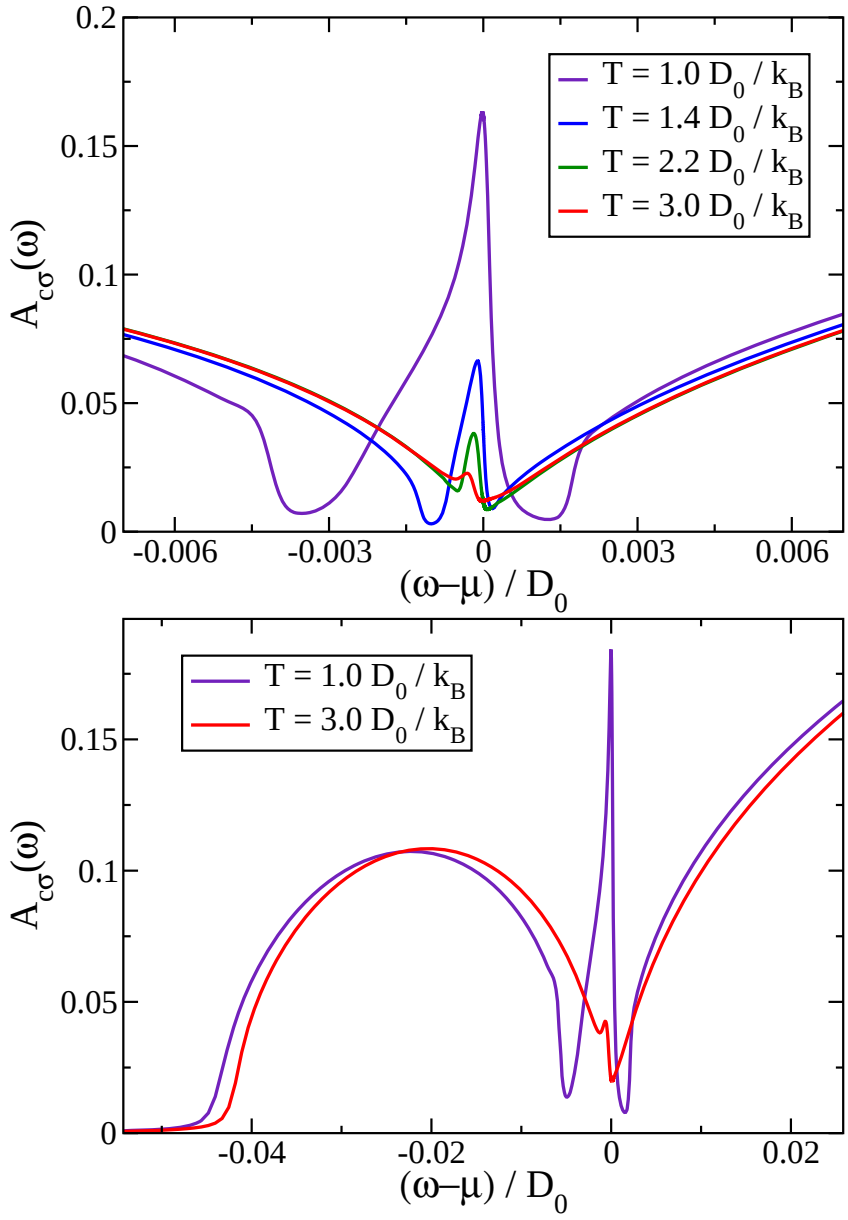


***Figure 7.1:*** Conduction band density of states $A_{c\sigma}(\omega)$ at several temperatures relative to the chemical potential $\mu$ in units of half conduction band width. The parameters are $E_d = -0.4D_0$, $\Gamma = \pi V^2 = 0.05D_0^2$, $n_I = 5.0\%$, $\Delta_0 = 0.576D_0$. A narrow resonance at $\omega \approx \mu$ occurs in the (metallic) low temperature regime.

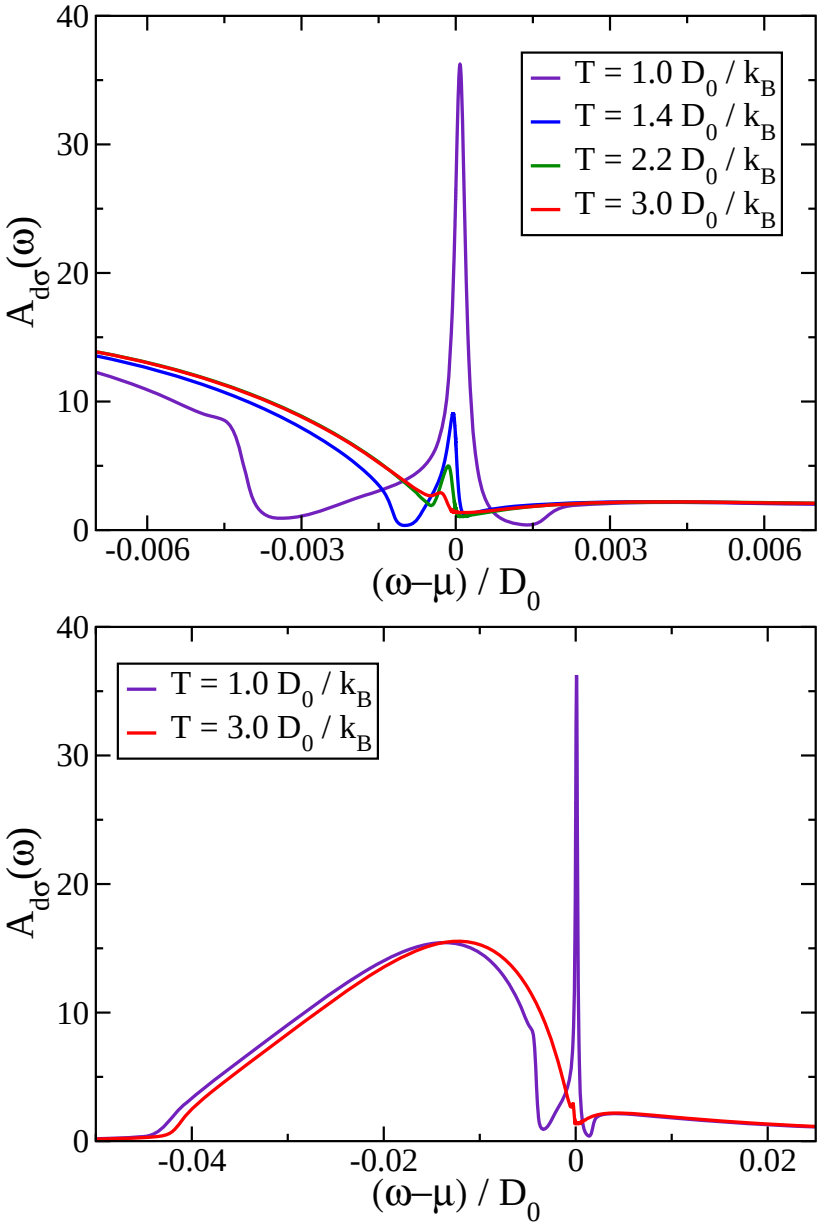


***Figure 7.2:*** Impurity density of states $A_{d\sigma}(\omega)$ at several temperatures relative to the chemical potential $\mu$. The system parameters are as in Fig. 7.1. We observe a Kondo resonance at $\omega = \mu$ corresponding to the central peak in $A_{c\sigma}(\omega)$.

In the following we have to discuss under which circumstances such a selfconsistent Kondo resonance like in Fig. 7.1 and Fig. 7.2 can occur. The most striking question is, how low $N_0$ is allowed to be in the high temperature phase if one wants to observe a Kondo resonance at low temperatures. Therefore we investigate the $\Delta_0$ dependence of the Kondo resonance. The results are presented in Fig. 7.3 and Fig. 7.4 , where we calculate the conduction band and the impurity density of states at $k_BT = 1.0D_0$ for various $\Delta_0$. All other parameters are chosen as in Fig. 7.1. The Kondo resonance at $\omega - \mu = 0$ obviously decreases

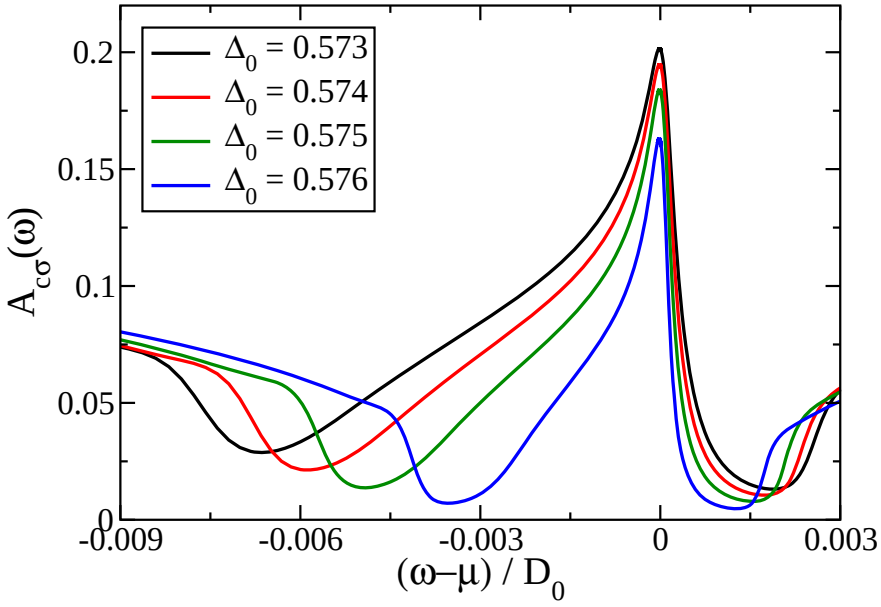


***Figure 7.3:*** Conduction band density of states at $k_BT = 1.0D_0$ related to the chemical potential $\mu$. The impurity induced Kondo resonance at $\omega - \mu \approx 0$ can be observed for various $\Delta_0$.

with increasing $\Delta_0$. Regarding the impurity density of states $A_{d\sigma}(\omega)$ in Fig. 7.4 it becomes particularly clear that besides the physical property of vanishing conduction band density of states one encounters severe numerical problems. Namely $A_{d\sigma}(\omega)$ becomes successively narrower the larger $\Delta_0$ gets. In that case the pseudo particle Green's function $A_{f,b}(\omega)$ defined in Chapter 4 are numerically very difficult to resolve at low temperatures. Finally, this leads to a breakdown of the selfconsistence loop at a certain $\Delta_0 = \Delta_{max}$. However, our numerical results suggest the assumption that $\Delta_{max}$ corresponds to the point where the overlap between the impurity induced side band and the upper conduction band is vanishing, leading to a gap in the high temperature phase. A finite overlap would lead to a low but finite density of states at the chemical potential as it is observed in Fig. 7.1. Consequently, we propose that the existence of a Kondo resonance

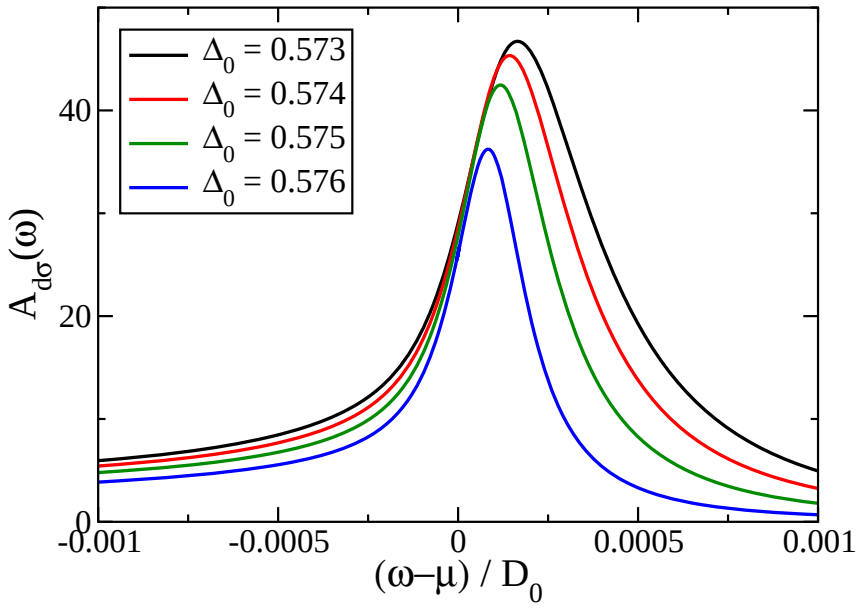


***Figure 7.4:*** Impurity density of states at $k_BT = 1.0D_0$ related to the chemical potential $\mu$. The Kondo resonance at $\omega - \mu \approx 0$ is decreasing with increasing $\Delta_0$.

in the low temperature regime is only possible for a bare conduction band centered at $\Delta_0 \leq \Delta_{max}$, while a gap in the high temperature phase would open at $\Delta_0 > \Delta_{max}$. Therefore the system is expected to obtain a gap at all temperatures ($\Delta_0 > \Delta_{max}$), while in the complementary parameter regime ($\Delta_0 \leq \Delta_{max}$) the density of states $N_0$ at the chemical potential remains finite.

## 7.2 Conductivity

In the case $\Delta_0 > \Delta_{max}$ the conductivity behaves like in a semiconductor. We calculate the conductivity for $\Delta_0 \leq \Delta_{max}$ using Eq. (5.28). Since the conduction band density of states at the chemical potential $N_0$ exhibits a pronounced peak at low temperatures in this regime, the conductivity is expected to be considerable large. Although the high temperature phase will obtain no gap in the conduction band, we expect a strong reduction of the conductivity, compared to the low temperature regime, since $N_0$ remains finite, but can at least be very low (cf. Fig. 7.1). In Fig. 7.5 we present the temperature dependent conductivity $\sigma(T)$ for various different $\Delta_0$. One can clearly observe a minimum of $\sigma(T)$ at a critical temperature $T_K$, which we identify with the Kondo temperature. Below $T_K$ the system is clearly in a metallic phase, while the minimum $\sigma(T_K)$ is up to three orders of magnitude below its maximum value. As expected the depth of the minimum thereby depends on $\Delta_0$, where we obtain the numerical maximum

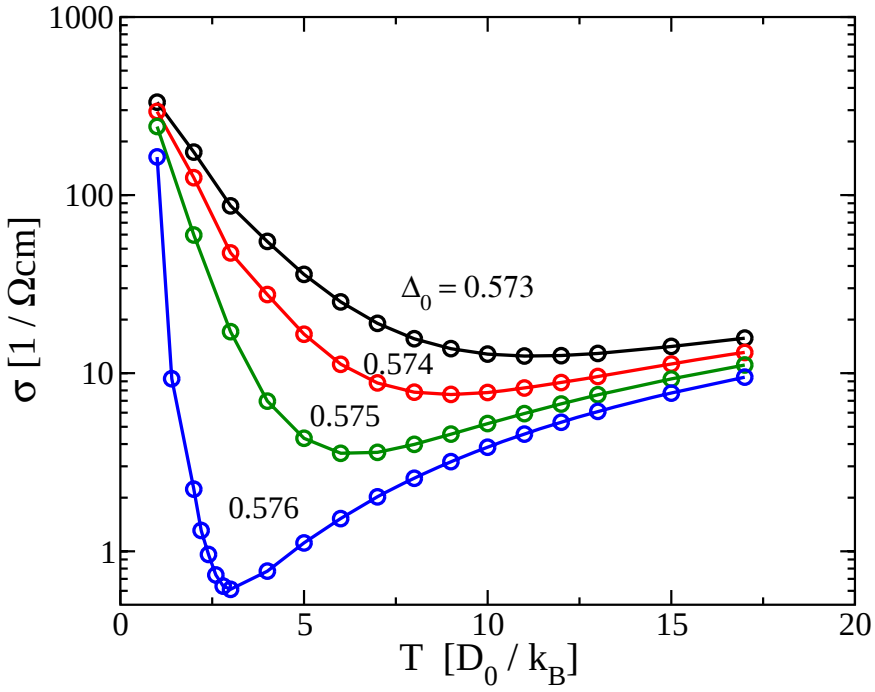


***Figure 7.5:*** Temperature dependent conductivity $\sigma(T)$ for various different $\Delta_0$. A strong drop of $\sigma(T)$ can be observed with increasing temperature $T \to T_K$, which we identify with the Kondo temperature. At $T_K$ the Kondo resonance in Fig. 7.1 and Fig. 7.2 breaks down, coinciding with the minimum of $\sigma(T)$.

$\Delta_{max} \approx 0.576 D_0$ for the chosen set of parameters. One should emphasize, that one might obtain a better approximation of $\Delta_{max}$ by means of different techniques instead of the NCA. For the future the paramagnetic model, as described in the present chapter may be worth to be treated from a principle point of view, employing for instance NRG-methods, which is not done in the present thesis since we are mainly dealing with the EuO-regime. However, we have demonstrated that in addition to the magnetic phase transition in EuO parameter regime, the general model contains a parameter subspace where a metal to insulator (or at least bad metal) transition can be observed. The underlying physics of this second type of transition is thereby in principle different from the previous one. In particular in the limit $\Delta_0 \approx \Delta_{max}$ the change in the conductivity is sufficiently large to predict an experimentally observable effect.

# 8 Summary

In the present thesis we investigate the ferromagnetic semiconductor europium monoxide in the off-stoichiometric $EuO_{1-x}$ and in the Gd-doped case $Gd_xEu_{1-x}O$. Both compounds are known to possess spectacular physical properties. While the high temperature phase corresponds to a paramagnetic semiconductor, one observes a ferromagnetic phase below the Curie temperature accompanied by a tremendously increasing conductivity. The corresponding electrical current appears to be nearly 100 % spin polarized. The strength of the resistivity change as well as the Curie temperature thereby strongly depend on the doping concentration. From x-ray absorption spectroscopy experiments it is well know that the magnetic phase transition causes a spin dependent band splitting of the Eu 5d conduction band.

**The EuO model:**

We develop a detailed theory containing what we consider the major constituents of these compounds. The model we propose consists of two subsystems coupled to a conduction band of Bloch electrons. The magnetic behavior turns out to be determined by the Eu 4f moments forming a Heisenberg ferromagnet, where the indirect exchange coupling is basically due to an induced magnetization of the valence band (Bloembergen-Rowland exchange). Furthermore the 4f spins with S=7/2 are coupled to the conduction band via an s-d type exchange interaction. For the Eu-rich $EuO_{1-x}$ and for $Gd_xEu_{1-x}O$ we need to supply a dilute concentration of impurities, providing excess charge carriers to the system. Theoretically this effect is incorporated by adding a second subsystem consisting of dilute Anderson impurities with an infinity local Coulomb repulsion acting on each impurity site. Hence, we conclude that the impurity level induced by the O-vacancies (each providing two excess electrons) as well as the trivalent Gd-state replacing a divalent Eu finally are only singly occupied. Due to the fact that the stoichiometric compound is a semiconductor with a large energy gap of 1.2 eV we conclude that the overall electron number must solely be provided by the excess charge carriers stemming from the dilute impurities.Together with the single occupancy we therefore claim that the total number of free electrons must be equal to the impurity concentration $n_I = x$. Note, that the limit $n_I \to 0$ is therefore included in a natural way within our model.

The goal of our project was to find a microscopic model that explains in particular the simultaneity of the magnetic phase transition and the change of the transport properties on the same footing. Hence, the model needs to be treated fully selfconsistently, in contrast to previous theoretical studies. Because of the complexity of each single constituent we decided to treat the magnetic part of the Hamiltonian within mean field approximation. The resulting physical interpretation turns out to be appealingly simple. Namely the local 4f moment are aligned by an effective magnetic field due to the conduction band magnetization acting on the Eu 4f Heisenberg ferromagnet and vice versa. Thereby the strength of the total conduction band magnetization obviously scales with the total electron number and hence with the impurity concentration. According to this the $n_I$ dependence of the Curie temperature is simply explained by the increasing electron number. This effect is even enhance by the polarization of the impurity states, forming local moments due to a strong onsite Coulomb repulsion.

The second effect of the finite impurity concentration amounts in the change of the transport properties in the low temperature phase. We solved the Anderson impurity part of the Hamiltonian by means of an impurity averaged non crossing approximation. In this case the impurities on the neighboring sites induce an additional side band around the single impurity level to the conduction band density of states. If the splitting of the conduction band which is induced by the polarized Eu 4f moments is large enough, its majority spin components finally has to overlap with the impurity induced side band. In this case the chemical potential has to be located somewhere in the conduction band because of particle number conservation. Hence, the low temperature phase needs to be metallic amounting in a finite conductivity which we calculate within linear response theory. The results we obtain according to the described procedure turn out to be in remarkable good agreement with the experiments. In particular we confirm the simultaneity of the phase transition and we reproduce the principle shape of the temperature dependent magnetization and resistivity. At least for low impurity concentrations $n_I \leq 4\%$ we find the Curie temperature increasing with $n_I$, while for larger concentration the model probably needs to be extended. However, the comparison to the experiment is still quite difficult because it is experimentally complicated to determine the correct impurity concentration.

As a perspective for future experiments and applications we also investigated the physical properties at different chemical potentials, starting from the value corresponding to the particle number constraint. We obtain, that the conductivity and the magnetization can be tuned via an applied gate voltage determining the chemical potential and hence the band filling. As a consequence we can either increase or decrease the Curie temperature at a given impurity concentration. To our knowledge there are no experiments up to now, investigating this behavior systematically. In particular for possible spintronics applications a voltage driven polarized metal to semiconductor metal would be of great interest.

**The paramagnetic model:**

Furthermore, we took a closer look at the non-magnetic model one obtains when decoupling the Eu 4f moment and the conduction band. Although this model does not describe EuO anymore it might be of principle interest. Physically it describes a conduction band coupled to dilute Anderson impurity with the chemical potential in the vicinity of the lower (bare) conduction band edge. As before we observe the formation of an impurity induced side band. Additionally we can clearly observe a Kondo resonance in the low temperature regime, which is emerging in the conduction band at the Fermi energy. Since the Kondo temperature $T_K$ is increasing with the density of states at the Fermi energy one can consider the observed effect to be self-amplified. As expected the Kondo resonance vanishes in the high temperature regime leaving a dip in the conduction band at the chemical potential. The depth of the dip depends on the distance between the bare conduction band and the impurity level. Hence, we obtain a high temperature phase with a conductivity that is up to 3 orders of magnitude below its maximum value at temperatures $T \ll T_K$.

**Outlook:**

Finally, the investigated model turns out to include two possible metal to insulator transitions. Both are caused by the dilute Anderson impurities but with a completely different origin. While the EuO phase transition is basically due to the magnetism of the 4f moments, the Kondo driven transition is dynamically generated between the impurity and the conduction band states. Even more, the two transitions appear to be in competition with each other. Namely a finite magnetization in the conduction band suppresses possible spin flip scattering processes leading to a Kondo resonance. For further investigations we suggest to consider systematically the crossover from the one regime to the other, using appropriate techniques, like for instance the NRG method.

# 9 Deutschsprachige Zusammenfassung

In der vorliegenden Arbeit untersuchen wir den ferromagnetischen Halbleiter Europiummonoxid. Im Mittelpunkt des Interesses stehen hierbei die Doping-Abhängigkeit, einmal für das nicht-stöchiometrische $EuO_{1-x}$ und desweitern für $Gd_xEu_{1-x}O$. In beiden Fällen lassen sich hierbei sehr eindrucksvolle physikalische Eigenschaften beobachten. Wie im stöchiometrischen Fall besteht die Hochtemperaturphase aus einem paramagnetischen Halbleiter. Unterhalb der kritischen Temperatur vollzieht das System einen magnetischen Phasenübergang der von einem dramatischen Abfall des spezifischen elektrischen Widerstands begleitet wird. Desweiteren ist der resultierende elektrische Strom zu fast 100 % spinpolarisiert. Sowohl die Intensität des Übergangs als auch die Curie-Temperatur hängen hierbei stark von der Störstellenkonzentration ab. Aus spektroskopischen Messungen der Bandstruktur ist bekannt, dass das Eu 5d Leitungsband unterhalb $T_C$ in zwei Spinkomponenten aufspaltet.

**Das EuO Modell:**

Ausgehend von den experimentellen Resultaten entwickeln wir ein theoretisches Model. Hierbei berücksichtigen wir insbesondere zwei Teilsysteme, die an ein elektronisches Leitungsband ankoppeln. Die magnetischen Eigenschaften sollen reproduziert werden durch die Kopplung an die lokalen Eu 4f-Momente, die mittels eines ferromagnetischen Heisenberg-Modells beschrieben werden. Die zugehörige 4f-Austauschwechselwirkung kann auf die lokale Magnetisierung des Valenzbandes (Bloembergen-Rowland Austausch) zurückgeführt werden. Die polarisierten 4f-Momente koppeln weiterhin effektiv an das elektronische Leitungsband. Sowohl für das sauerstoffverarmte $EuO_{1-x}$ als auch für $Gd_xEu_{1-x}O$ muss zusätzlich eine endliche Konzentration $n_I = x$ an Störstellen in das System eingebracht werden, damit freie Ladungsträger zur Verfügung gestellt werden.

Diesem Effekt wird durch das Ankoppeln einer verdünnten Konzentration aus Anderson -Störstellen Rechnung getragen, wobei die lokale Coulomb-Abstoßung auf jeder Störstelle als unendlich stark angenommen wird. Demzufolge können wir sowohl für $EuO_{1-x}$ als auch für $Gd_xEu_{1-x}O$ jede Störstelle als einfach besetzt annehmen. Hieraus und aus dem Verschwinden des Metal-Halbleiter Übergangs im stöchiometrischen Fall ohne Störstellen folgern wir, dass die totale Beset-

zungszahl pro Gitterplatz von Elektronen im Leitungsband gleich der zugehörigen Störstellendichte sein muss. Insbesondere der Grenzfall des stöchiometrischen EuO ist hierdurch auf natürliche Weise gewährleistet.

Das wesentliche Ziel der vorliegenden Arbeit war es, ein mikroskopisches Modell zu entwickeln, das die experimentell beobachteten simultanen Phasenübergänge in gedopten EuO im vollen Umfang selbskonsistent behandelt. Aufgrund der Komplexität des Gesamtsystems behandeln wir die Eu-4f Momente und deren Kopplung an das Leitungsband im Rahmen einer Molekularfeldtheorie. Die physikalische Interpretation erweist sich hierbei als sehr instruktiv, indem die Eu-4f Momente und die Spins des Leitungsbandes wechselseitig in dem effektiven Magnetfeld des jeweils anderen Systems ausgerichtet werden. Da die Stärke der gesamten Leitungsband-Magnetisierung mit der Störstellenkonzentration skaliert, lässt sich so das Verhalten der Curie-Temperatur in Abhängigkeit von $n_I$ erklären. Neben den magnetischen werden insbesondere die Transporteigenschaften durch eine endliche Störstellenkonzentration beeinflußt. Der Anderson-Störstellen Hamiltonian wird mittels der sogenannten Non-Crossing-Approximation diagrammatisch behandelt. Aufgrund der selbstkonsistenten Kopplung an die benachbarten Störstellen wird ein zusätzliches Seitenband auf Höhe der Störstellenniveaus in der Leitungsband-Zustandsdichte induziert. Für den Fall, dass die spinabhängige Aufspaltung des Leitungsbandes stark genug ist, kommt es zu einem Überlapp zwischen dem Majoritätsspin-Band und dem induzierten Seitenband. Folglich muss das chemische Potential aufgrund der Teilchenzahlerhaltung im Leitungsband liegen. Demzufolge ist die magnetische Tieftemperaturphase metallisch, was sich in der mittels Linear Response Theory berechneten Leitfähigkeit widerspiegelt. Die so erhaltenen Resultate für die Magnetisierung und den elektrischen Widerstand sind qualitativ in sehr guter Übereinstimmung mit den Experimenten. Insbesondere das simultane Auftreten der Phasenübergänge wird aufgrund des zugrundeliegenden Prinzips erklärt. Für nicht zu große Störstellenkonzentrationen $n_I \leq 4\%$ finden wir eine mit $n_I$ ansteigende Curie-Temperatur, analog zu den experimentellen Befunden. Im Falle größerer $n_I$ ist zu erwarten, dass unser Modell erweitert werden muss, obwohl aufgrund der experimentell komplizierten Bestimmung der Störstellenkonzentration noch keine sehr genauen Daten existieren.

Zusätzlich zu den bisherigen Betrachtungen haben wir die Änderung der magnetischen und der Transporteigenschaften unter Anwendung einer Gate-Spannung untersucht. Hierdurch kann experimentell das chemische Potential in der Probe verändert werden. Dies entspricht einer Änderung der Bandfüllung, wodurch insbesondere die oben erwähnte Teilchenzahlbedingung nicht mehr erfüllt sein muss. Als Konsequenz kann sowohl die Magnetisierung als auch die Leitfähigkeit, die immer noch an die magnetischen Eigenschaften gekoppelt ist spannungsabhängig gesteuert werden. Ausgehend von dieser Vorhersage möchten wir eine experimentelle Untersuchung dieses Effekts anregen, insbesondere in Hinblick auf die eventuelle Anwendbarkeit im Bereich der Spintronic.

**Das paramagnetische Modell:**

Neben dem EuO Modell betrachten wir ein paramagnetisches Modell, ausgehend von dem selben Hamiltonian, wobei die Eu 4f-Momente entkoppelt werden. Obwohl das so definierte Modell nicht mehr EuO beschreibt, ist die Untersuchung von grundsätzlichem Interesse. Wir untersuchen also ein System in dem verdünnte Anderson-Störstellen an ein Leitungsband gekoppelt werden, wobei die Störstellenniveaus in der Umgebung der unteren Kante des ungestörten Leitungsbandes liegen. Wie erwartet beobachten wir demzufolge die Formierung eines störstelleninduzierten Seitenbandes. Für tiefe Temperaturen beobachten wir zusätzlich das Auftreten einer Kondo-Resonanz an der Fermienergie, sowohl in der Green's Funktion der Störstelle als auch in der des Leitungsbandes. Da die Kondo-Temperatur direkt von der Leitungsbandzustandsdichte an der Fermienergie abhängt, kann man die Resonanz als sich selbst erzeugend betrachten. Für Temperaturen oberhalb der Kondo-Temperatur verschwindet die Kondo-Resonanz wie erwartet. Als Konsequenz erhalten wir ein lokales Minimum der Zustandsdichte an der Fermienergie, dessen Wert unmittelbar durch den Abstand zwischen ungestörtem Leitungsband und Störstellenniveau bestimmt wird. Im besten Fall beobachten wir ein Anwachsen der Leitfähigkeit um bis zu 3 Größenordnungen für tiefe Temperaturen.

**Ausblick:**

Insgesamt gibt es im betrachteten Modell einen magnetischen Phasenübergang, der direkt an einen Übergang in den Transporteigenschaften des Systems gekoppelt ist. Desweiteren gibt es einen Metal-Isolator Übergang der zwar ebenso an die Existenz von Störstellen gebunden ist, aber dem ein prinzipiell anderer Mechanismus zugrunde liegt. Es ist sogar so, dass, aufgrund des polarisierten Leitungsbandes und der dadurch verminderten Spin-Flip Streuung, die endliche Magnetierung eine mögliche Kondo-Resonanz unterdrückt . Für zukünftige Untersuchungen wäre es interessant den Übergang zwischen beiden Modellen mit geeigneten Methoden (z.B. Numerical Renormalization Group, etc. ) systematisch zu untersuchen.

# A Impurity averaged conduction electron selfenergy

In Chapter 3 we showed that the conduction electron selfenergy for a dilute impurity concentration yields

$$\Sigma_{k\sigma}(i\omega_n) = n_I \cdot t_\sigma(i\omega_n) = n_I \cdot |V|^2 G_{d\sigma}(i\omega_n) \tag{A.1}$$

To derive the selfenergy we calculate the impurity averaged second summand of the Dyson equation, sketched in Fig. A.1, using $t_i = t_\sigma(i\omega_n)$ and $G$ the bare electron propagator

$$\begin{aligned}
\langle ... \rangle_{imp} &= \prod_{j=1}^{N} \int \frac{d^3R_j}{V} \sum_{i=1}^{N} t_i G\left(R_i, x\right) G\left(x', R_i\right) && \text{(A.2)} \\
&= \prod_{j=1}^{N} \int \frac{d^3R_j}{V} \sum_{i=1}^{N} \sum_{k,k'} \frac{e^{iR_i(k-k')}}{(2\pi)^3} e^{-ikx} e^{ik'x'} G_k G_{k'} && \text{(A.3)} \\
&= \frac{1}{V} \sum_{i,k} \prod_{j \neq i} \int \frac{d^3R_j}{V} t_i G_k^2 e^{-ik(x-x')} = \frac{N}{V} t_i \sum_k G_k^2 e^{-ik(x-x')} && \text{(A.4)}
\end{aligned}$$

The prefactor of the squared Green's function yields the electron selfenergy according to Eq. (A.1), since $N$ is the total impurity number and $V$ is the corresponding volume.

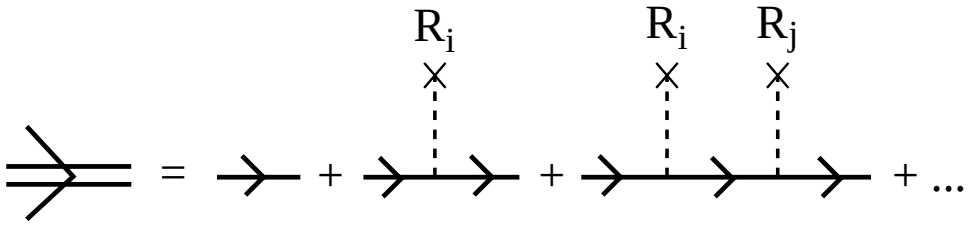


***Figure A.1:*** Diagrammatic expansion of the conduction electron Green's function with impurity scattering at sites $R_i$.

# B Derivation of the current operator

In Chapter 5 we derived the current Eq. (5.24), using the commutator $[H, \rho(\vec{q})]$ of the Hamiltonian and the total charge density. Here, we present the contributing constituents in detail.

$$H = H_c + H_d + H_{hyb} + H_{4f} + H_{c4f} \tag{B.1}$$

$$H_c = \sum_{k\sigma} (\epsilon_k - \mu) c^\dagger_{k\sigma} c_{k\sigma} \tag{B.2}$$

$$H_d = E_d \sum_{i\sigma} d^\dagger_{i\sigma} d_{i\sigma} \qquad H_{hyb} = V \sum_{i\sigma} (c^\dagger_{i\sigma} d_{i\sigma} + h.c.) \tag{B.3}$$

$$H_{4f} = -\sum_{i,j} J_{i,j} \vec{S}_i \vec{S}_j \quad H_{c4f} = -J_{cf} \sum_i \vec{\sigma}_i \vec{S}_i \tag{B.4}$$

The total charge density operator is given by

$$\rho(\vec{q}) = \sum_{k\sigma} c^\dagger_{k-q,\sigma} c_{k\sigma} + \sum_{j\sigma} e^{-i\vec{q}\vec{R}_j} d^\dagger_{j\sigma} d_{j\sigma} \tag{B.5}$$

$$= \sum_{i\sigma} e^{-i\vec{q}\vec{R}_i} c^\dagger_{i\sigma} c_{i\sigma} + \sum_{j\sigma} e^{-i\vec{q}\vec{R}_j} d^\dagger_{j\sigma} d_{j\sigma} \tag{B.6}$$

where the $j$ summation runs over the impurity distribution and the $i$-summation over the local conduction electron states at site $\vec{R}_i$ in the corresponding basis. Thus, all commutators including only local particle number operators vanish

$$[\rho(\vec{q}), H_d] = [\rho(\vec{q}), H_{4f}] = [\rho(\vec{q}), H_{c4f}] = 0 \tag{B.7}$$

In the following we will derive the remaining two commutators.

$$[\rho(\vec{q}), H_c] = \sum_{kp,\sigma\tau} \left[ c^\dagger_{k-q\sigma} c_{k\sigma}, c^\dagger_{p\tau} c_{p\tau} \right] (\epsilon_p - \mu)$$

$$= \sum_{kp,\sigma\tau} \left( c^\dagger_{k-q\sigma} c_{k\sigma} c^\dagger_{p\tau} c_{p\tau} - c^\dagger_{p\tau} c_{p\tau} c^\dagger_{k-q\sigma} c_{k\sigma} \right) (\epsilon_p - \mu)$$

$$= \sum_{kp,\sigma\tau} \left( c^\dagger_{k-q\sigma}(\delta_{pk}\delta_{\tau\sigma})c_{p\tau} + c^\dagger_{k-q\sigma}c^\dagger_{p\tau}c_{p\tau}c_{k\sigma} - c^\dagger_{p\tau}c_{p\tau}c^\dagger_{k-q\sigma}c_{k\sigma} \right) (\epsilon_p - \mu)$$
$$= \sum_{k\sigma} c^\dagger_{k-q\sigma}c_{k\sigma}\,(\epsilon_k - \mu) - \sum_{kp,\sigma\tau} c^\dagger_{p\tau} \left\{ c^\dagger_{k-q\sigma}, c_{p\tau} \right\} c_{k\sigma}\,(\epsilon_p - \mu)$$

Hence the contribution of the free electron Hamiltonian yields

$$[\rho(\vec{q}), H_c] = \sum_{k\sigma} (\epsilon_k - \epsilon_{k-q})\, c^\dagger_{k-q\sigma}c_{k\sigma} \tag{B.8}$$

The commutator due to the hybridization Hamiltonian reads

$$\begin{aligned}[\rho(\vec{q}), H_{hyb}] &= V \sum_{i\sigma} e^{-i\vec{q}\vec{R}_i} \sum_{j\tau} \left[ c^\dagger_{i\sigma}c_{i\sigma}, c^\dagger_{j\tau}d_{j\tau} + d^\dagger_{j\tau}c_{j\tau} \right] \\ &+ V \sum_{j\sigma} e^{-i\vec{q}\vec{R}_j} \sum_{i\tau} \left[ d^\dagger_{j\sigma}d_{j\sigma}, c^\dagger_{i\tau}d_{i\tau} + d^\dagger_{i\tau}c_{i\tau} \right]\end{aligned}$$

Therefore one has to evaluate

$$\left[ c^\dagger_{i\sigma}c_{i\sigma}, c^\dagger_{j\tau}d_{j\tau} \right] = c^\dagger_{i\sigma}c_{i\sigma}c^\dagger_{j\tau}d_{j\tau} - c^\dagger_{j\tau}d_{j\tau}c^\dagger_{i\sigma}c_{i\sigma}$$
$$c^\dagger_{i\sigma} \left\{ c_{i\sigma}, c^\dagger_{j\tau} \right\} d_{j\tau} = c^\dagger_{i\sigma}d_{j\tau}\delta ij\delta\tau\sigma$$

Utilizing the relation $\left[A, B^\dagger\right] = \left[B, A^\dagger\right]^\dagger$ for two operators $A, B$ and by interchanging $d, c$ one can obtain all relations needed

$$\Rightarrow \left[ c^\dagger_{i\sigma}c_{i\sigma}, c^\dagger_{j\tau}d_{j\tau} \right] = c^\dagger_{i\sigma}d_{j\tau}\delta ij\delta\tau\sigma \qquad \left[ c^\dagger_{i\sigma}c_{i\sigma}, d^\dagger_{j\tau}c_{j\tau} \right] = -d^\dagger_{j\tau}c_{i\sigma}\delta ij\delta\tau\sigma$$
$$\left[ d^\dagger_{j\sigma}d_{j\sigma}, d^\dagger_{i\tau}c_{i\tau} \right] = d^\dagger_{i\sigma}c_{i\tau}\delta ij\delta\tau\sigma \qquad \left[ d^\dagger_{j\sigma}d_{j\sigma}, c^\dagger_{i\tau}d_{i\tau} \right] = -c^\dagger_{i\tau}d_{i\sigma}\delta ij\delta\tau\sigma$$

Hence one obtains for the commutator including the hybridization term

$$[\rho(\vec{q}), H_{hyb}] = 0 \tag{B.9}$$

Consequently the total commutator is given by

$$[\rho(\vec{q}), H] = \sum_{k\sigma} (\epsilon_k - \epsilon_{k-q})\, c^\dagger_{k-q\sigma}c_{k\sigma} \tag{B.10}$$

reflecting the fact that the current in the system is only carried by the conduction electron states.

# C Pseudo particle spectral functions

Previously, we restricted ourselves to the presentation of the physical electron Green's function $G_d(\omega)$ which is derived via a convolution of pseudo particle Green's functions $A_{f,b}(\omega)$ yielding

$$A_{f\sigma}(\omega) = \frac{1}{\pi}\frac{\mathrm{Im}\Sigma_{f\sigma}(\omega)}{(\omega+\mu+\lambda_0-i0-E_d-\mathrm{Re}\Sigma_{f\sigma}(\omega))^2+\mathrm{Im}\Sigma_{f\sigma}(\omega)^2} \quad \text{(C.1)}$$

$$A_b(\omega) = \frac{1}{\pi}\frac{\mathrm{Im}\Sigma_b(\omega)}{(\omega+\lambda_0-i0-\mathrm{Re}\Sigma_b(\omega))^2+\mathrm{Im}\Sigma_b(\omega)^2} \quad \text{(C.2)}$$

where the corresponding selfenergies are obtained by the NCA Eqs. (5.15)-(5.16). For completeness we will therefore present the pseudo particle spectral function in the following. We choose the same set of parameter like in Chapter 6 at a constant impurity concentration $n_I = 0.9\%$.

As before, we distinguish between the ferromagnetic and the paramagnetic phase for the EuO model. The pseudo fermion Green's function is either spin dependent ($T < T_C$) or degenerate ($T > T_C$). It is remarkable that in the high temperature regime $A_{f\sigma}$ appears to be very narrow around the chemical potential, while $A_b$ (Fig. C.2) possesses a peak at $\omega_0 \approx -(E_d-\mu)+\Sigma_b(\omega_0)$ corresponding to the renormalized impurity level relative to the chemical potential. Furthermore, no Kondo resonance is observed at $\omega-\mu \approx 0$ , implying that the critical temperature $T_C \gg T_K$ is well above the Kondo temperature $T_K$. For $T < T_C$ $A_{f\sigma}$ is broadened as compared to the high temperature regime and obtains its maximum value at $\omega_0 \approx -(E_d-\mu)+\Sigma_\sigma(\omega_0)$. The slave boson function $A_b$ is located around the chemical potential. The latter is due to the particle number condition Eq. (5.9) enforcing the physical Green's function to energies in the vicinity of the chemical potential. Physically this can be understood by the depopulation of the impurity d-level in the low temperature regime. Hence, the d-Green's function must obtain a significant overlap with the chemical potential. As a result of the convolution between $A_{f\sigma}$ and $A_b$ the slave boson function therefore also exhibits a similar behavior.

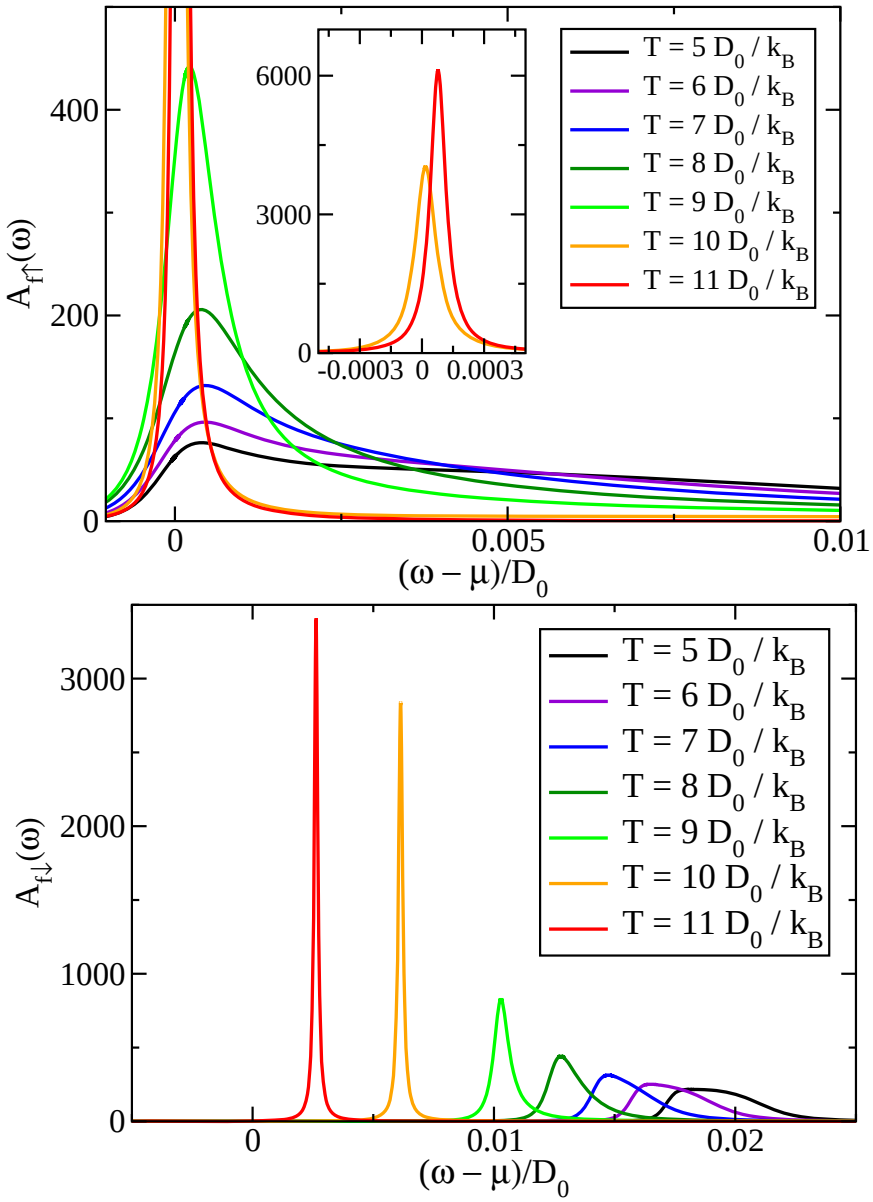


***Figure C.1:*** Imaginary part of the pseudo fermion Green's function for both spin directions. The impurity concentration is $n_I = 0.9\%$. Spin degeneracy is lifted below the Curie temperature. In the paramagnetic phase $A_{f\sigma}$ is spin degenerate and sharply centered close to the chemical potential.

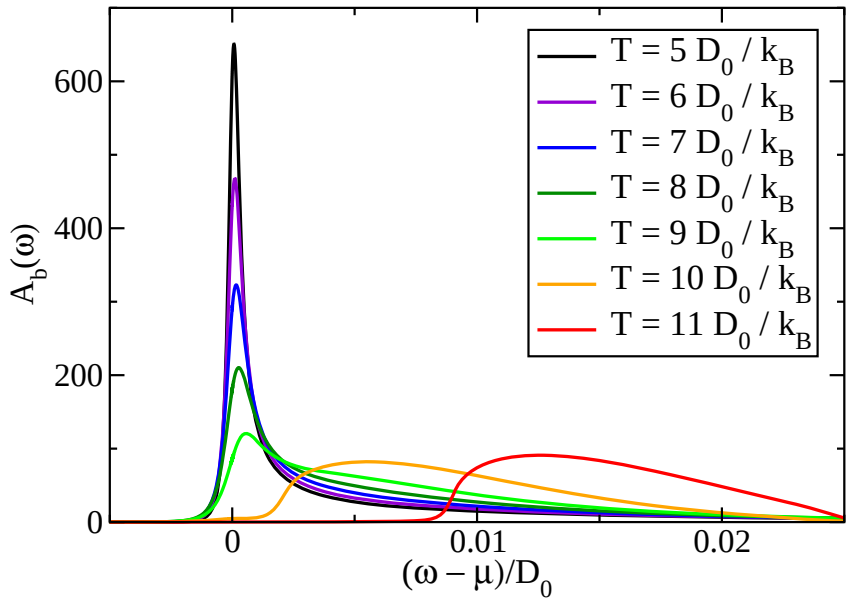


***Figure C.2:*** Imaginary part of the slave boson Green's function. Below the critical temperature the slave bosons are centered in a narrow peak around the chemical potential. In the paramagnetic peak $A_b$ is broadened and located around the negative renormalized impurity level.

# Bibliography


[1] B.T. Matthias, R.M. Bozorth and J.H. Van Vleck G. Pálsson *Phys. Rev. Lett.* **7**, 160 (1961)

[2] M. R. Oliver, J. A. Kalafas, J. Dimmock und T. B. Reed, *Phys. Rev. Lett.* **24**, 1064 (1970)

[3] M. R. Oliver, J. O. Dimmock, A. L. Mc Worther und T. B. Reed, *Phys. Rev. B* **5**, 1078 (1972)

[4] Y. Shapira, S. Foner and T. B. Reed, *Phys. Rev. B* **8**, 2299 (1973); **8**, 2316 (1973)

[5] T. Penney, M. W. Shafer and J. B. Torrance, *Phys. Rev. B* **5**, 3669 (1972)

[6] P. G. Steeneken, L. H. Tjeng, L. Elfimov, G. A. Sawatzky, G. Ghiringhelli, N. B. Brookes und D.-J. Huang, *Phys. Rev. Lett.* **88**, 047201 (2002)

[7] T. Matsumoto, K. Yamaguchi, M. Yuri, K. Kawaguchi, N. Koshizaki, and K. Yamada , *J.Phys.* **16**,6017 (2004)

[8] M. Imada, A. Fujimori, and Y. Tokura *Rev. Mod. Phys.* **70**,1039 (1998)

[9] P.W. Anderson , *Phys.Rev.* **124** , 41 (1961)

[10] P.W. Anderson , *J.Phys.C: Solid State Phys.* **3** , 2436 (1970)

[11] J. Kondo , *Prog.Theo.Phys.* **32** , 37 (1964)

[12] K.G. Wilson *Rev.Mod.Phys.* **47** , 773 (1975)

[13] N.Andrei , *Phys.Rev.Lett.* **45** , 379 (1980)

[14] P.B. Wiegmann *Sov.Phys. JETP Lett.* **31** , 392 (1974)

[15] A.C. Hewson , *The Kondo Problem to Heavy Fermions,* Cambridge University Press (1993)

[16] H. Keiter and J. C. Kimball , *J. Appl. Phys.* **42** , 1460 (1971)

[17] N. Grewe and H. Keiter , *Phys. Rev. B* **24** , 4420 (1981)

[18] Y. Kuramoto, *Z. Phys. B* **53** , 37 (1983)

[19] H. Kojima, Y. Kuramoto and M. Tachiki , *Z. Phys. B* **54** , 293 (1984)

[20] Y. Kuramoto and H. Kojima , *Z. Phys. B* **57** , 95 (1984)

[21] Y. Kuramoto , *Z. Phys. B* **65** , 29 (1986)

[22] V.-C. Lee and L. Liu , *Phys. Rev. B* **30** , 2026 (1984)

[23] M. W. Shafer, J. B. Torrance and T. Penney , *J. Phys. Chem. Solids* **33**, 2251 (1972)

[24] D. E. Eastman, F. Holtzberg and S. Methfessel, *Phys. Rev. Lett.* **23**, 226 (1969)

[25] I. Tsubokawa, *J. Phys. Soc. Japan* **15**, 1664 (1960)

[26] O. W. Dietrich, A.J. Henderson Jr. and H. Meyer, *Phys. Rev. B* **12**, 2844 (19)

[27] W. Heisenberg, *Z. Phys.* **49**, 619 (1928)

[28] R. Schiller, W. Müller, and W. Nolting, Phys. Rev. B **64**,134409 (2001)

[29] A. Mauger , *Phys. Rev. B* **27**, 2308 (1983)

[30] A. Mauger and D. L. Mills , *Phys. Rev. B* **28**, 6553 (1983)

[31] J. B. Torrance, M. W. Shafer, and T. T. McGuire , *Phys. Rev. Lett.* **29**, 1168 (1972)

[32] H. Ott, S. J. Heise, R. Sutarto, Z. Hu, C. F. Chang, H. H. Hsieh, H.-J. Lin, C. T. Chen, and L. H. Tjeng, *Phys. Rev. B* **73**, 094407 (2006)

[33] T. Haupricht, *Diploma thesis*, Universität Köln, (2006)

[34] T. Haupricht, *private communication*

[35] P. Sinjukow und W. Nolting, Phys. Rev. B **68**, 125107 (2003)

[36] P. Sinjukow und W. Nolting, Phys. Rev. B **69**, 214432 (2004)

[37] M. A. Rudermann and C. Kittel , *Phys.Rev.* **96** , 99 (1954)

[38] T. Kasuya , *Prog. Theor. Phys.* **16** , 45 (1956)

[39] K. Yosida , *Phys.Rev.* **106** , 893 (1957)

[40] N. Bloembergen and T. J. Rowland , *Phys.Rev.* **97** , 99 (1955)

[41] K. Yosida *Theory of Magnetism* Springer (1996)

[42] A. Auerbach *Interacting Electrons and Quantum Magnetism* Springer (1997)

[43] J. Zinn-Justin *Quantum Field Theory and Critical Phenomena* Oxford University Press (1993)

[44] F. Bloch , *Z. Physik* **61** , 206 (1930)

[45] J. Als-Nielsen, O. W. Dietrich, W. Kunnmann and L. Passell , *Phys.Rev. Lett.* **27** , 741 (1971)

[46] A. Georges, G. Kotliar, W. Krauth and M. J. Rozenberg , *Rev. Mod. Phys.* **68** , 13 (1996)

[47] A. Georges und G. Kotliar, Phys. Rev. B **45**, 6479 (1992)

[48] W. Metzner and D. Vollhardt , *Phys. Rev. Lett.* **62** , 324 (1989)

[49] J. Hubbard , *Proc. Roy. Soc.* **276** , 238 (1963)

[50] J. Kondo , *Prog.Theo.Phys.* **32** , 37 (1964)

[51] J. Schrieffer and P. Wolff, *Phys.Rev.* **149** , 491 (1966)

[52] W. J. de Haas, J. H. de Boer and G. J. van den Berg , *Physica* **1** , 1115 (1934)

[53] D. Goldhaber-Gordon,J. Göres, M. A. Kastner, Hadas Shtrikman, D. Mahalu, and U. Meirav , *Phys. Rev. Lett.* **81** , 5225 (1998)

[54] A. Abrikosov , *Physics* **2** , 21 (1965)

[55] S. E. Barnes , *J. Phys. F* **6** , 1375 (1976)

[56] S. E. Barnes , *J. Phys. F* **7** , 2637 (1977)

[57] P. Coleman, *Phys. Rev. B* **29** , 2 (1984)

[58] G. Baym and L. P. Kadanoff, *Phys. Rev.* **124** , 287 (1961)

[59] G. Baym, *Phys. Rev.* **127** , 1391 (1962)

[60] N. E. Bickers, *Rev. Mod. Phys.* **59** , 845 (1987)

[61] E. Müller-Hartmann, *Z. Phys.* **B57** , 281 (1984)

[62] T. A. Costi, J. Kroha and P. Wölfle, *Phys. Rev. B* **53** , 1850 (1996)

[63] S. Kirchner and J. Kroha, *J. Low. Temp. Phys.* **126** , 1233 (2002)

[64] J. Kroha, P. Wölfle and T. A. Costi *Phys. Rev. Lett.* **79** , 261 (1997)

[65] S. Kirchner, J. Kroha and P. Wölfle *Phys. Rev. B* **70** , 165102 (2004)

[66] J. Kroha and P. Wölfle, Invited Article, Proceedings of the International Conference on "Mathematical Methods in Physics", Montreal 2000; in "Theoretical Methods for Strongly Correlated Electrons", D. Senechal, A.-M. Tremblay, and C. Bourbonnais Eds., CRM Series in Mathematical Physics (Springer, New York, 2003)

[67] G. Kotliar and A. E. Ruckenstein, *Phys. Rev. Lett.* **57**, 1362 (1986)

[68] J. Kroha, P. J. Hirschfeld, K. A. Muttalib and P. Wölfle, *Solid State Comm.* **83 (12)**, 1003 (1992)

[69] R. Kubo, *J. Phys. Soc. Japan* **12**, 570 (1957)

[70] H. Schweitzer and G. Czycholl *Phys. Rev. Lett.* **67** , 3724 (1991)

[71] G. Czycholl and H. J. Leder *Z. Phys. B* **44** , 59 (1981)

[72] T. Pruschke, M. Jarrell and J. Freericks, *Adv, Phys.* **44** , 187 (1995)

[73] G. Pálsson and G. Kotliar, *Phys. Rev. Lett.* **80**, 4775 (1998)

# Publications

- *Simultaneous ferromagnetic and semiconductor-metal transition in electron-doped EuO*,
  Michael Arnold and Johann Kroha, Preprint cond-mat/0708.0416,
  submitted to Physical Review Letters

- *Simultaneous ferromagnetic and semiconductor-metal transition in EuO*,
  Michael Arnold and Johann Kroha, Physica C 460,1137 (2007)

- *Universality in Voltage-driven Nonequilibrium Phase Transitions*,
  Johann Kroha, Michael Arnold, and Beate Griepernau,
  J. Low Temp. Phys. 147 (3-4), 505 (2007);

- *Stable two-channel Kondo fixed point of an SU(3) quantum defect in a metal: renormalization group analysis and conductance spikes*,
  Michael Arnold, Tobias Langenbruch, and Johann Kroha,
  Phys. Rev. Lett. 99, 18660 (2007)

- *Conserving approximation for the Anderson impurity model in Kotliar-Ruckenstein slave boson representation*,
  Michael Arnold, Johann Kroha, and Antoine Georges, Preprint

## Manuscripts in preparation:

- *Magnetic and semiconductor-metal transitions in Heisenberg-Semiconductor models with quantum defects*,
  Michael Arnold and Johann Kroha, to be submitted to Phys. Rev. B

- *A quantum defect with partially broken SU(3) symmetry in a metal: two-channel Kondo fixed point and conductance spikes*,
  Tobias Langenbruch, Michael Arnold, and Johann Kroha,
  to be submitted to Phys. Rev. B

# Danksagung

Zuerst möchte ich Prof. Kroha für die immer interessanten wissenschaftlichen Anregungen und Ideen danken, die unter anderem das hier bearbeitete Thema beinhalteten. Weiterhin danke ich Prof. Flume, Prof. Maier und Prof. Sokolowski für ihre Bereitschaft an der Promotionskommission teilzunehmen. Außerdem gilt mein Dank dem Team der theoretischen Physik im physikalischen Institut. Die angenehme und familiäre Atmosphäre bei der Arbeit, aber auch bei zahlreichen Feiern und anderen Gelegenheiten hat die letzten Jahre zu einer sehr angenehmen Erfahrung gemacht. Ein wesentlicher Beitrag hierzu bestand sicherlich im alltäglichen Miteinander innerhalb unserer gesamten Arbeitsgruppe. Sowohl in wissenschaftlicher, als auch in menschlicher Hinsicht war dieses Umfeld stets inspirierend.

Abschließend möchte ich natürlich noch meiner Familie danken, die in Gestalt meiner Eltern und meiner Schwester immer einen starken Rückhalt bildeten. Besonderer Dank gilt meiner Frau Geesche, die mich tatsächlich vom ersten bis zum letzten Semester begleitet hat, was gar nicht ausreichend gewürdigt werden kann. Meiner Tochter Mieke danke ich einfach dafür, dass sie da ist.